



**University of Kerbala
College of Science
Department of Chemistry**

Biosynthesis of Zinc Oxide Nanoparticles *Ziziphus-spina christi* Leaves Extract: Characterization and Their Effects in Male Rats Exposed to Adenine

A Thesis

Submitted to the Council of the College of Science-University of Kerbala
as a Partial Fulfillment of the Requirement for the Master Degree in
Chemistry Science

By

Hayder Hussein Abbas

B.Sc. Chemistry/College of Science /University of Kufa (2009)

Supervised by

**Prof. Dr. Narjis Hadi Al-Saadi
Ph. D. Biochemistry**

**Prof. Dr. Ayyed Hameed Hasan
Ph. D. Animal Physiology**

2023 A.D

1445 A.

Certification of Supervisor

We certify that this thesis "**Biosynthesis of Zinc Oxide Nanoparticles *Ziziphus-spina christi* Leaves Extract: Characterization and Their Effects in Male Rats Exposed to Adenine**" was prepared under our supervision at the Department of Chemistry, College of Science, University of Kerbala, as partial fulfillment of the requirements for the degree of Master of Chemistry.

Signature: 

Name: **Dr. Narjis Hadi Al-Saadi**

Title: Professor

Address: University of Kerbala / College of Science / Department of Chemistry

Date: 15/10/2023

Signature 

Name: **Dr. Ayyed Hameed Hasan**

Title: Professor.

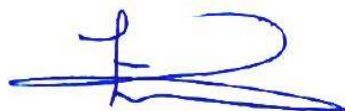
Address: University of Kerbala / College of Dentistry

Date: 17/10/2023

Report of the Head of Chemistry Department

According to the recommendations presented by the Supervisor and the Postgraduate Studies Director, I forward this thesis "**Biosynthesis of Zinc Oxide Nanoparticles *Ziziphus-spina christi* Leaves Extract: Characterization and Their Effects in Male Rats Exposed to Adenine**" for examination.

Signature:



Name: **Prof. Dr. Luma Majeed Ahmed**

Head of Chemistry Department

Address: University of Kerbala /College of Science/ Department of Chemistry.

Date: 25/ 10/ 2023

Examination Committee Certification

We, the examining committee, certify that we have read this thesis "**Biosynthesis of Zinc Oxide Nanoparticles *Ziziphus-spina christi* Leaves Extract: Characterization and Their Effects in Male Rats Exposed to Adenine**" and examined the student (Hayder Hussein Abbas) in its contents and that in our opinion; it is adequate as a thesis for the degree of Master of Science in Chemistry.

Signature:



Name: **Rana Majeed Hameed**

Title: Assist. Prof. Dr.

Address: University of Kerbala, College of Medicine

Date: 17/10/2023

(Chairman)

Signature:

Name: **Dr. Amer Hasan Abdullah**

Title: Assist. Prof. Dr.

Address: University of Mustansiriyah,
College of Sciences, Department of
Chemistry

Date: 25/10/2023

(Member)

Signature:



Name: **Dr. Afaf Khairi Esmail**

Title: Assist. Prof. Dr.

Address: University of Kerbala,
College of Sciences, Department
of Biology

Date: 15/10/2023

(Member)

Signature:



Name: **Dr. Narjis Hadi Al-Saadi**

Title: Professor

Address: University of Kerbala, College
of Sciences, Department of Chemistry

Date: 15/10/2023

(Member & Supervisor)

Signature:



Name: **Dr. Ayyed Hameed Hasan**

Title: Professor

Address: University of Kerbala,
College of Dentistry

Date: 17/10/2023

(Member & Supervisor)

Approved by the Council of the College of Science

Signature:

Name: **Dr. Jasem Hanoon Hashim Al-Awadi**

Title: Professor

Address: Dean of College of Science, University of Kerbala.

Date: 26/10/2023



Dedication

To the messenger of mercy, the Prophet Muhammad “Allah blessing and peace be upon him and his pure family” ...

To my homeland, Iraq, and its noble people...

To my loving mother, who was of help and support for me, and her blessed supplication had the greatest effect in facilitating the search ship to dock on this image...

To those with whom I have shared all my life, and from whom I derive my pride and determination, my dear mother, dear brother (Karrar) and sisters (Fatimah and Zainab)...

To the spring that never stops giving, who always weaves my beautiful happiness with strings from her great heart

my dear wife (Enas)

To my beloved sons who were patient with me through hardship and fatigue... (Adam, Aula and Akram)

To family, friends, and everyone who benefits from this work....

Hayder

Acknowledgments

First of all, I would like to thank Allah, for giving me wisdom and bliss Thank you my God for all the goods that have been given in my life, and the prayer and peace upon the messenger, mercy to the worlds, our Prophet Mohammad, and to his household. Thanks to the dean of the College of Science, University of Kerbala (Prof. Dr. Jasem Hanoon Hashim Al-Awadi). I, also want to thank the head of the department of Chemistry (Prof. Dr. Luma Majeed Ahmed), and the whole staff in the Department of Chemistry for their help.

I would like to express my sincerely grateful and deep appreciation to my supervisor **Prof. Dr. Narjis Hadi Mansor Al-Saadi** for her patience, generosity, assistance, great interest, kindness candidness, and never-ending encouragement in pursuing my thesis. Without her guidance and persistent help, this thesis would not have been possible to be finished. I am very grateful to her for her continuous encouragement and support during the completion of the work. Calling on God Almighty to give her long health and more scientific prosperity.

I would like to thank my co-supervisor **Prof. Dr. Ayyed Hameed Hasan Al-Mossawi** for his guidance and advisement throughout the period of the project. I am forever grateful for his enthusiastic supervision, his sharp and perceptive observation of my research, and most importantly, his kindness. His insightful opinion and advice helped me through many technical and professional difficulties. My deepest appreciation is extended to her and I wish her a lifetime of happiness.

To my angel in life, to the meaning of love, compassion, and dedication to the smile of life. To the secret of existence and to those who were the secret of my success (my dear mother, my brother and sisters, my wife and my children).

I would like to thank those who have great credit for encouraging me and their presence acquired strength. My thanks go to all the professors and staff of the Faculty of Pharmacy, University of Kufa.

I would like to thank my colleagues in the study, who built a fun and breezy environment for me to study and help together.

Hayder Hussain Abbas

Summary

Zinc oxide nanoparticles (ZnO-NPs) have been widely studied in recent decades due to their nano-medicine applications based on their physiological and biochemical agents often added as a food supplement in animal diets. This study aimed to synthesis and characterization of (ZnO-NPs) by the biological method using the plant extract and then investigated its effects in adenine-exposed male rats. Biosynthesized ZnO-NPs were synthesized using the crude aqueous extract of *Ziziphus-spina christi* leaves and zinc nitrate hexahydrate ($\text{Zn}(\text{NO}_3)_2 \cdot 6\text{H}_2\text{O}$). The reaction medium was maintained with a temperature of 60°C and a pH of 9. The change of color from yellow to brown indicates the production of ZnO-NPs. The produced ZnO-NPs were characterized using several techniques. Ultraviolet-visible (UV-Vis) spectrum showed the maximum peak at 362 nm, this was strong evidence for the forming of ZnO-NPs. Fourier Transform-Infrared (FT-IR) spectrum revealed the appearance of absorption peaks between 400 and 500 cm^{-1} returned to Zn-O bonding. X-ray diffraction (XRD) analysis revealed that the hexagonal Wurtzite structure for nanoparticles with an average crystallite size was 38.177 nm. Transmission electron microscopy (TEM) showed that nanoparticles had a spherical shape and fell in the range of 35 - 45 nm in diameter, also the images of scanning electron microscope (SEM) showed the semispherical shape and these particles are in a highly agglomerated form with an average particle size was ranged at diameter: D_1 (39.74 nm), D_2 (42.25 nm), and D_3 (48.19 nm). Finally, atomic force microscopy (AFM) displays a uniform surface with cone-like grains covering the surface of ZnO-NPs, and the surface roughness in the range of 42 to 45 nm. Thirty-six male rats were used in this study and divided randomly into six equal groups (six rats each). Group-I

received orally dimethyl sulfoxide (5% v/v/day) alone for 30 days and served as the control group, group-II administered adenine orally (100 mg/Kg. Bw/day) for 30 days, group III received *Ziziphus-spina christi* leaves extract (10 mg/Kg. Bw/day) for 30 days, group-IV was administered ZnO-NPs (10 mg/Kg. Bw/day) for 30 days, group-V was co-administered adenine (100 mg/Kg. Bw/day) plus *Ziziphus-spina christi* leaves extract (10 mg/Kg. Bw/day) for 30 days and the last group-VI received the adenine combined with ZnO-NPs in the same previous doses for 30 days. At the end of the experiment, the kidney function tests (uric acid, urea, and creatinine) and liver function tests (alanine aminotransferase ALT, aspartate aminotransferase AST and alkaline phosphatase ALP) were determined. Antioxidant status (superoxide dismutase SOD, catalase CAT, total antioxidant capacity TAC, and reduced glutathione GSH) and oxidative stress (Malondialdehyde MDA and nitric oxide NO) were performed. Furthermore, histopathological alterations of kidney and liver tissues were investigated. *In vivo* of this study, the synthesized ZnO-NPs and *Ziziphus-spina christi* leaves extract at a dose (10 mg/Kg. Bw) were exhibited the potential effects against adenine-exposed male rats, these confirmed by ameliorative growth rats and the significant decreases in kidney and liver function parameters, uric acid, urea, creatinine, ALT, AST, and ALP in comparison to adenine exposed rats ($P \leq 0.05$). Significant elevation was also demonstrated in antioxidants levels SOD, CAT, TAC, and GSH associated with depletion in oxidative stress MDA and NO in both treatment groups fifth and sixth when compared to adenine group rats. Moreover, there were improvements in the marked histological changes of the kidney and liver by comparing with the adenine group. In conclusion, *Ziziphus-spina christi* leaves extract and ZnO-NPs have ameliorative effects against adenine-exposed male rats, implying that they may be used safely against kidney and liver

damage, and no significant effects were observed in normal renal and hepatocyte tissues, indicating that they may be powerful antioxidant, anti-inflammatory, and antitoxic agents for biomedical applications.

List of Contents

Subject No.	Subject	Page No.
	Summary	I
	List of Contents	IV
	List of Tables	VII
	List of Figures	VIII
	List of Abbreviations	X
Chapter One: Introduction and Literature Review		
1-1	Introduction	1
1-2	Literature Review	4
1-2-1	<i>Ziziphus-spina christi</i> plant	4
1-2-2	Constitutes of <i>Ziziphus -spina christi</i>	5
1-2-3	Biological applications of <i>Ziziphus -spina christi</i>	6
1-2-4	Effect of <i>Ziziphus spina- christi</i> on kidney diseases	7
1-3	Nanoparticles	8
1-3-1	Classification of Nanoparticles	9
1-3-2	Synthesis Approaches of Nanoparticles	10
1-3-3	Synthesis Methods of nanoparticles	12
1-3-3-1	Physical synthesis Methods	12
1-3-3-2	Chemical Synthesis Methods	13
1-3-3-3	Biological synthesis Methods	13
1-3-4	Synthesis of Nanoparticles from Plants	14
1-3-5	Characterization of Nanoparticles	16
1-4	Zinc Oxide Nanoparticle (ZnO-NPs)	17
1-4-1	Biosynthesis of Zinc Oxide Nanoparticles	18
1-4-2	Optimization of ZnO-NPs Synthesis	19
1-4-3	Biological Applications of Zinc Oxide Nanoparticles	20
1-4-4	Antioxidant Activity of Zinc Oxide Nanoparticles	20
1-5	Kidney and Liver Toxicity	21
1-6	Role of Zinc Oxide Nanoparticles in Ameliorating Renal-Hepatic Toxicity	22
1-7	Adenine	24
1-8	Mechanism Action of Adenine	25
1-9	The objectives of the Study	28
Chapter Two: Materials and Methods		
2	Materials and Methods	29
	Instruments	29

	Chemicals and Kits	30
	Methods	31
2-1	Experimental design of the study	31
2-2	Collection of plants	32
2-3	Preparation of Plant Extract	32
2-4	Phytochemicals screening in the plant extract	33
2-5	Preparation of 1 mM Zn(NO ₃) ₂ .6H ₂ O Solution	35
2-6	Biosynthesis and purification of Zinc Oxide nanoparticles	36
2-7	Optimization of the ZnO-NPs biosynthesis	37
2-7-1	Effect of the Reaction time	38
2-7-2	Effect of the boiling time	38
2-7-3	Effect of the plant extract volume	38
2-7-4	Effect of ZnNO ₃ .6 H ₂ O concentration	38
2-7-5	Effect of pH	38
2-7-6	Effect of temperature	38
2-8	Characterization of zinc oxide nanoparticles	39
2-8-1	UV-Visible Spectroscopy	39
2-8-2	Fourier transform infrared FT-IR spectroscopy	39
2-8-3	X-ray diffraction (XRD)	39
2-8-4	Transmission Electron Microscopy (TEM)	40
2-8-5	Scanning electron microscopy (SEM)	40
2-8-6	Atomic Force Microscopy (AFM)	40
2-9	<i>In vivo</i> applications of Zinc oxide Nanoparticles	41
2-9-1	Animals of the Study	41
2-9-2	Preparation of Adenine	41
2-9-3	The Experimental Design	42
2-9-4	Collection of blood and Tissues	42
2-9-4-1	Blood Specimens	42
2-9-4-2	Tissue Sampling	43
2-10	Biochemical Analysis	43
2-10-1	Estimation of Kidney Function Tests	43
2-10-1-1	Estimation of Uric Acid	43
2-10-1-2	Estimation of Urea	46
2-10-1-3	Estimation of Creatinine	47
2-10-2	Estimation of Liver Function Tests	49
2-10-2-1	Estimation of Alanine Aminotransferase Activity	49
2-10-2-2	Estimation of Aspartate Aminotransferase activity	51

2-10-2-3	Estimation of Alkaline Phosphatase Activity	54
2-10-3	Estimation of Antioxidant Statuses	55
2-10-3-1	Estimation of Total Antioxidant Capacity Assay	55
2-10-3-2	Estimation of Catalase Activity Assay	58
2-10-3	Estimation of Superoxide Dismutase activity assay	59
2-10-3-4	Estimation of Reduced Glutathione Assay	61
2-10-3-5	Estimation of Malondialdehyde Assay	62
2-10-3-6	Estimation of Nitric Oxide Assay	64
2-11	Histological Study	66
2-12	Statistical Analysis	67
Chapter Three: Results and Discussion		
3	Results and Discussion	68
3-1	Qualitative Analysis of the Phytochemicals in the <i>Ziziphus-spina christi</i> Leaves Aqueous and Alcoholic Extracts	68
3-2	Biosynthesis of Zinc Oxide Nanoparticles	69
3-3	Characterization of Synthesized Zinc Oxide Nanoparticles	73
3-3-1	Ultraviolet-Visible Spectroscopy (UV-Vis Spectroscopy)	73
3-3-2	Fourier Transform Infrared Spectroscopy (FT-IR)	80
3-3-3	X-ray Diffraction (XRD)	82
3-3-4	Transmission Electron Microscopy (TEM)	84
3-3-5	Scanning Electron Microscope (SEM)	85
3-3-6	Atomic Force Microscopy (AFM)	86
3-4	Bioc hemical Analysis	88
3-4-1	Body Weight Changes	88
3-4-2	Estimation of Kidney Function Tests	90
3-4-3	Estimation of Liver Function Tests	92
3-4-4	Effect on Antioxidants Statuses	94
3-4-5	Histological Study	97
3-4-5-1	Kidney Section	97
3-4-5-2	Liver Section	99
Conclusion and Future Studies		
	Conclusions	102
	Future Studies	103
References		
	References	104

List of Tables

Table No.	Title	Page No.
2-1	Instruments and tools with their suppliers	29
2-2	Chemicals and kits used with their origin and company	30
2-3	Preparation of standard solutions to determination of uric acid	44
2-4	Mixing of reagents to determination of uric acid	45
2-5	Addition of reagents to determination of urea	47
2-6	Addition of reagents to determination of creatinine	48
2-7	Preparation of standard solutions to determination of ALT	50
2-8	Mixing of reagents to determination of ALT	51
2-9	Preparation of standard solutions to determination of AST	52
2-10	Mixing of reagents to determination of AST	53
2-11	Addition of reagents to determination of ALP	54
2-12	Preparation of standard solutions to determination of TAC	56
2-13	Addition of reagents to determination of SOD	60
2-14	Addition of reagents to determination of GSH	61
2-15	Addition of reagents to determination of MDA	63
2-16	Preparation of standard solutions to determination of NO	65
3-1	Qualitative analysis of phytochemicals in the <i>Ziziphus-spina christi</i> leaves aqueous and alcohol extracts	69
3-2	Effect of ZnO-NPs and <i>Z.-spina christi</i> leaves extract on adenine-induced body weight changes	89
3-3	Effect of ZnO-NPs and <i>Z.-Spina Christi</i> leaves extract on kidney function parameters in adenine-exposed male rats	91
3-4	Effect of <i>Z.-spina christi</i> leaves extract and ZnO-NPs on liver function parameters in adenine-exposed male rats	92
3-5	The effect of <i>Z.-spina christi</i> leaves extract and ZnO-NPs on the antioxidant levels in adenine-exposed male rats	95

List of Figures

Figure No.	Title	Page No.
1-1	<i>Ziziphus -spina christi</i> tree	5
1-2	The basic chemical structure of essential phytochemicals of <i>Z. spina-christi</i> leaves extract	6
1-3	Top-Down synthesis method of nanoparticles	11
1-4	Bottom-Up synthesis method of nanoparticles	11
1-5	Schematic synthesis methods of nanoparticles	14
1-6	Synthesis of metal-nanoparticles from plant extracts	15
1-7	Techniques used in nanoparticles characterization	17
1-8	Main crystal structures of ZnO-NPs	18
1-9	The chemical structure of adenine	25
1-10	Scheme of metabolic pathways for the disposal of adenine in animals	27
2-1	Experimental Design of the study	31
2-2	Schematic biosynthesis of zinc oxide nanoparticles	37
2-3	The chemical reaction to determination of uric acid	44
2-4	Standard curve of uric acid	45
2-5	The chemical reaction to determination of urea	46
2-6	The chemical reaction to determination of creatinine	47
2-7	The chemical reaction to determination of ALT	49
2-8	Standard curve of ALT	50
2-9	The chemical reaction to determination of AST	51
2-10	Standard curve of AST	53
2-11	The chemical reaction to determination of ALP	54
2-12	The chemical reaction to determination of TAC	56
2-13	Standard curve of TAC	57
2-14	The chemical reaction to determination of SOD	59
2-15	The chemical reaction to determination of GSH	61
2-16	The chemical reaction to determination of MDA	62
2-17	The chemical reaction to determination of NO	64
2-18	Standard curve of NO	66
3-1a	The gradual change in the color of the synthesized ZnO-NPs from <i>Z.-spina christi</i> leaves and zinc nitrate hexahydrate with time (0 min-48 hours)	71
3-1b	Yellowish-white powder of the synthesized ZnO-NPs	71
3-2	UV-Visible spectra of the synthesized ZnO-NPs at different times	72

3-3	UV-Visible spectra of the synthesized ZnO-NPs	73
3-4	UV-Visible spectra of the synthesized ZnO-NPs at different boiling times of extract	74
3-5	UV-Visible spectra of ZnO-NPs at different volumes of extract	75
3-6	UV-Visible spectra of ZnO-NPs at different concentrations of Zn(NO ₃) ₂ .6H ₂ O	76
3-7	UV-Visible spectra of Zn-NPs at different pH	78
3-8	UV-Vis spectra of Zn-NPs at different temperatures	79
3-9	FT-IR spectrum, (a) <i>Z.-spina christi</i> leaves extract (b) ZnO-NPs	82
3-10	XRD diffractogram, (a) ZnO- card No. 36-1451. (b) the synthesized ZnO-NPs	83
3-11	TEM micrograph of the synthesized ZnO-NPs. (a) Scale at 100 nm. (b) Scale at 200 nm. (c) The size distribution histogram of ZnO-NPs	84
3-12	SEM images of synthesized ZnO-NPs at different magnifications (a) At 50 nm. (b) At 200 nm. (c) SEM images at 100 nm with the particle size at different average diameters D1, D2, and D3	86
3-13	AFM analysis of synthesized ZnO-NPs (a) 2-Dimension image (b) 3-Dimension image (c) The granularity distribution chart	87
3-14	Effects of ZnO-NPs and <i>Z.-spina christi</i> leaves extract on the histological appearance of kidney tissues in male rats with renal failure induced by adenine.	98
3-15	Effects of ZnO-NPs and <i>Z.-spina christi</i> leaves extract on the histological appearance of liver tissues in male rats with renal failure induced by adenine	101

List of Symbols and Abbreviations

Abbreviations	Meaning
ADA	Adenosine deaminase
AFM	Atomic Force Microscopy
ALP	Alkaline phosphatase
ALT	Alanine aminotransferase
AMP	Adenosine monophosphate
ANOVA	Analysis of Variance ANOVA
APRT	Adenine phosphoribosyl transferase
AST	Aspartate amino transferase
ATP	Adenosine triphosphate
Å	Angstrom
Bw	Body weight
BUN	Blood urea nitrogen
Caspase 3	Protein coding gene
CAT	Catalase
CHCl ₃	Chloroform
CH ₃ COOH	Acetic Acid
cm ⁻¹	Wavenumber
CuSO ₄ .5H ₂ O	Cupric sulphate pentahydrate
CP	Cisplatin
CO ₂	Carbon dioxide
C ₅ H ₅ N	Chemical formula of adenine
D	The average crystalline size in Debye–Scherrer's equation
DHA	2,8-Dihydroxyadenosine
DHBS	3,5-dichloro-4-hydroxybenzene-1-sulfonic acid
DMN	Dimethyl nitrosamine
DMSO	Dimethyl sulfoxide
DNA	Deoxyribonucleic acid

eq.	Equation
ESRD	End Stage Renal Disease
FAD	Flavin adenine dinucleotide
FDA	Food and Drug Administration
FeCl ₃	Ferric chloride
FeSO ₄ .7H ₂ O	Ferrous sulfate heptahydrate
Fe ²⁺ , Fe ³⁺	Ferrous and ferric ions respectively
TPTZ	(2,4,6-tris(2-pyridyl)-1,3,5-triazine)
FT-IR	Fourier transform infrared spectroscopy
FWHM	Full width at half maximum
GMP	Guanine monophosphate
GPx	Glutathione peroxidase
GR	Glutathione reductase
Griess I	Sulfanilamide
Griess II	Naphthyl ethylenediamine
gm	Gram
g/dL	Grams per deciliter
GTP	Guanine triphosphate
GSH	Glutathione reductase
H&E	Hematoxylin and Eosin stain
G2 (HepG2)	Hepatoma cell line
H ₂ SO ₄	Sulfuric acid
H ₂ O ₂	Hydrogen peroxide
HCl	Hydrochloric acid
HGPRT	Hypoxanthine-guanine phosphoribosyl transferase
HNO ₃	Nitric acid
IMP	Inosine monophosphate
IL-6	Interleukin-6
<i>k</i>	Isotope factor or Scorer's constant (0.98)

KD	Kidney disease
Kg	Kilogram
KI	Potassium Iodide
KOH	Potassium hydroxide
(K ₃ Fe (CN) ₆)	Potassium ferrocyanide
Kv	Kilovolt
mA	Milliamperere
MDA	Malonaldehyde
μmol/L	Micromole per liter
μmol/mL	Micromole per milliliter
mL	Milliliter
μL	Microliter
mM	Millimolar
MO-NPs	Metal oxide nanoparticles
NAD	Nicotinamide adenine dinucleotide
NaOH	Sodium hydroxide
Na ₂ CO ₃	Anhydrous sodium carbonate
NH ₄ ⁺	Ammonium ion
NPs	Nanoparticles
NaNO ₂	Sodium nitrite
NO	Nitric oxide
O ₂ ⁻	Superoxide anion
p	Probability
pH	"Potential of hydrogen" (or "Power of hydrogen")
PBS	Phosphate-buffer saline
PNP	Purine nucleoside phosphorylase
RF	Renal failure
RNA	Ribonucleic acid
RNS	Reactive nitrogen species

ROS	Reactive oxygen species
SD	Standard deviation
SEM	Scanning electron microscopy
SOD	Superoxide dismutase
STZ	Streptozotocin
SPR	Surface plasmon resonance
TAA	Paracetamol
TAC	Total antioxidant capacity
TBA	2-Thiobarbituric acid
TCA	Trichloroacetic acid
TNB	2-nitro-5-thiobenzoic acid
TNF- α	Tumor Necrosis Factor- α proteins
U/ml	Units per milliliter
UV	Ultraviolet
UV-vis.	UV-visible spectroscopy
WST-1	Water-soluble tetrazolium salt
XDH	Xanthine dehydrogenase
XMP	Xanthosine monophosphate
XRD	X-ray diffraction
ZnO-NPs	Zinc oxide nanoparticles
Zn (NO ₃) ₂ .6H ₂ O	Zinc nitrate hexahydrate
<i>Z.-spina christi</i>	<i>Ziziphus-spina christi</i>
(0D) NPs	Zero-Dimensional nanoparticles
(1D) NPs	One-Dimensional nanoparticles
(2D) NPs	Two-dimensional nanoparticles
(3D) NPs	Three-dimensional nanoparticles
λ	Wavelength
θ	Incident Bragg's diffraction angle
β	Incident XRD peak full width at half maximum

Chapter One

Introduction

and

Literature Review

1-1 Introduction

In the few past years, nanoparticles have been different applications because they are reliable to provide a broad range of unusual uses and improved technologies for multiple applications such as industry, environment, medicine, and communications [1]. One of the reasons behind the intense interest in nanoparticles is that nanoparticles permit the preparation of substances where at least one dimension of the structure normally ranged from 1 to 100 nanometers, which is 1,000 times smaller than a micron. Nanoparticles are comparable to naturally occurring proteins and molecules in the human cell, and the great interest is due to their small size and large surface area to volume ratio [2], [3]. The biological activity of nanoparticles increased as the total surface area of the particles increased, which gives rise to some of the superior properties to their bulk phase such as antimicrobial, catalytic, electronic, magnetic, and optical properties [4], [5].

Medicinal plants are a great resource to be useful for medicine purposes to reduce diseases and improve human health. The medicinal advantages of these plants involved in some chemical compounds that produce a specific physiological action that can be used in the synthesis and production of drugs, due to the acceptability, compatibility, adaptability, and the little or no side effects of these natural drugs on the human body [6]. Biologically synthesized nanoparticles from plant extracts are usually prepared from the biological part of plants. Plant parts, for instance, leaf, root, stem, and seed, are widely used for synthesizing metal-NPs. Moreover, plant extracts contain bioactive compounds (phytochemicals) such as flavonoids, followed by saponins, carbohydrates, alkaloids, steroids, coumarins, quinines, fats and phenolic compounds, etc. [7]. Phytochemical constituents are playing a

significant role in reducing the metallic ions and later stabilizing them [8].

Metal oxide nanoparticles (MO-NPs) have been widely studied in recent years because they are highly valuable materials in various fields among the drug and health-related industries [9]. Some of MO-NPs were utilized in the therapy and clinical practice as well as promoting wound healing and antioxidant, nanoparticles of oxides such as titanium oxide (TiO_2), silver oxide (AgO), zinc oxide (ZnO), magnesium oxide (MgO), cerium oxide (CeO_2), iron oxide (Fe_2O_3), cadmium oxide (CdO), nickel oxide (NiO) and zirconium oxide (ZrO) [10]. These MO-NPs are the most promising candidates for biomedicine, with a considerable amount of research data available in recent literature regarding their biological *in vitro* and *in vivo* activity. Moreover, due to their reduced size, MO-NPs can interact on the more in-depth level with various cellular structures compared to their bulk counterparts, and, more importantly, they do not cause toxicity due to their highly improved biocompatibility [11]. Among metal oxide nanoparticles, ZnO-NPs which are a nontoxic, biocompatible biomaterial, with unique abilities that may vary depending on their size, shape, orientation, morphology and aspect ratio.

Biological synthesis of ZnO-NPs using plant extracts or microorganisms such as bacteria and fungi has attracted the great consideration from many researchers because of the advantages it has over the chemical and physical methods. Plant extracts have been more advantageous over the microbes and fungi because it does not require high isolation cost, cultivation, and maintenance, additionally can be obtained an agreeable yield in a short time [12].

The improvement effects of ZnO-NPs on oxidative stress were observed in rats, birds and fish when the toxic materials led to a

significant increase in malonaldehyde (MDA) and decrease in superoxide dismutase (SOD) and catalase (CAT) activities, while concentrations of MDA was significantly reduced and activities of SOD and CAT significantly increased after treatment with ZnO-NPs [13-15]. Zinc concentration was increased from the dissociation of ZnO-NPs, where zinc is the core constituent of antioxidant enzymes (as superoxide dismutase) and it is a protector for sulfhydryl groups and impair lipid peroxidation by displacing transition metals (as copper and iron) from catalytic sites [16]. Finally, ZnO-NPs are protected cell membranes against oxidative damage, decrease free radicals and lipid peroxidation levels, as well as increase the antioxidant enzyme levels, and then protect against kidney diseases [17].

1-2. Literature review

1-2-1 *Ziziphus-spina christi* Plant

Traditional plants use as a main source of popular medicines by many people in the world. So, in many developing countries, a large proportion of the population depends on traditional plants, and concern much research on medicinal plants in order to meet health care needs. Although modern medicine may exist side by side with such traditional practices, herbal medicines have often maintained their popularity for historical and cultural reasons [18]. The high concentrations of phytochemical contents in some plants draw attention to evaluate their possible health enhancing effects [19]. Due to artificial drugs are not always inexpensive or safe, many previous studies were performed to investigate new natural molecules that have vital activity, which is considered to be safe and without side effects [20], [21]. An example of such plants is *Ziziphus -spina christi* that belongs to the Rhamnaceous family (Figure 1-1). It is commonly in Arabic the tree called Sider and the fruit (Nabag) indicating the specific importance of this plant to local people [22]. *Ziziphus -spina christi* is consisting of about a hundred varieties of deciduous or evergreen trees and shrubs distributed throughout the tropical and subtropical regions of the world [23], from which twelve species are cultivated [24]. *Z.-spina christi* is a spiny shrub and sometimes a tall tree, reaching a height of 20 m that strongly resists heat and drought [25]. However, little research has been conducted on the rich nutritional content of its fruits and leaves, as well as on its well-known antimicrobial effects [26]. Moreover, *Z.-spina christi* is still growing along with several plants, and it is one of the important fruits that grows in the dry parts of tropical Asia and Africa [27].



Figure 1-1: *Ziziphus-spina christi* tree.

1-2-2 Constitutes of *Ziziphus -spina christi*

The chemical nature of plants is based upon the phytochemical compounds. Plants with a high concentration of chemical constituents can be therapeutically active or inactive. Active components may be found in each part of the plant (leaf, flower, stem, bark, root, fruit, and seed) [28]. Phytochemicals are classified into primary and secondary metabolites. Primary metabolites such as amino acids, proteins, carbohydrates and chlorophyll, while secondary metabolites are flavonoids, alkaloids, saponins, tannins, steroids, coumarins, quinines, fats and phenolic compounds (Figure 1-2) [29]. *Z.-spina christi* is rich in many biologically important compounds that were investigated by the phytochemical analysis which indicated the presence of flavonoids, alkaloids, tannins, coumarins, carbohydrates, and fats [30]. In addition, leaves also are rich in calcium, iron, and magnesium [31].

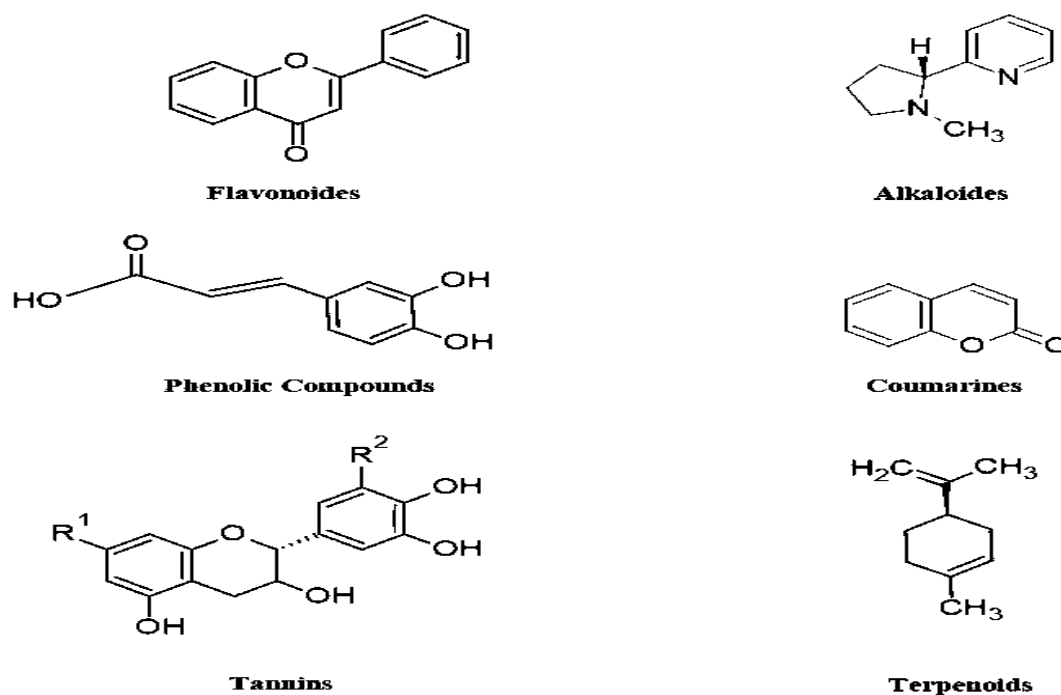


Figure 1-2 The basic chemical structure of the essential phytochemicals of *Z. spina-christi* leaves extract [32].

1-2-3 Biological Applications of *Ziziphus -spina christi*

The majority of rural people have no knowledge of modern medicine and depend mostly on folk therapies, often produced by plants [33]. *Z. spina-christi* is known for its medicinal properties as a hypoglycemic, hypotensive, anti-inflammatory, antimicrobial, antioxidant, anti-tumor, kidney and liver protective agent, and as an immune system stimulant [34]. The contents of *Z. spina-christi* fruits are good diets and rich in diverse vitamins that are used in folk medicine to treat blisters, bruises, chest pains, dandruff, fractures, headaches, and mouth problems [35]. It has been described as anti-laxative, astringent, diuretic and tonic[36] while the seeds are used to relieve pain and cut off vomiting and abdominal pain associated with pregnancy [37]. The roots are used to recover and prevent skin diseases [38]. Some pharmacological analysis studies indicated that the aqueous extract of *Z. spina-christi* root bark has antinociceptive activity in mice and rats, as well as reduces the tension and anxiety in mice [39], [40].

Z. spina-christi extract has also been reported to possess a protective effect against aflatoxicosis and anti-conceptive properties in rats and have a calming effect on the central nervous system [41], [42]. Moreover, the extract of *Z. spina-christi* stem bark has antidiarrheal effects in rats [43]. Finally, fruits have cleaning properties such as purifying the stomach, removing impurities from blood as well as being restorative for the health system [44].

1-2-4 Effect of *Ziziphus spina-christi* on Kidney Diseases

Ziziphus-spina christi is one of the most widely used medicinal herbs in the world. Unlike pharmaceutical medicines, which have been created for a specific condition regardless of their side effects, the entire plant of *Z.-spina christi* not only has no side effects, but also the presence of some minerals and vitamins in the diet is very important, and the deficiency in their normal levels may be cause many diseases, among them kidney diseases [45]. *Z.-spina christi* leaves were regarded a high-value resource, and numerous studies have shown that the phytochemicals content is exceptional, including flavonoids and phenolic compounds which are crucial compounds for the improvement of renal failure due to their antioxidant and anti-inflammatory agents [46 - 48]. It has been demonstrated that significant decrease in the level of urea, creatinine, uric acid, and also free radicals. Because of the improved preservation of bio-active components of *Z.-spina christi* leaves, it can be considered as a more appropriate ingredient for food enrichment [49]. Moreover, an extract of *Z.-spina christi* could be used not only as a safe potential natural functional food ingredient or as a therapeutic drug in the treatment of kidney diseases but also it is effective in reducing both lipid peroxidation products and reactive oxidative stress accompanying renal failure [50], [51].

1-3 Nanoparticles

Nanotechnology deals with the design, production and characterization of nano-meter sized objects which is extended to broad area in medical, chemical and engineering applications due to its unique properties [52]. Nanoparticles (NPs) are basically defined as small objects have the size approximately of 1-100 nm to create and use structures that have novel properties [53]. They can also be designed to improve the pharmacological and therapeutic effects of the drugs, as well as have a very big surface area and they permit many functional groups to be adhered to them which in turn, can bind to tumor cells. Additionally, they have proven to be an excellent replacement for radiation and chemotherapy as they can easily be used to remove the tumor [54]. On the other hand, biomolecules derived NPs are getting famous because of the growing demand of biocompatible and biodegradable NPs. Moreover, biological NPs are easily available and non-immunogenic. Apart from their own unique functions, biomolecules can conjugate with other inorganic NPs to generate special biomolecule-NPs hybrids. Biomolecules such as proteins, nucleic acids, lipids and polysaccharides-based NPs have been used in various applications [55], [56].

Recent studies have developed a number of nanoparticles such as metals oxides, semiconductors and polymeric particles utilized in molecular imaging and particulate delivery vehicles [57], [58]. Liposomes, silica nanoparticles, micelles and cytosans play an important role in drug delivery with minimized side effects. They have also been utilized as anticancer agents. So, basically, nanotechnology deals with construction of artificial cells, enzymes and genes or repair in the synthesis of protein [59]. Furthermore, these particles possess highly favorable optical and chemical properties for biomedical

imaging and therapeutic applications, a high density of therapeutic agents can often be encapsulated, dispersed or dissolved in these nanoparticles, which in turn depends on the preparation process to yield different properties and release characteristics of the entrapped agent [60]. Finally, nanoparticles are good candidates to be shown as adjuvant for vaccines and advantageous features of nanoparticles include increased interaction of drug molecules with epithelial cells can be achieved leading to maximal absorption of the drug molecule [61].

1-3-1 Classification of Nanoparticles

In the field of NPs synthesis and fabrication techniques in the past two decades have ripened the classification of nanosized particles. Any particle is classified as nanoparticle when at least one of the dimensions of particles are in the order of nanometers. Generally, NPs are broadly classified into four different categories based on their dimensionality, regardless of their location or chemical properties [62].

- **Zero-Dimensional (0D) NPs:** All three dimensions of the NPs are in the nanoscale; i.e., up to 100 nm. quantum dots (carbon, graphene, inorganic) and other spherical NPs (noble metals, fullerenes, polymers, metal organic framework are some popular examples of 0D NPs class [63]. Due to their chemical inertness, biocompatibility, optical stability, cell permeability, and wavelength-dependent photoluminescence, they are interesting for biomedical and optical electronic applications [63].
- **One-Dimensional (1D) NPs:** (One dimension between 1 and 100 nm). In this class, nanotubes, nanorods, nanowires, and nanofibers are made of polymer, carbon, metals, and metal oxides [64]. Due to their important surface-to-volume ratio and small pores, they are used for filtration and catalysis and as scaffolds and super-absorbents for wound dressing and tissue engineering [65].

- Two-dimensional (2D) NPs: (Two dimensions > 100 nm) include metal oxides, platelet-like forms, graphene (graphene oxide and re-reduced graphene oxide), silicates, black phosphorus, hexagonal boron nitride, boron nanosheets, etc. [66]. Their physicochemical, biological, and optical properties explain their uniform shape, surface charge, and high surface-to-volume ratio [67].
- Three-dimensional (3D) NPs: (No dimension in the nanoscale range) include nanopores powders, nanowire bundles, nanotube bundles, nanolayers, and nanostructured electrodes. Much research has been done on the development, fabrication, and evaluation of 3D NPs for storage devices (super capacitors and batteries) for wastewater treatment and electrochemical conversion [68]. These complex NPs are important components of biomedical devices, solar cells, and microelectromechanical systems [69].

1-3-2 Synthesis Approaches of Nanoparticles

There are many developments in science and engineering that have progressed very fast toward the synthesis of nanoparticles to achieve unique properties that are not the same as the properties of bulk materials. The synthesized particle reveals interesting properties at the dimension below 100 nm with stable form, mostly from several effects, temperature, pH, pressure, time, cost of preparation and pore size [70]. These effects are the quantization of electronic states apparent leading to very sensitive size-dependent effects such as optical and magnetic properties and the high surface-to-volume ratio modifies the thermal, mechanical, and chemical properties of nanoparticles [71].

There are three general approaches for the synthesis of nanoparticles in the function of the starting raw materials: top-down, bottom-up, and hybrid approaches [72].

- Top-Down Approach : In this approach, nanoparticles are produced by breaking down the bulk material into nanomaterials (Figure 1-3), as it bases on converting large pieces of metal by grinding and crushing into nanoparticles, and the addition of specific material led to stability of nanoparticles [73].

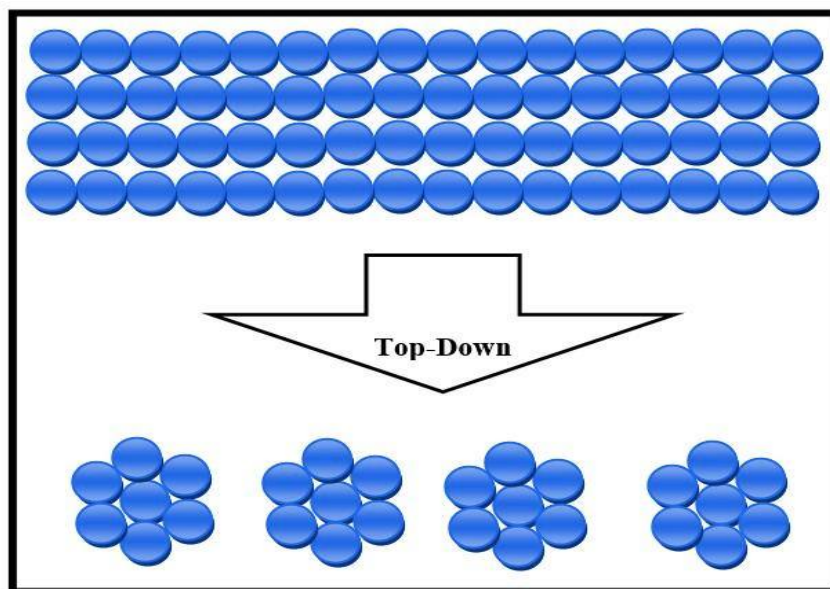


Figure 1-3: Top-down synthesis method of nanoparticles [74].

- Bottom-Up Approach : In this approach, a very small size material is converted into a larger size material (Figure 1-4), as it depends on the atom-to-atom or molecule-to-molecule assembly process [75].

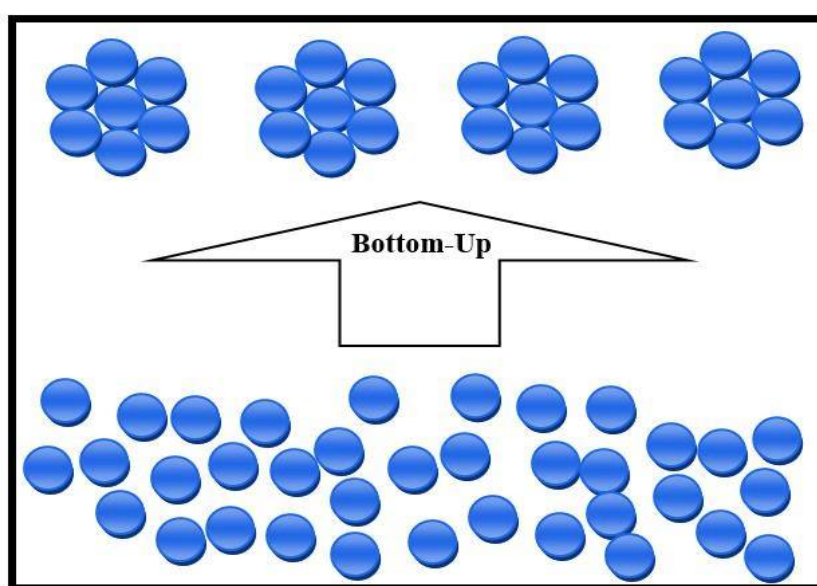


Figure 1-4: Bottom-up synthesis method of nanoparticles [74].

- Hybrid Approaches: In the hybrid approach, top-down and bottom-up fabrication techniques are combined to develop nanostructured platforms. These hierarchically organized structures are generally difficult or impossible to fabricate using only top-down or bottom-up techniques [76].

1-3-3 Synthesis Methods of Nanoparticles

Nanoparticles are synthesized by variety methods, which include physical, chemical and biological methods, and these methods can be broadly classified into bottom-up and top-down approaches (Figure 1-5). Depending upon the requirements, the synthesis methods of nanoparticles are selected. Every method has some advantages as well as disadvantages; the production method is selected based upon the availability of the facilities. Physical methods are suitable for small-scale production whereas chemical methods are selected where the cost of production is a concern. Biological synthesis methods have different significance compared to physical and chemical methods as they are non-toxic, gives rapid synthesis, low in waste production and also give large-scale production [77].

1-3-3-1 Physical Synthesis Methods:

Physical methods include arc plasma, thermal evaporation, physical vapor deposition, ultrasonic irradiation, and laser ablation. These processes are chemically pure and technically simple, which makes them ideal for carrying out industrial processes at high production rates [78]. For example, arc plasma which is based on electrical arc discharge synthesis, is one of the most commonly used physical methods for converting bulk materials into nanomaterial via condensation and evaporation [79]. On the other hand, metal oxide (e.g., ZnO) nanoparticles can be synthesized using the thermal evaporation method [80].

1-3-3-2 Chemical Synthesis Methods:

Hydrothermal sol-gel, chemical vapor deposition, solvothermal processes, polymerization, and other chemical precipitation techniques are examples of chemical techniques for the synthesis of NPs [81]. Wet chemical synthesis, which is based on the physical states of the solid and liquid phases, is the most commonly used method for producing NPs [82]. During industrial-scale wet chemical synthesis, capping agents/stabilizers are used extensively in spite of their toxicity to control particle size and to prevent the agglomeration. The parameters of the hydrothermal and solvothermal techniques used for the synthesis affect the structure, morphology, composition, and assembly of the resulting ZnO-NPs. Using the hydrothermal technique for the synthesis of ZnO-NPs [83], and described the solvothermal technique for the synthesis of gallium-indium-ZnO-NPs for electrolyte-gated transistors [84].

1-3-3-3 Biological Synthesis Methods:

Biological methods are promising alternatives to physical and chemical synthesis methods because they are eco-friendly [85]. Biological synthesis methods include microorganism-assisted, biotemplate-assisted, and plant extract-assisted biogenesis are green synthesis approaches for nanoparticle synthesis [86]. Many plant biomolecules, including enzymes, vitamins, polysaccharides, organic acids, amino acids, and proteins, are used for nanoparticle synthesis in a medium enriched with metal ions. The first step involves the preparation of leaf tinctures and the use of biomolecules from plant extracts and various microorganisms, including fungi, bacteria, and lactobacilli. Many active compounds are present in plant extracts, for instance, alkaloids, phenols, terpenoids, quinines, amides, flavonoids, proteins, and alcohols [87]. Some of them contribute to the green

synthesis of metallic nanoparticles by reducing metal cations to nanoparticles (i.e., reducing agents, such as flavonoids and polyphenols) and by concomitantly performing stabilization functions to avoid nanoparticle aggregation. Several previous studies based on biological methods to the synthesis of metal oxide nanoparticles among them, ZnO-NPs [88], [89].

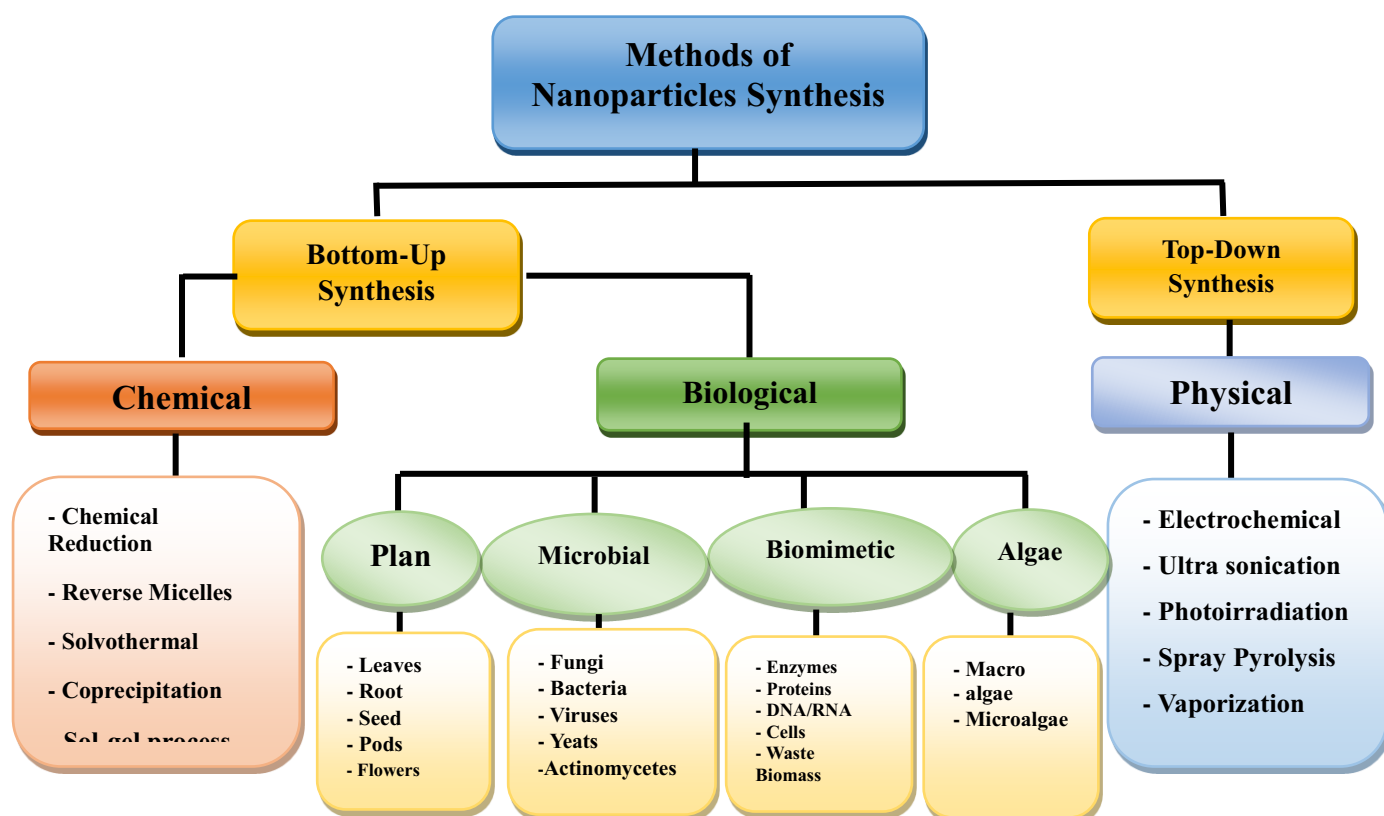


Figure 1-5: Scheme the synthesis methods of nanoparticles [90].

1-3-4 Synthesis of Nanoparticles from Plants

Green synthesis of NPs using the natural plant extracts was important to explore the role of biological components, essential phytochemicals (e.g., flavonoids, alkaloids, terpenoids, amides, and aldehydes) as reducing agents and solvent systems [91]. Extraction is a solid-liquid separation process for isolating specific plant components in which the plant components (i.e., the solid object) are dissolved and entrapped in the solvent (i.e., the liquid). The plant extract concentration, pH, temperature, and the time of incubation are known

to affect the size, shape, and yield of the NPs. Compared with the other previously described methods, the use of plant extracts for NPs synthesis is particularly interesting because it is less expensive, more environmentally friendly, can be scaled up for industrial applications, and can be performed without high pressure, energy, temperature, or toxic chemicals [92]. Indeed, for NPs synthesis, plant extracts are simply mixed with a metal salt solution at ambient temperature for a few minutes. Any plant part can be used to synthesize NPs, such as leaves, stems, stalks, and flowers (Figure 1-6). Some of the examples of synthesis of ZnO-NPs using plant extract include the use of *Lepidium sativum* seed [93], *Cassia auriculata* leaf [94], *Amomum longiligulare* Fruits [95], *Phoenix dactylifera* root [96], etc. Leaf extracts are environmentally friendly, non-hazardous, and non-toxic reducing agents. Researchers should now focus on whether plant biomass or extracts can be used to fabricate noble metal (silver, gold, platinum, and palladium) NPs with a specific shape and size. Indeed, due to the great plant diversity, it is not known whether they could be useful for the production of such NPs [97].

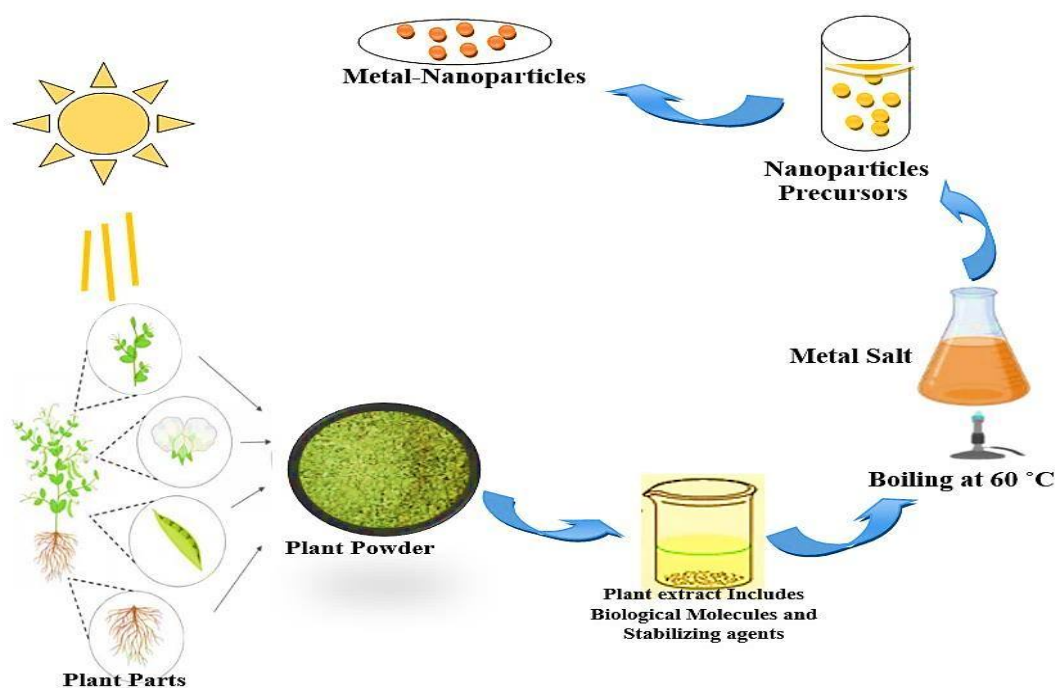


Figure 1-6: Biosynthesis of metal-nanoparticles from plant extracts [98].

1-3-5 Characterization of Nanoparticles

The characterization is necessary to identify the properties of the synthesized NPs. The experimental methods that are used to quantify the dimensions, crystal orientation, elemental composition, and other physical and chemical properties of synthesized NPs are termed as characterization techniques [99]. Various *in vitro* and *in vivo* techniques are used to characterize a new system and predict its clinical efficacy. These techniques enable efficient comparison across NPs and facilitate a product optimization process [100]. Nowadays, many more types of NPs are synthesized than only a decade ago, and in larger amounts than before, requiring the development of more precise and credible protocols for their characterization. However, such characterization is sometimes incomplete. This is because of the inherent difficulties of NPs to be properly analyzed, compared to the bulk particles (e.g., too small size and low quantity in some cases following laboratory-scale production) [101]. In fact, quite often a wider characterization of NPs is necessary, requiring a comprehensive approach, by combining techniques in a complementary way. Different techniques may be used to identify NPs, in order to know if in some cases the use of only one or two of them is enough to provide reliable information when studying a specific parameter (e.g., particle size). Moreover, these techniques are sometimes exclusive for the study of a particular property, while in other cases they are combined [102]. So, to discuss all these techniques in a comparative way, considering factors such as their availability, cost, selectivity, precision, non-destructive nature, simplicity and affinity to certain compositions or materials. The techniques are always studied in depth according to their availability. There are techniques provide further information on the structure, elemental composition, optical properties, functional groups and other common and more specific physical properties of the nanoparticle samples (Figure 1-7). Examples of these techniques include Uv-vis.

spectroscopy, Fourier Transform Infrared (FT-IR) and x-ray Diffraction (XRD). Other techniques which provide information on the size, morphology and crystal structure of the NPs are microscopy-based techniques for example, scanning electron microscopy (SEM), transmission electron microscopy (TEM) and atomic force microscopy (AFM) [103].

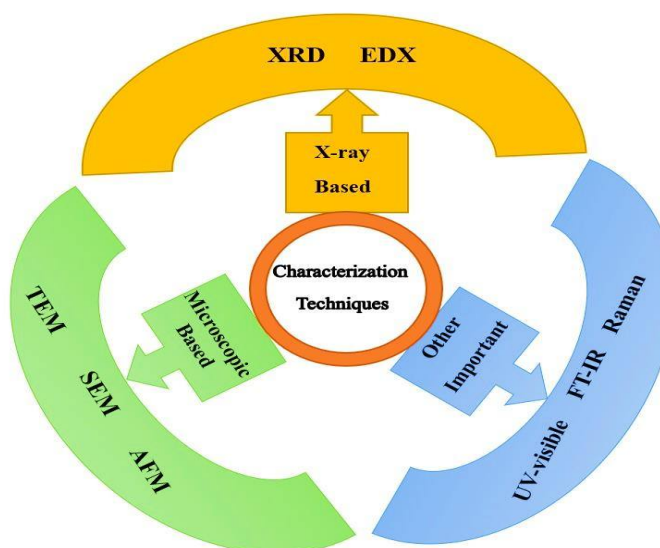


Figure 1-7: Techniques used in nanoparticles characterization [104].

1-4 Zinc Oxide Nanoparticle (ZnO-NPs)

Zinc oxide is an inorganic compound with the formula ZnO as a white powder, and is a metal oxide semiconductor. ZnO-NPs, as one of the most important metal oxide nanoparticles have been extensively studied and popularly employed in various fields due to their peculiar physical and chemical properties [105]. ZnO-NPs are nontoxic, insoluble in water with density of 5.606 g.cm^{-3} and appear as a white powder with refractive index of 2.0041. It also possesses a high boiling and melting points which are $2360 \text{ }^\circ\text{C}$ and $1975 \text{ }^\circ\text{C}$ respectively [106]. ZnO-NPs as three main crystal structures under ambient condition (pressure and temperature), hexagonal wurtzite, cubic zinc blende and cubic rock salt (Figure 1-8), The hexagonal wurtzite structure is the most thermodynamically stable and hence most common among the

three structures [107]. The hexagonal wurtzite structure, where oxygen atoms (blue spheres) are tetrahedrally coordinated to zinc atoms (yellow spheres). The wurtzite structure as a hexagonal unit cell as shown in figure 1-8a.

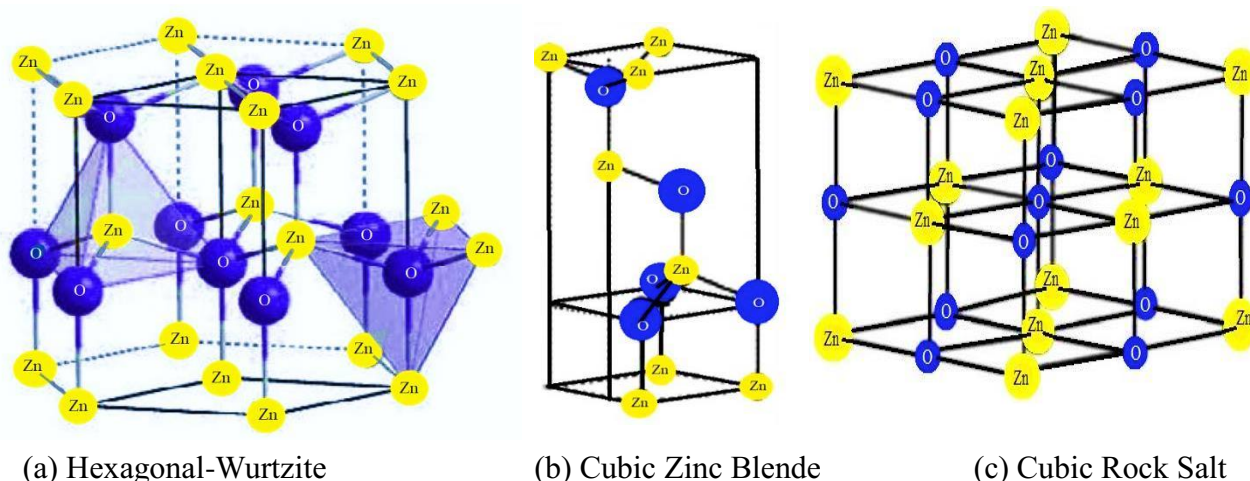


Figure 1-8: Main crystal structures of ZnO-NPs [108].

In Hexagonal-Wurtzite, two interpenetrating hexagonal-close-pack (hcp) sublattices are alternatively stacked along the c-axis. One sublattice consists of four Zn atoms and the other sublattice consists of four oxygen atoms in one unit cell; every atom of one kind is surrounded by four atoms of the other kind and forms a tetrahedral structure [109].

1-4-1 Biosynthesis of Zinc Oxide Nanoparticles

Physical and chemical methods for ZnO-NPs preparations have been widely developed. ZnO-NPs can be synthesized using aqueous or alcoholic plant extracts, microorganisms (bacteria, fungi, aquatic algae, and yeasts) and other biosynthesis methods [110]. A broad variety of plant extracts are used for the biosynthesis of ZnO-NPs [111-113]. ZnO-NPs prepared by biosynthesis methods exhibited strong potential for biomedical applications such as its excellent anticancer and antibacterial activity. In general, for the ZnO-NPs synthesis, the desired quantity of zinc oxide, zinc nitrate, zinc acetate, or zinc sulfate is used

and dissolved in distilled water. To the zinc solution, a defined volume of plant extract is added and mixed well in a magnetic stirrer. Plants consist of phytoconstituents like flavonoids, amino acids, terpenoids, alkaloids, polyphenols, and polysaccharides which can act as reducing agents as well as capping or stabilizing agents. Also, these phytoconstituents reduce metal ions or metal oxides into zero valence metal nanoparticles. Hence, no capping or stabilizing agents are needed in this green approach to nanoparticle synthesis [114].

1-4-2 Optimization of ZnO-NPs Synthesis

Different factors like temperature, pH, time, and both concentrations of metal ion and plant extract have important roles in obtaining desired size, shape, and stability, and enhancing the product yield of the nanoparticle [115]. Temperature plays a very crucial role in all reactions. It has recently been found that temperature also plays a role in determining the size, shape, and yield of nanoparticles synthesized using plant extracts. Both the reaction and particle

however, the average particle size decreases, and the particle conversion rate steadily rises as the temperature rises [116]. The best results for ZnO-NPs synthesis are obtained by varying the pH of the reaction medium within the desired range [117]. The synthesis of nanoparticles is greatly dependent on the concentrations of substrate (metal salt) and biomass (plant extract) [118]. As example, when plant extract and zinc salt are combined, the color changes from yellow to brown, indicating the first appearance of ZnO-NPs. Zinc salt has a significant impact on the size and structure of ZnO-NPs. As the concentration of salt increases, the surface plasmon bands shift to a higher frequency, indicating aggregation [119]. The incubation time of the reaction determines the efficiency of ZnO-NPs [120]. Formation of

ZnO-NPs is confirmed with UV spectroscopy based on its surface plasmon resonance (SPR) effect. Different morphologies of ZnO-NPs are nanoflower, nanoflake, nanorods, nanowires, and nanobelt [121].

1-4-3 Biological Applications of Zinc Oxide Nanoparticles

The biological activity of ZnO-NPs depends on many factors, surface chemistry, size distribution, particle morphology, and particle reactivity in solution. Therefore, the development of ZnO-NPs with controlled structures that are uniform in size, morphology, and functionality is essential for various biomedical applications [122]. Moreover, ZnO-NPs are soluble in biological fluids and subsequently release zinc ions. On oral administration first pass effect, gastrointestinal barrier, kidney, liver, and gut wall function decreases the bioavailability of ZnO-NPs; whereas on intravenous administration shows 100% bioavailability. Different factors like pH, particle size, concentration, and the presence or absence of organic compounds influence the solubility of ZnO-NPs [123]. Dissolution, absorption, and distribution of ZnO-NPs depend upon the exposure dose amount and do not depend upon the particle size of the nanoparticle. On oral administration, ZnO-NPs are distributed in the kidney, liver, and spleen whereas on intraperitoneal administration, zinc oxide nanoparticles are distributed in the lungs, kidney, spleen, heart, and liver. Kidneys and the liver are the common target organ in both administrations [124]. Distribution of ZnO-NPs in the organs depends upon the type of experimental animals, route of exposure, and physicochemical properties of the nanoparticles [125].

1-4-4 Antioxidant Activity of Zinc Oxide Nanoparticles

Zinc oxide nanoparticles exhibit antioxidant properties because of the electron density transfer at oxygen and the property rely on the structural configuration of the oxygen atoms [126]. The naturally

obtained substance shows the significant protective activity of natural antioxidants from higher plants against several diseases which originated from oxidative processes [127]. In the biological system, over production of highly reactive radical species or their precursor leads to oxidative stress which has been observed in various diseases such as cancer, cardiovascular disease, renal diseases, diabetes and arthritis. In few studies antioxidant and free radical scavenging activities of ZnO-NPs in biological system has been described. Many studies have shown that ZnO-NPs plays a significant role against various toxic effects, including cytotoxicity, genotoxicity, inflammation, and oxidative stress, also known to have anti-inflammatory properties by blocking pro-inflammatory cytokines, proved that ZnO-NPs synthesized from the plant extract have antioxidant and anti-inflammatory properties and they are used in several disease prevention and therapies [128], [129].

1-5 Kidney and Liver Toxicity

The kidney filters all harmful substances and metabolites are eliminated through the urine. Endogenous and exogenous chemicals are secreted mostly by the kidneys [130]. Because it filters a huge number of toxins that can accumulate in the renal tubules when a vast volume of blood flows through it, the kidney is extremely vulnerable to toxicants. This can then lead to systemic toxicity, which can impair bodily functions such as maintaining the fluid and electrolyte balance, decreasing the production of essential hormones, and impairing the body's ability to remove wastes [131]. The liver is one of the largest organs in the human body and the primary focus of metabolic and excretory activity. It is responsible for the detoxification and excretion of a wide range of endogenous and exogenous substances and any damage to it or impairment of its functioning can have serious consequences for one's health [132].

The main factors causing renal-hepatic toxicity are toxic materials, exposure to hazardous or toxic materials can affect the body in many ways. In general, when chemicals and other hazardous substances are absorbed, they pass through the various body systems and can affect a particular organ or organs, called the “target organ” Fortunately, the body has mechanisms, mainly in the liver and kidneys, to process and eliminate many of these substances. This ability to eliminate toxic substances can reduce the effect on the target organ [133], [134]. Damage to the kidney and liver can be acute or chronic. An acute process generally refers to a relatively short period of time (hours to weeks) between exposure to the toxin and the onset of symptoms or medical findings. A chronic process generally refers to a long period of time (years) between exposure to the toxin and the onset of symptoms or medical findings. The detection of either an acute or chronic process or disease can be complex, depending on the type of toxin and the extent of exposure [135], [136].

1-6 Role of Zinc Oxide Nanoparticles in Ameliorating Renal-Hepatic Toxicity

Zinc oxide nanoparticles are among the most widely used metal oxide-NPs in a variety of sectors and research-based organizations due to their wide range of applications [137]. They can be used for a variety of medical applications because they are less toxic, inexpensive, safe, and simple to prepare, as well as may be easily absorbed in the human body [138]. In the previous study, the ameliorative potential of green tea-mediated ZnO-NPs was shown against ochratoxin-A-induced hepatotoxicity and nephrotoxicity in albino rats. Zinc oxide nanoparticles were found to reverse the damage caused by ochratoxin A and were also involved in reducing alanine aminotransferase (ALT), aspartate aminotransferase (AST), urea, and creatinine levels, in addition to the biochemical analysis showed improvement in kidney

tissues, with slight congestion in a few areas [139]. Another study showed the protective effects of ZnO-NPs (50 mg/kg) against Dimethyl nitrosamine (DMN) induced liver injury in rats, ZnO-NPs were reduced lipid peroxidation, oxidative stress, and fibrosis of the liver, which indicates a reduction in the levels of proinflammatory cytokines. An increase in the levels of reduced glutathione (GSH) and glutathione peroxidase (GPx) was also observed, thereby improving liver and kidney function [140]. Similarly, ZnO-NPs reduced potassium bromate P-induced hepatotoxicity in Swiss albino rats. The overall health of the treated animals was improved profoundly by maintaining the levels of glutathione reductase (GR), glutathione peroxidase (GPx), superoxide dismutase (SOD), and catalase (CAT) and decreasing the levels of malondialdehyde (MDA), hydrogen peroxide (H₂O₂), and nitric oxide (NO) [141]. Thioacetamide (TAA) is a powerful hepatotoxic and hepato-carcinogenic chemical that causes hepatotoxicity by producing thioacetamide-S-dioxide, an unstable reactive metabolite that stimulates the production of reactive oxygen species (ROS) by binding covalently to macromolecules [142]. As ZnO-NPs possess various therapeutic properties, they were employed against TAA-induced hepatotoxicity to evaluate their protective effects. ZnO-NPs significantly lowered oxidative stress and reduced the expression of inflammatory markers (interleukin-6 (IL-6) and Tumor Necrosis Factor-alpha (TNF- α) proteins) and liver enzymes and also helped in returning the antioxidant status to its normal level [143]. Likewise, *Eclipta prostrata*-derived ZnO-NPs showed a dose-dependent cytotoxic effect against the hepatoma G2 (HepG2) cell line. DNA fragmentation assays and activation of caspase 3 validated the apoptotic features of ZnO-NPs at a concentration of 100 mg/mL [144]. Moreover, cisplatin (CP), a chemotherapy drug used to treat a variety of malignancies, can cause platinum to build up in the kidney,

impairing its function. CP-induced nephropathy raised serum creatinine, blood urea nitrogen, and microalbuminuria, all of which are indicators of renal function. These characteristics, on the other hand, were downregulated after ZnO-NPs treatment. ZnO-NPs prevented CP-induced decreases in renal SOD, CAT, and GSH, and an increase in renal MDA levels [145]. Similarly, streptozotocin (STZ) therapy led to diabetic nephropathy in male rats, which was demonstrated by an increase in the blood glucose level, renal oxidative stress markers, and glomerular basement membrane thickness. Administration of ZnO-NPs intraperitoneally for seven weeks significantly improved nephropathy and enhanced renal function [146]. Finally, ZnO-NPs are a great option for treating hepato-renal impairments because of their anti-inflammatory, antioxidant, and pro-oxidant mechanisms. As the impact of ZnO-NPs can vary depending on the disease condition, its cellular response, however, can be crucial. More research is still required to determine the precise molecular mechanism by which ZnO-NPs act to ameliorate adverse reactions to the organs upon administration of hazardous substances [147].

1-7 Adenine

Adenine (6-Aminopurine), is a nitrogen heterocycles (Figure 1-9) and one of the four nucleobases in the nucleic acids of deoxyribonucleic acid (DNA) and ribonucleic acid (RNA). Adenine also plays an important role in biochemistry involved in cellular respiration, the form of both adenosine triphosphate (ATP) and the cofactors nicotinamide adenine dinucleotide (NAD) and flavin adenine dinucleotide (FAD), and protein synthesis [148]. Adenine is derived from the nucleotide inosine monophosphate (IMP) that finally metabolites to uric acid. It is produced on a pre-existing ribose phosphate via a specific pathway by using substrates from amino acids (glycine, glutamine, and aspartic acid), and fusion with the enzyme

tetrahydrofolate [149]. It presents at very low level in the blood and excess adenine is transformed to 2,8-dihydroxyadenine when oxidized by xanthine dehydrogenase in the kidney. Adenine produces adenosine, a nucleoside, by linking with ribose, and then forms ATP, a nucleotide, by adding three phosphate groups to adenosine. Adenosine triphosphate is used in cell metabolism as one of the most important methods of transferring chemical energy between chemical reactions, and maintaining energy balance [150]. In addition, the level of adenosine and the expression of adenosine receptors are regulated so that the signaling via one or more of the receptors increases in cellular stress and distress. Adenosine via its receptors will tend to limit the consequences of the potentially damaging stimuli. This is achieved in multiple ways. There is a strong link between adenosine and signaling in hypoxia [151]. Thus, the increased adenosine in the kidney indicated renal lesions due to ischemia or hypoxia, and decreased levels of adenosine in the kidney may result from increased cell apoptosis, functional destruction, and ATP depletion [152].

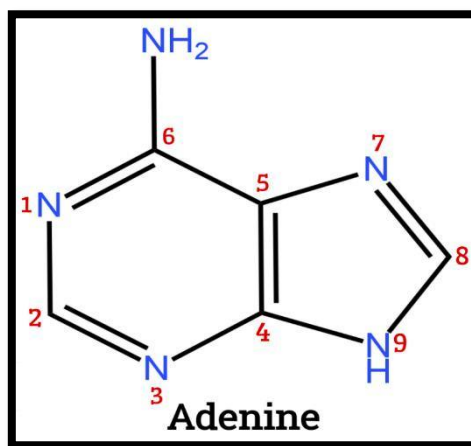


Figure 1-9: The chemical structure of adenine [153].

1-8 Mechanism Action of Adenine

Several previous studies have shown that adenine-rich diet induced the model of renal failure in animal [154]–[156]. The

consumption of oral adenine thus might cause the occlusion of renal tubules which retards the excretion of nitrogenous substances leading to a biochemical and physiological status resembling kidney diseases in humans [157]. When adenine presents in high levels at mammalian metabolism, it is endogenously produced as a by-product of the polyamine pathway and is cleared by adenine phosphoribosyl transferase (APRT) [158], [159]. APRT deficiency causes 2,8-dihydroxyadenine (2,8-DHA) accumulation, leading to nephrolithiasis and crystalline nephropathy (Figure 1-10). In the absence of APRT activity, adenine cannot be converted to adenosine. Adenine is metabolized through an alternative pathway where it is oxidized by xanthine dehydrogenase (XDH) to 2,8-DHA via the generation of an intermediate compound, 8-hydroxyadenine. Because 2,8-DHA is insoluble at any physiological urine pH, it forms 2,8-DHA crystals eventually leading to 2,8-DHA nephrolithiasis and/or crystalline nephropathy [160]. Adenine and 2,8-DHA are released in the urine and low solubility of 2,8-dihydroxyadenine led to its precipitation in the kidney tubules of the nephron [161]. The low solubility of 2,8-DHA makes its precipitation in kidney especially in nephron tubules of kidney. Waste compounds excretion from kidney are stopped by obstruction of renal tubular due to 2,8-DHA. This, in turn, will lead to elevation of creatinine and urea nitrogen concentration in the blood and leading to elevation of various guanidine compounds, then resulted in renal failure [162].

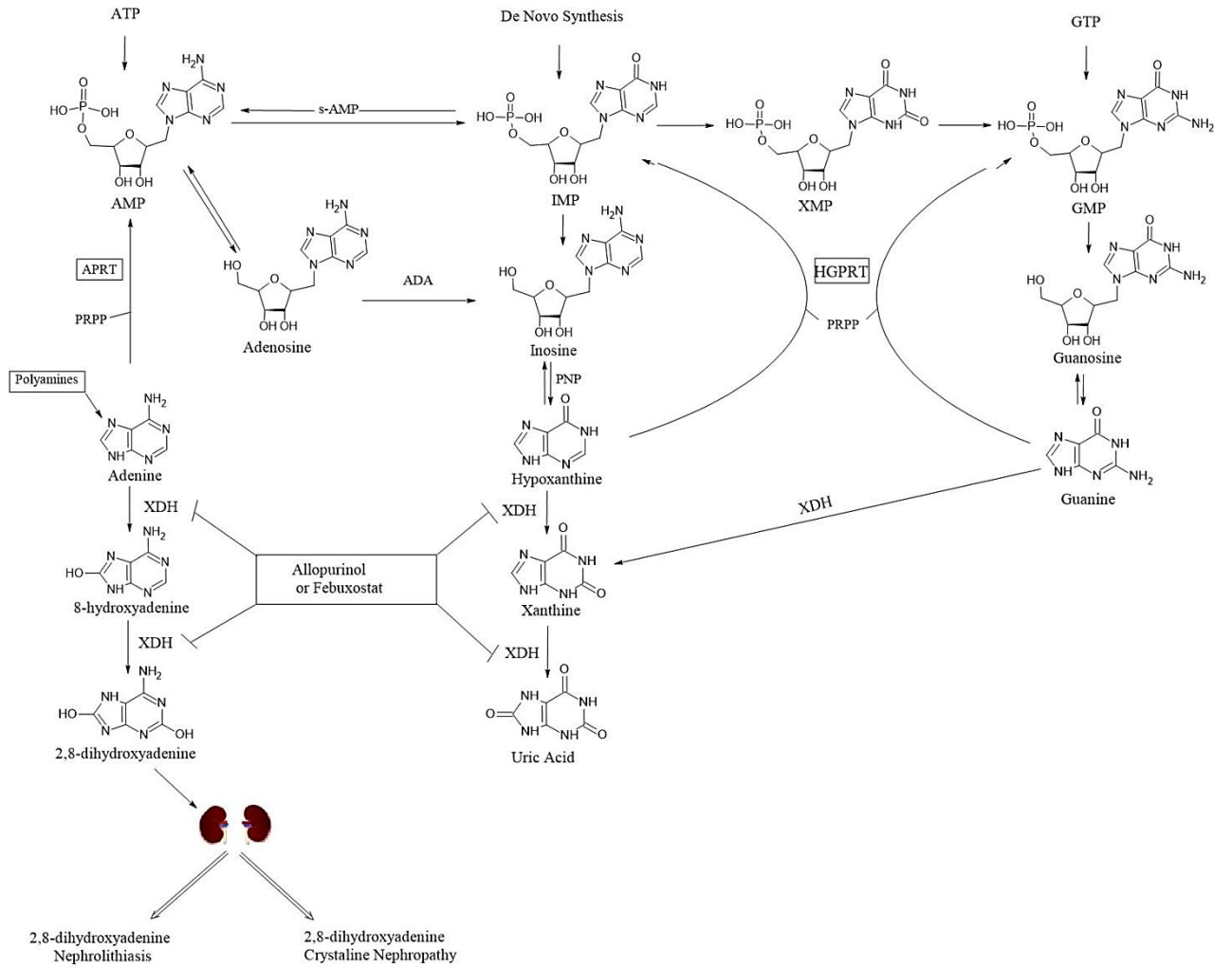


Figure 1-10: Scheme of metabolic pathways for the disposal of adenine in animals [163].

1-9 The objectives of the study

The current study was designed to possible biosynthesis of zinc oxide nanoparticles using an aqueous extract of *Z.-spina christi* leaves and zinc nitrate hexahydrate and evaluated the ameliorative effects in the treatment of kidney injury induced by adenine in male albino rats (*Sprague-Dawley* rats) through the following objectives:

- 1- Characterization and optimization of the biosynthesized ZnO-NPs using many techniques UV-visible, FT-IR, XRD, SEM, TEM and AFM.
- 2- Estimation of kidney function tests (uric acid, urea and creatinine) and liver function tests (ALT, AST and ALP) as well as antioxidant levels (TAC, CAT, SOD, GSH) and oxidative stress (MDA and NO).
- 3- Histological study which includes histological change in kidneys and livers tissues.

Chapter Two

Materials and Methods

2 Materials and Methods

• Instruments

Tools and instruments used with their origin and company are listed in Table 2-1.

Table 2-1: Instruments and tools with their suppliers.

No.	Type of Instruments and tools	Company/Source
1	Analytical sensitive balance	METTLER TOLEDO/Switzerland
2	Atomic force microscopy (AFM)	AFM NT-MDT/Russia
3	Balance for animals	India
4	Centrifuge	China
5	Cooling centrifuge	Sigma 2-16PK/Germany
6	Digital camera	Nikon Z50/Tailand
7	Gel tube	Jordan
8	Eppendorf tube	China
9	Whatman No. 1 filter paper	Labtex/Bangladesh
10	Freezer	Hitachi/Japan
11	Fourier Transform Infrared (FT-IR)	IRPrestige-21, SHIMADZU/Japan
12	Gel tubes	Jordan
13	Lab Glasses	China
14	Gloves	China
15	Hot plate with a magnetic stirrer	LAB INCO L-81/ Netherlands
16	Light microscope	Olympus BH-2/ Japan
17	Micropipette 100-1000 μ l	DragoLAB/China
18	Masks	China
19	Oven	D-91126 Schwabach FRG/ Germany
20	Oven	TAU STERIL-2000/Germany
21	Rack for blood standing	China
22	Scanning electron microscopy (SEM)	TESCAN MIRA3-SEM/France
23	Spectrophotometer	Thermo-Spectronic/USA
24	Sterile syringes (1, 3, and 5 ml)	China
25	Test tubes	China
26	Transmission electron microscopy (TEM)	JEOL JEM-1200 EX/Japan
27	Vacuum filtration	
28	Water bath	Gallen Kamp/ England
29	UV-vis spectrophotometer	UV-1650PC, SHIMADZU/Japan
30	X-ray diffraction (XRD)	XRD-600, SHIMADZU/Japan

- **Chemicals and Kits**

Chemicals and kits used in the current study are listed in Table 2-2.

Table 2-2: Chemicals and kits used with their origin and company.

No.	Type of Chemicals and Kits	Company/Source
1	Acetic Acid (CH ₃ COOH)	HiMedia
2	Adenine Powder	Solarbio /China
3	Anhydrous sodium carbonate (Na ₂ CO ₃)	BDH Chemical Ltd Pool/U. K.
4	Alkaline phosphatase colorimetric kit (ALP)	Solarbio /China
5	Alanine aminotransferase colorimetric kit (ALT)	Solarbio /China
6	Aspartate amino transferase colorimetric kit (AST)	Solarbio /China
7	Basic nitrate bismut	Basic nitrate bismut
8	Catalase Activity Assay Kit (CAT)	Solarbio /China
9	Chloroform (CHCl ₃)	Noorbok/England
10	Creatinine colorimetric kit	Solarbio /China
11	Cupric sulphate pentahydrate (CuSO ₄ .5H ₂ O)	Analar Trade Mark
12	Dimethyl sulfoxide (DMSO)	Xi'an Seererb/China
13	Eosin- methoxylin stain	Merck/Germany
14	Ethanol (96% v/v)	Fluka /Switzerland
15	Ferric chloride (FeCl ₃)	BDH Chemical Ltd Pool/U. K.
16	Formalin 10%	TEBIA/USA
17	Hydrochloric acid (HCl)	BDH Chemical Ltd Pool/U. K.
18	Litmus paper strips	Lo and/China
19	Malondialdehyde content assay kit (MDA)	Solarbio /China
20	Nitric acid (HNO ₃)	BDH Chemical Ltd Pool/U. K.
21	Nitric oxide assay kit (NO)	Solarbio /China
22	Paraffin wax	Merck/Germany
23	Potassium hydroxide (KOH)	Analar Trade Mark
24	Potassium Iodide (KI)	Analar Trade Mark
25	Reduced Glutathione content assay kit (GSH)	Solarbio /China
26	Sodium hydroxide (NaOH)	BDH Chemical Ltd Pool/U. K.
27	Sulfuric acid (H ₂ SO ₄)	Belgium
28	Superoxide Dismutase activity assay kit (SOD)	Solarbio /China
29	Total antioxidant capacity assay kit (TAC)	Solarbio /China
30	Urea colorimetric kit	Solarbio /China
31	Uric acid colorimetric kit	Solarbio /China
32	Zinc nitrate hexahydrate (Zn(NO ₃) ₂ .6H ₂ O, 99.9%)	CDH/India

- Methods

2-1 Experimental Design of the study

The general steps for the biosynthesis of zinc oxide nanoparticles and their applications are shown in Figure 2-1.

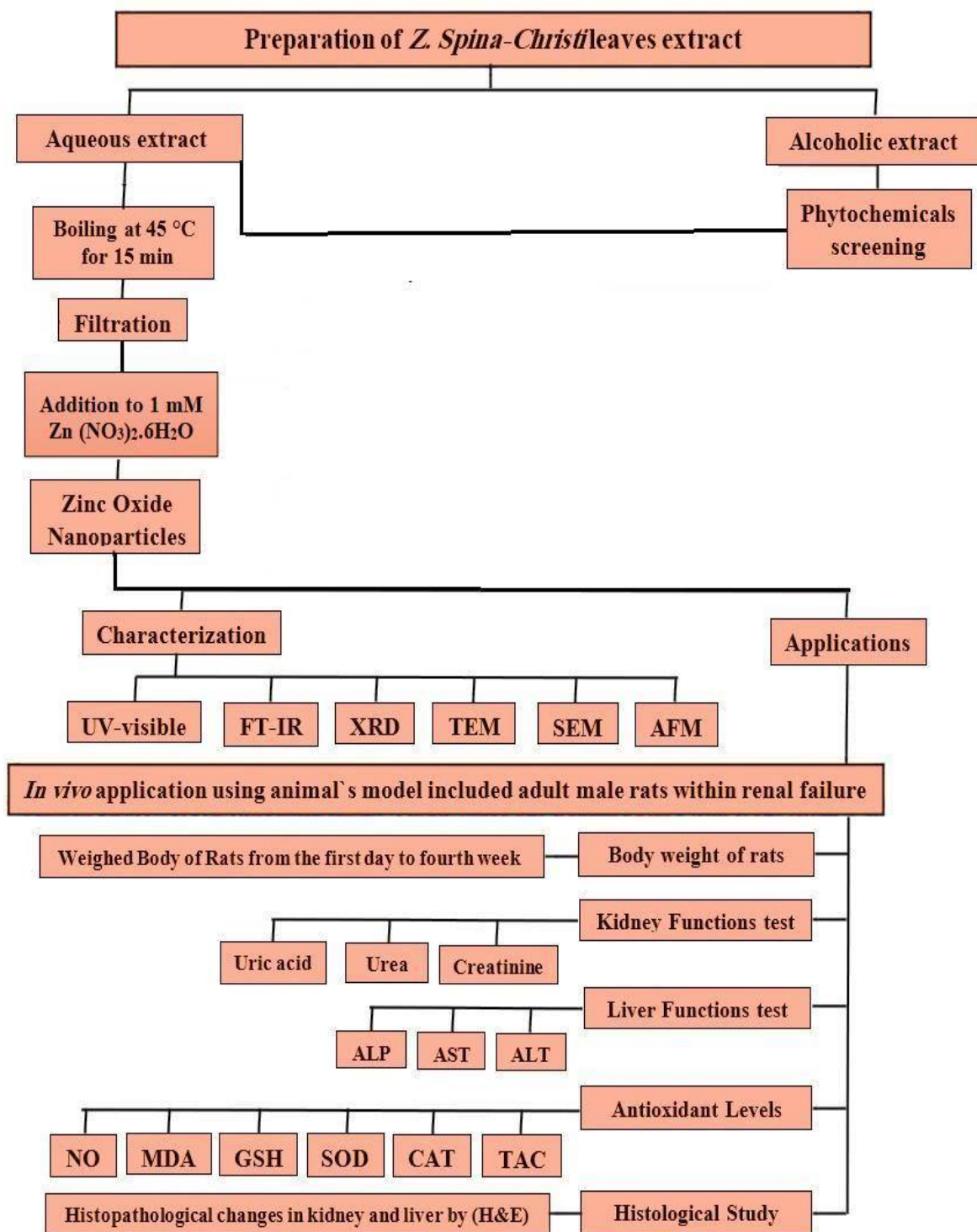


Figure 2-1: Schematic diagram for the experimental design of the study.

2-2 Collection of Plants

Fresh *Ziziphus-spina christi* leaves were collected from the University of Kufa-College of Medicine campus. The fresh leaves were thoroughly washed under tap water to remove the adhered and then rinsed with distilled and de-ionized water to remove dust and other particles. The washed plant part was dried by exposing it to the sun through a window to protect it from direct sunlight. Then the dried leaves were sliced into small pieces and crushed using a mortar and pestle.

2-3 Preparation of Plant Extract

• Preparation of Aqueous Extract for *Ziziphus-spina christi* Leaves

Ten grams of crushed leaves were dissolved in 100 mL de-ionized water in conical flasks and heated at 45 °C for 15 minutes using heating stirrer, and then cooled to room temperature. The mixture was filtered through vacuum filtration with Whatman No. 1 filter paper followed by muslin cloth and centrifuged at 3000 rpm for 15 minutes to remove any unnecessary particles that might have entered into the extract. To investigate the functional groups in *Z.-spina christi* leaves, the crude extract was dried in an air oven for 3 hours at 60 °C to obtain a powder for FT-IR analysis, while to investigate the phytochemicals are presented in *Z.-spina christi* leaves or to the biosynthesis of ZnO-NPs, freshly of *Z.-spina christi* leaves extract were prepared.

• Preparation of Alcohol Extract for *Ziziphus-spina christi* Leaves

For alcoholic (ethanolic) extraction, 10 gm from the leaf pieces were transferred into the conical flask and 100 mL of ethanol (95% V/V) was added. The mixture was adjusted at room temperature and kept for 10 hours. The extract was subjected to vacuum filtration with the Whatman filter paper No. 1. The extraction was then used without any further purification for investigations the phytochemical screening only.

2-4 Phytochemicals screening in the plant extract

The phytochemical analysis of an extract of *Z.-spina christi* leaves showed the presence or absence of many phytochemical components such as (flavonoids, alkaloids, terpenoids, phenolic compounds, steroids, saponins, tannins, proteins, amino acids, quinines, cardiac glycosides, and carbohydrates) were prominently presented in the plant. The both crude aqueous and alcoholic extracts of *Z.-spina christi* leaves was submitted to phytochemical analysis.

- **Detection of Proteins and Amino acid**[164]

1- Xanthoproteic test: An aqueous extract was treated with a few drops of concentrated nitric acid. The formation of the yellow color indicates the presence of proteins.

2- Biuret test: A 2 mL aqueous extracts and an equal volume of NaOH were dissolved. A few drops of 2% Copper sulphate were added. The pink or violet color indicates the presence of amino acids and proteins.

- **Detection of Alkaloids**[165]

Dragendorff's test: The spot of alcoholic extract and spraying over it of Dragendorff's reagent will give orange color indicating the alkaloids present. To Prepare of spraying reagent of Dragendorff's for alkaloids tests, was made of two portions:

Reagent (1) A 0.85 g of bismut substrate was dissolved in a solution of 10 ml acetic acid (CH_3COOH) and 40 mL water.

Reagent (2) A 8 g of potassium iodide (KI) was dissolved in 20 ml of water, a stock solution mixture of equal parts of solution 1 and 2. The spray reagent was prepared by mixing 1mL of the stock solution with 2 mL of fresh acetic acid and 10 ml of water. Detection of alkaloids and other nitrogen compounds is by orange-brown spots on white background.

- **Detection of Flavonoids**[166]

A 1 mL aqueous extract treated with 1 ml 50% NaOH and 1 mL of 50% ethyl alcohol was added. A dirty yellowish-brown precipitate indicates the presence of flavonoids.

- **Detection of Saponins**[167]

Foam Test: A 0.2 gm of the aqueous extract was vigorously shaken with 5 mL of distilled water in a test tube for a few minutes. The formation of foaming (appearance of creamy mass of small bubbles) shows the presence of saponins.

- **Detection of Phenolic Compounds**[165]

Ferric chloride test: A 1 mL aqueous extract was treated with few drops of 2% Ferric chloride. Changing the color to brownish indicates the presence of phenolic compounds.

- **Detection of Carbohydrates**[168]

Benedict's test: one mL of aqueous extract and 4 mL of benedict's reagent were dissolved and then heated in a boiling water bath for a few minutes orange red color precipitate indicates the presence of carbohydrates.

Preparation of Benedict's reagent: One liter of Benedict's reagent can be prepared by dissolving 100 gm of anhydrous sodium carbonate (Na_2CO_3) and 173 gm of sodium citrate in 800 mL of distilled water. The mixture was boiled and filtrated. A 17.3 gm of cupric sulphate pentahydrate ($\text{CuSO}_4 \cdot 5\text{H}_2\text{O}$) is mixed in 100 mL of distilled water, then added to the filtrate, and then the volume was completed to one liter by distilled water with constant stirring.

- **Detection of Terpenoids and Steroids**[169]

Salkowski test: Two mL of the alcoholic extract was dissolved in 2 mL of chloroform and evaporated to dryness. Then 2 mL of concentrated sulfuric acid (H_2SO_4) were added slowly and the mixture was heated by put in the water bath for 10 minutes. The

presence of terpenoids was indicated by the reddish-brown color, while the steroids were indicated by the green-blue color.

- **Detection of Coumarins**[169]

Two ml of alcoholic extract was added to 3 ml 10% NaOH in a test tube and then boiled in a water bath for 5 minutes observation of yellow color fluorescence was observed with positive results.

- **Detection of Tannins**[164]

Sodium hydroxide (NaOH) test: A fresh solution of 10% NaOH was prepared, and 1 ml was added to 1 ml of aqueous extract. Formation of emulsion indicates the positive results of tannins.

- **Detection of Resins**[164]

Turbidity test: Two ml of alcoholic extract treated with a few drops of 4% HCl, the appearance of the strong turbidity indicates resins present.

- **Detection of Quinines**[169]

Alcoholic KOH test: When alcoholic KOH was added to the plant extract, the red to blue color appeared reacting positively with quinines.

- **Detection of Fats and Oils**[170]

Paper test: A small amount of both aqueous and alcoholic extract was pressed between two filter papers. The stain on filter papers indicates the presence of the oils.

2-5 Preparation of 1 mM $Zn(NO_3)_2 \cdot 6H_2O$ Solution

A one millimolar (1mM) of $Zn(NO_3)_2 \cdot 6H_2O$ solution was prepared by dissolving 0.02975 gm from salt in 100 ml de-ionized water and stored in a dark and dry place for the synthesis of zinc oxide nanoparticles.

2-6 Biosynthesis and Purification of Zinc Oxide Nanoparticles

Zinc oxide nanoparticles were prepared by adding 10 mL of the crude aqueous extract of *Z.-spina christi* leaves to 90 mL of 1 mM $\text{Zn}(\text{NO}_3)_2 \cdot 6\text{H}_2\text{O}$ at room temperature (Figure 2-2). Freshly prepared 0.5 M of sodium hydroxide (NaOH) was added dropwise to the solution while being gently stirred to adjust the pH to 9. The mixture was heated on the magnetic stirrer for 2 hours at 60 °C until it transformed into a brownish colored pellet. After that the mixture was cooled and centrifuged at 5000 rpm for 15 minutes, to purify the obtained pellet because it contains impurities on the surface of particles, and then washed with ethanol followed by de-ionized water three times to eliminate the water-soluble substances and any contaminants of otherwise organic materials present on the surface of synthesized nanoparticles. The pure pellet was desiccated in a warm air oven at the temperature of 100°C for 90 minutes followed by the calcination step at 300 °C for 1 hour, that is important to forming ZnO-NPs. The calcinated ZnO-NPs were ready for characterization and further uses.

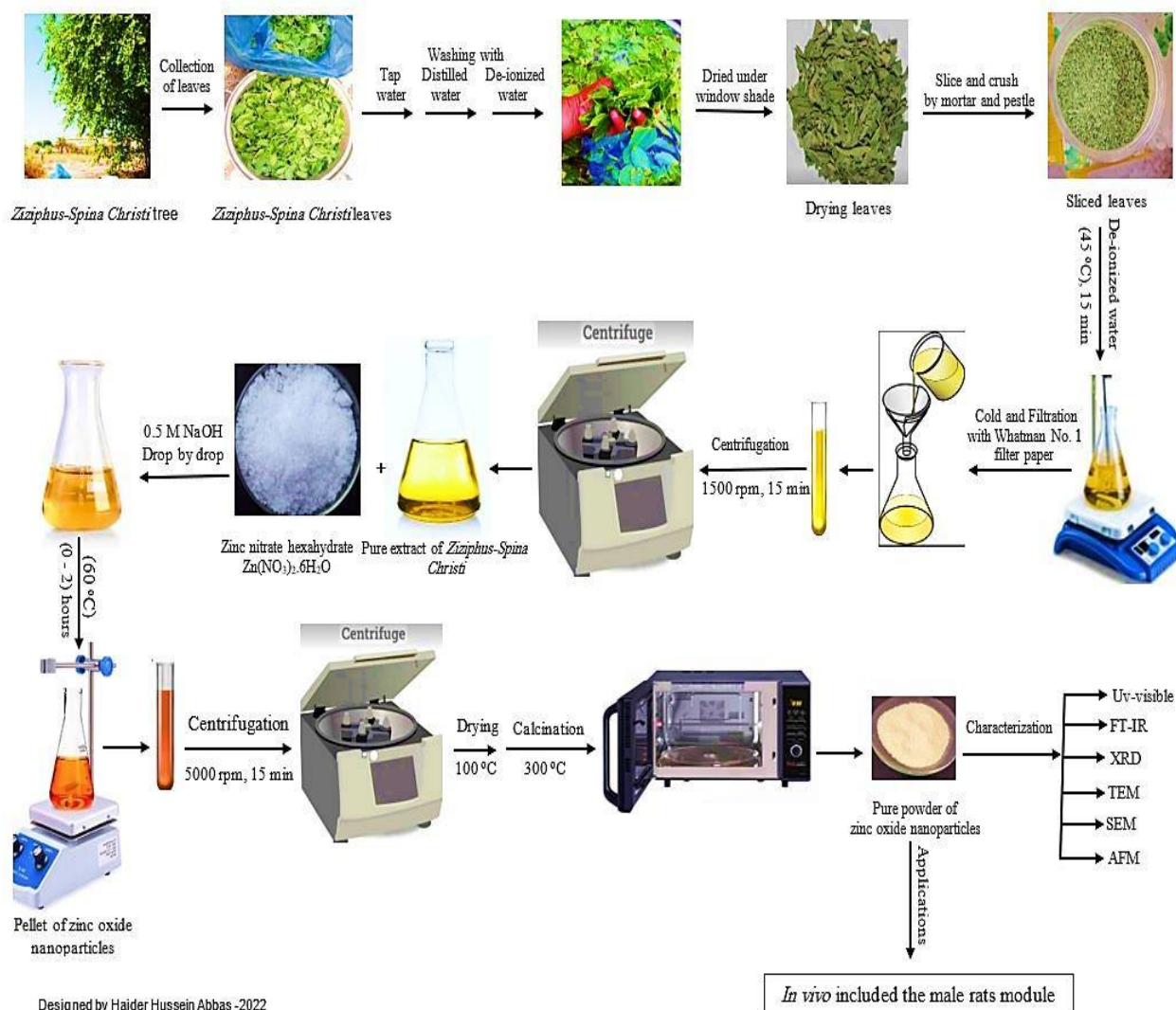


Figure 2-2: Scheme the biosynthesis of zinc oxide nanoparticles [171]

2-7 Optimization the Biosynthesis of ZnO-NPs

Synthesis of ZnO-NPs may be regulated by manipulating the reaction parameters. As a result, optimizing reaction conditions in the biosynthesis process is required to achieve the control size and formation rate of ZnO-NPs. In this study, the optimization process was managed by controlling five experimental parameters that include boiling time of plant extract, the volume of plant extract, precursor zinc ion concentration, pH, and reaction temperature to production of ZnO-NPs with stable and good yield. Optimization of reaction conditions were carried out using UV-visible spectrophotometer.

2-7-1 Effect of the Reaction time

The Reaction time is considered a crucial role in the chemical reactions, in this study was followed the reaction of *Z.-spina christi* with zinc nitrate hexahydrate at the different times (0 minute to 48 hours) and followed the change of color using Uv-visible spectroscopy.

2-7-2 Effect of the Boiling Time

The effect of boiling time of the plant leaves in preparation for the aqueous extract of *Z.-spina christi* leaves was considered in this study. Ten grams of dry leaves were boiled for (10, 15, and 20 minutes) with 100 mL of de-ionized water. Then followed the change of mixture color from green to yellow with the time and using Uv-visible spectroscopy.

2-7-3 Effect of the Plant Extract Volume

Biomass quantity plays a very important role in the synthesis of ZnO-NPs. The various volumes of *Z.-spina christi* leave extract (5 mL, 10 mL, and 15 mL) respectively were added to 1 mM of Zn (NO₃)₂.6H₂O and followed the change of color with time and using Uv-visible spectroscopy.

2-7-4 Effect of ZnNO₃.6 H₂O Concentration

The synthesis of nanoparticles is greatly dependent on the substrate concentration. The concentrations of ZnO-NPs (1mM, 2 mM, and 3m M) were studied with the constant other factors.

2-7-5 Effect of pH

The pH of the reaction mixture determines the types of ZnO-NPs formed, the different pH values (pH 5, 6, 7, 8, 9, and 10) were maintained using 0.5 M NaOH. The boiling time, quantity of plant extract, salt concentration, and reaction temperature were kept constant.

2-7-6 Effect of temperature

Temperature plays a very important role in all reactions. Optimization studies about temperature were carried out with temperatures ranging from 40°C to 70°C with a difference of 10°C.

2-8 Characterization of Zinc Oxide Nanoparticles

The synthesized ZnO-NPs were characterized using different modern techniques as follows:

2-8-1 UV-Visible Spectroscopy

The optical properties of ZnO-NPs were evaluated using UV–vis spectrophotometer at the central laboratory in Faculty of Pharmacy-University of Kufa. The spectra were set in between the wavelength of 300–700 nm range. In the spectrophotometer de-ionized water was set as an available reference.

2-8-2 Fourier Transform Infrared FT-IR Spectroscopy

FT-IR spectroscopy was used to determine the various functional groups involved in *Z.-Spina Christi* leaves extract and synthesized ZnO-NPs. These were recorded and compared using FT-IR spectrophotometer under the spectral range of (4000–400) cm^{-1} at the central laboratory in Faculty of Pharmacy-University of Kufa. Identification of functional groups present in the sample was recorded at room temperature, and the dried extract and synthesized ZnO-NPs were carried out by the KBr pellet method. The presence of the various vibrational modes in aqueous extract and synthesized ZnO-NPs were investigated.

2-8-3 X-Ray Diffraction (XRD)

To determine the average crystalline size of biosynthesized ZnO-NPs and identification its crystalline features were characterized by XRD technique at Ministry of Sciences and Technology-Baghdad-Iraq with $\text{Cu K}\alpha$ radiation (Voltage = 40 kV, Current =30 mA, $\lambda=1.5406 \text{ \AA}$, scan rate of $5.0^\circ \text{ min}^{-1}$ and scan range of 2θ from $20 - 80^\circ$). From the XRD data obtained; the crystalline size of the synthesized ZnO-NPs was calculated according to Debye–Scherrer's equation [172].

$$D = \frac{k\lambda}{\beta \cos \theta} \text{ ----- eq. (1)}$$

Were, D is the average crystalline size, λ is the wavelength of X-ray (1.5406 Å), θ is the Bragg's diffraction angle, β is the XRD peak full width at half maximum (FWHM) of the peak in radians, and k is the shape factor or Scherrer's constant (0.98).

2-8-4 Transmission Electron Microscopy (TEM)

Transmission electron microscopy (TEM) is a microscopy technique whereby a beam of electrons is transmitted through an ultra-thin sample and interacting with it to form an image involved information about the structure, crystallization, morphology, and stress of a substance. TEM images for synthesized ZnO-NPs were investigated using the TEM technique at University of Kasan-Iran. For TEM characterization, operating at 100 Kv, the ultrasound bath was used to disperse a small amount of ZnO NPs into ethanol. The size and morphology of ZnO-NPs were investigated by suspending 0.01 g of the ZnO-NPs in 100 mL 95% ethanol and sonication of the suspension for 20 minutes.

2-8-5 Scanning Electron Microscopy (SEM)

The surface morphology of green synthesized ZnO-NPs was performed by using a SEM technique at University of Kasan-Iran. ZnO-NPs were added to SEM slides to make a thin layer. Then the slide was set for SEM analysis after coating it with carbon copper grids. After that ZnO-NPs were observed under SEM at an increasing voltage of 20 KV, and the images were recorded.

2-8-6 Atomic Force Microscopy (AFM)

Atomic force microscopy offers ultra-high resolution in particle size measurement and is based on a physical scanning of samples at the sub-micron level using a probe tip of atomic scale. The instrument provides a topographical map of the sample based on forces between the tip and the sample surface. Samples are usually scanned in contact

or noncontact mode depending on their properties. In contact mode, the topographical map is generated by tapping the probe onto the surface across the sample, and the probe moves over the conducting surface in non-contact mode. Moreover, particle size obtained by the AFM technique provides a real picture which helps understand the effect of various biological conditions. The surface topology study of the synthesized ZnO-NPs by AFM analysis was at University of Kasan-iran. A thin film of ZnO-NPs was deposited on a silica glass slide by dropping a few drops of the ZnO-NPs solution on the slide and then allowed to dry at 30 °C overnight. The deposited film on a silica glass plate was scanned with AFM Model Ntegra Prima AFM (NT-MDT, Russia) for the determination of the nanoparticle's size.

2-9 In Vivo Applications of Zinc Oxide Nanoparticles

2-9-1 Animals of the Study

The experiment on animals was carried out at the laboratory animal facilities at the College of Sciences-University of Kufa. Thirty-six healthy male rats (*Sprague Dawley rats*) were used in this study weighing from 200 to 205 gm obtained from the animal house in the College of Sciences-University of Kufa. Rats were kept in the animal houses for acclimation to the laboratory condition for two weeks before using them. The study was performed during the period from May to August 2022. These animals were kept with standard environment situations temperature (25-27 C°) and relative humidity (50%-60%) conditions. The animals were divided and housed in plastic cages with dimensions of 50×35×15 cm [173].

2-9-2 Preparation of Adenine

Adenine (C₅H₅N₅) with high purity grade, CAS NO.: 73-24-5 was obtained from Solarbio Company (China). A 10 gm of adenine was

dissolved in 10 mL DMSO and completed to 100 mL with de-ionized water.

2-9-3 The Experimental Design

Thirty-six male rats were used in this study and divided into six equal groups; each group consisted of 6 male rats as follows:

1-First group (G-I): Rats were received 0.5 mL DMSO one time daily for 30 days and served as control group.

2- Second group (G-II): Rats in this group were gavaged 0.5 mL adenine (100 mg/kg. BW) dissolved by DMSO one time daily for 30 days. The dose of adenine was chosen from the previous study by [174], based on the original method by [175].

3- Third group (G-III): Rats were received 0.5 mL of *Z.-spina christi* leaves extract (10 mg/kg.BW) one time daily for 30 days. The dose of *Z.-spina christi* leaves extract according to previous study [176].

4- Fourth group (G-IV): Rats were received 0.5 mL of ZnO-NPs (10 mg/kg.bw) one time daily for 30 days [177].

5- Fifth group (G-V): Rats in this group were co-administrated 0.25 mL adenine (100 mg/kg.BW) and 0.25 mL *Z.-Spina Christi* leaves extract (10 mg/kg.BW at the same time for 30 days [178].

6- Sixth group (G-VI): rats in this group were co-administrated 0.25 mL adenine (100 mg/kg.BW) and 0.25 mL of ZnO-NPs (10 mg/kg.BW) at the same time for 30 days, this was chosen in based on the previous experiment by [179].

* The rats were weighed and recorded the weights before the beginning of the treatment and weekly during the treatment period.

2-9-4 Collection of Blood and Tissues

2-9-4-1 Blood Specimens

After 30 days of experiment and On the 31st day, fasted rats were anesthetized by placing them in a closed jar containing cotton rinsed with chloroform to be sedated for the next step which is blood drawn

via cardiac puncture in sterile syringes by needle prick in the heart draining (2-3 ml) of blood carefully, then blood placed in a test tube containing gel which leaves for 30 minutes in room temperature and then used for getting serum by centrifuge at 3000 rpm for 15 minutes and put it in Eppendorf tubes which kept at freezer (-20°C) till the time of biochemical analysis.

2-9-4-2 Tissue Sampling

After blood collection and heart puncture, rats were sacrificed to isolate kidneys and liver by order. The kidneys and livers of each animal were quickly removed and rapidly weighed then prepared for histological study according to Mescher's method [180].

2-10 Biochemical Analysis

2-10-1 Estimation of Kidney Function Tests

Kidney function tests of serums (uric acid, urea, and creatinine) concentrations were spectrophotometrically determined according to special kits.

2-10-1-1 Estimation of Uric Acid

- **Principle**

Uricase can catalyze the decomposition of uric acid into allantoin, CO₂, and H₂O₂. Then Fe²⁺ in potassium ferrocyanide is oxidized by H₂O₂ to form Fe³⁺. Fe³⁺ can further react with 4-aminoantipyrine and 3,5-dichloro-4-hydroxybenzene-1-sulfonic acid (DHBS) in the presence of peroxidase to form quinonimine derivative, a red-colored complex that has a characteristic absorption peak at 505 nm.

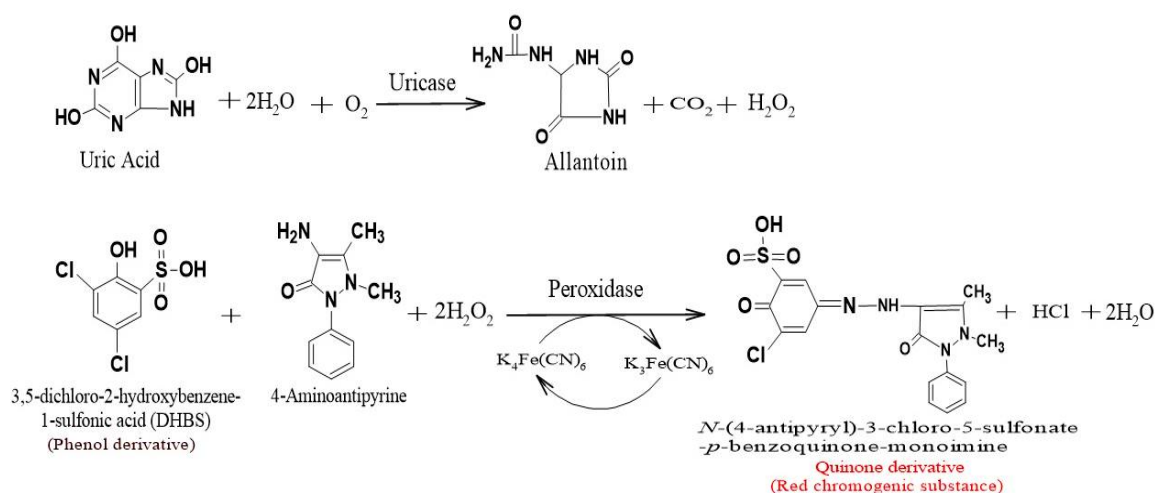


Figure 2-3: The chemical reaction to determination of uric acid

- **Reagents**

Reagent I: Uric acid standard 10 mg/dL.

Reagent II (Buffer): Phosphate buffer and 3,5-DHBS.

Reagent III: (Enzymes): Uricase, peroxidase, potassium hexacyanoferrate (II) and 4-aminoantipyrine.

- **Preparation of Standard Solution**

1- The spectrophotometer was run for 30 minutes, then the wavelength was adjusted at 505 nm, and set the counter to zero with de-ionized water.

2- Preparation of standard curve by dilution of 1 mg/dL of standard solution with de-ionized water to 20, 40, 60, 80, and 100 mg/dL for standby.

Table 2-3: Preparation of standard solutions to determination of uric acid

Number	Standard Concentration (mg/dL)	Uric Acid Standard (μL)	De-ionized Water (μL)
1	0	0	1000
2	20	20	980
3	40	40	960
4	60	60	940
5	80	80	920
6	100	100	900

3- The concentration of each standard solution been at the x-axis, and the corresponding ΔA standard at the y-axis. Then the linear regression equation $y=kx+b$ is obtained. ΔA were brought into the equation to get x (mg/dL).

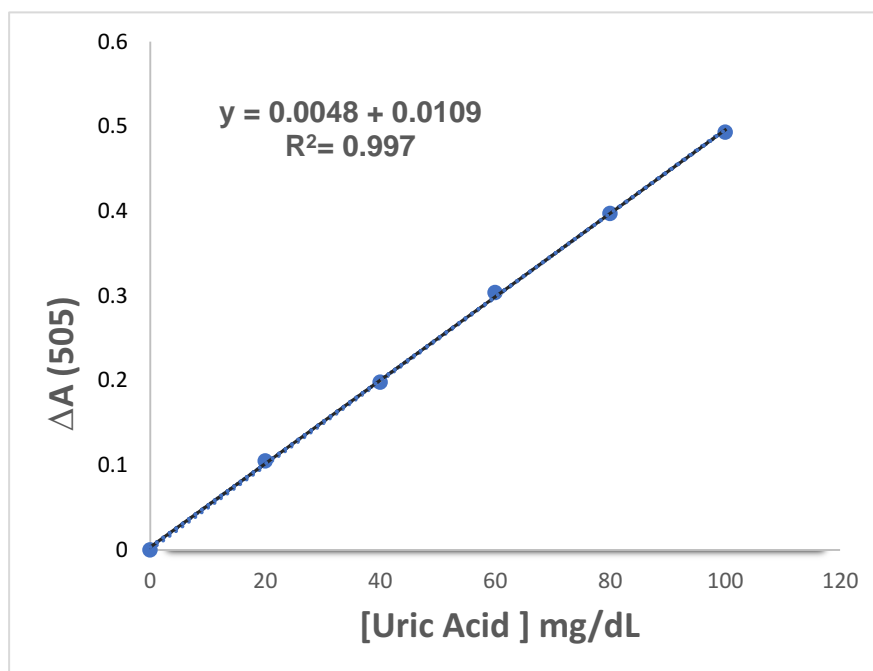


Figure 2-4: Standard curve of uric acid

- **Procedure**

In 5 ml centrifuge tube, were mixed reagents as following:

Table 2-4: Mixing of reagents to determination of uric acid

Reagent name (mL)	Control Tube (A _{Control})	Specimen tube (A _{Specimen})	Standard tube (A _{Standard})	Blank tube (A _{Blank})
Specimen (mL)	0.25	0.25	-	-
Standard solution (mL)	-	-	0.25	-
De-ionized water	-	-	-	0.25
Working solution A		0.75	0.75	0.75
Working solution B	0.75	-	-	-
The mixture was mixed completely and placed in a water bath at 25°C for 30 min.				

To measure the absorption value (A) at 505 nm used 1mL glass cuvette. The absorption was measured as A_{Control}, A_{Specimen}, A_{Standard}, and A_{Blank}. $\Delta A_{Control} = A_{Specimen} - A_{Control}$. $\Delta A_{Blank} = A_{Specimen} - A_{Blank}$. Each test tube needs to set up a contrast tube and the standard curve only needs to test once or twice.

- **Calculation:**

$$\text{Uric acid concentration} \left(\frac{\text{mg}}{\text{dL}} \right) = \frac{x \times VS}{VS \times M.wt} = 168x$$

Where, k= The slope of the standard curve, b= The intercept of standard curve, VS: Sample volume=0.25 mL, VE: Extract solution volume=1 mL, M: Molecular weight of uric acid=168 g/mol.

2-10-1-2 Estimation of Urea

- **Principle**

The colorimetric estimation method of urea based on the specific action of urease which hydrolyses urea to form ammonium and carbon dioxide. In the presence of sodium nitroprusside, the ammonium ions (NH_4^+) combine with alkaline hypochlorite and sodium salicylate to form a blue-green 2,2-dicarboxy indophenol.

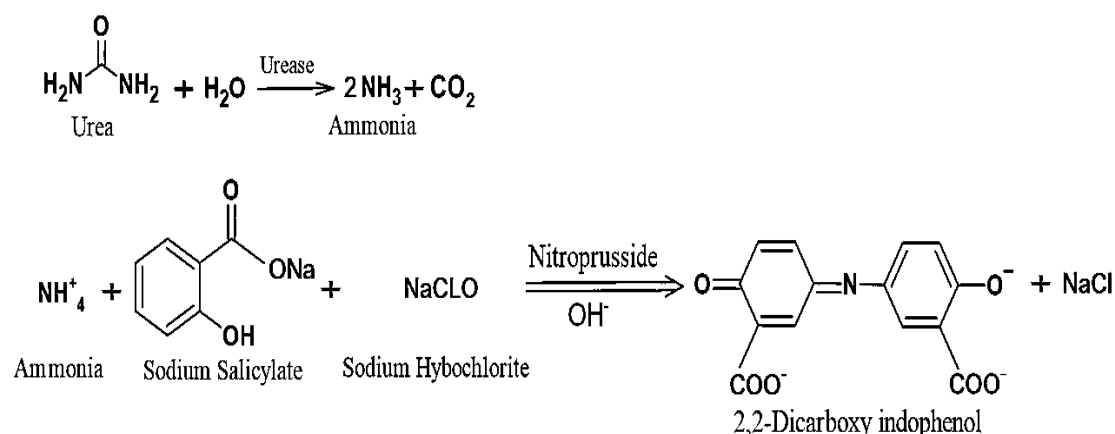


Figure 2-5: The chemical reaction to determination of urea

The intensity of the color is directly proportional to urea concentration in the specimen, which is measured at 600 nm.

- **Reagents**

Reagent I: Urea standard, 50 mg/dL (8.3 mmol/L)

Reagent II (Enzyme reagent): Urease > 500 U/mL Stabilizer.

Reagent III (Buffered chromogen): Phosphate buffer, sodium salicylate and sodium nitroprusside.

Reagent IV (Alkaline hypochlorite): Sodium hypochlorite and sodium hydroxide.

- **Procedure**

1-The spectrophotometer was run for 30 minutes, then the wavelength was adjusted at 600 nm, and set the counter to zero with de-ionized water.

2-Standard solution: Urea standard solution was diluted (1 mg/dL) to 0.25 mg/dL with de-ionized water.

3- Reagents were added to the following list:

Table 2-5: Addition of reagents to determination of urea

Reagent name (μL)	Blank tube (A _{Blank})	Standard tube (A _{Standard})	Specimen tube (A _{Specimen})	Control tube (A _{control})
Reagent III	500	500	500	500
De-ionized water	200	-----	-----	-----
The mixture was shaken well, then placed at 25°C in water bath for 10 min.				
Reagent II	Drop (100)	Drop (100)	Drop (100)	Drop (100)
Mixed thoroughly, then added				
Standard solution	-----	200	-----	-----
Specimen	-----	-----	200	200
The mixture was shaken well, then placed at 25°C in water bath for 10 min.				
Reagent IV	200	200	200	200
The mixture mixed well, incubated at room temperature for 10 min, then measured the absorbance at 600 nm as, $\Delta A_{\text{Standard}} = (A_{\text{Standard}} - A_{\text{Blank}})$, $\Delta A_{\text{Specimen}} = (A_{\text{Specimen}} - A_{\text{control}})$.				

- **Calculation**

$$\text{Urea concentration} \left(\frac{\text{mg}}{\text{dL}} \right) = \frac{\Delta A_{\text{Specimen}}}{\Delta A_{\text{Standard}} \times C_s} = \frac{0.25 \times \Delta A_{\text{Specimen}}}{\Delta A_{\text{Standard}}}$$

Where, C_s: concentration of standard solution = 0.25 mg/dL.

2-10-1-3 Estimation of Creatinine

- **Principle**

The principal assay is depended on the reaction of creatinine with picric acid in an alkaline solution to form yellow – a red complex as following:

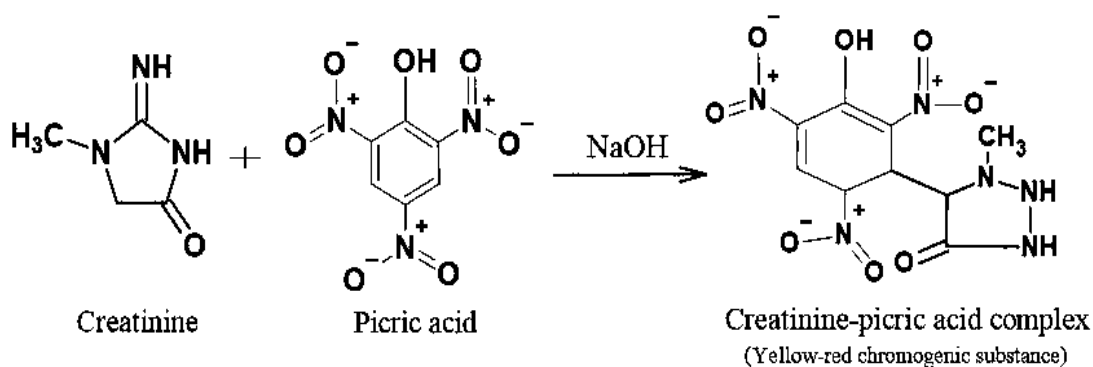


Figure 2-6: The chemical reaction to determination of urea concentration

The intensity of the produced color is proportionate with the creatinine solution in the serum. Creatinine was determined by measuring the absorbance at 520 nm.

- **Reagents**

Reagent I: Creatinine standard.

Reagent II: Picric acid.

Reagent III: Sodium hydroxide.

Additional reagent was required but not provided: Trichloroacetic acid (TCA).

- **Procedure**

Serum preparation

A 0.5 mL of serum was taken and added 0.5 mL of additional reagent (TCA). The mixture was centrifuged at 4°C, 12000 g for 10 minutes, then the supernatant was collected for testing.

1-The spectrophotometer was run for 30 minutes, then the wavelength was adjusted at 520 nm, and set the counter to zero with de-ionized water.

2- Reagents were added as the following list:

Table 2-6: Addition of reagents to determination of creatinine

Reagent Name (mL)	Specimen tube (A _{Specimen})	Blank tube (A _{Blank})	Standard tube (A _{Standard})
Specimen	1	-----	-----
De-ionized water	----	0.5	-----
Standard solution (RI)	-----	-----	0.5
TCA	-----	0.5	0.5
working solution (RII + RIII)	1	1	1
The mixture was mixed completely and placed at 25°C for 10 min.			

The absorbance was determined at 520 nm. They are respectively recorded as A_{Specimen}, A_{Blank}, and A_{Standard}.

$$\Delta A_{\text{Specimen}} = (A_{\text{Specimen}} - A_{\text{Blank}}), \Delta A_{\text{Standard}} = (A_{\text{Standard}} - A_{\text{Blank}}).$$

- **Calculations**

$$\text{Creatinine concentration } \left(\frac{\text{mg}}{\text{dL}} \right) = \frac{CS \times \Delta A_{\text{Specimen}}}{\Delta A_{\text{Standard}}} \times \frac{VU+VE2}{VE1+VL} = 2612.5 \times \frac{\Delta A_{\text{Specimen}}}{\Delta A_{\text{Standard}}}$$

Where, CS: standard tube concentration=20 mg/dl, VU: volume of supernatant during extraction= 0.75 ml, VE1: add the volume of extracting solution I=1 ml, VE2: add the volume of extracting solution II=0.25 ml, VL: the volume of liquid sample=0.1 ml.

2-10-2 Estimation of Liver Function Tests

For determination of hepatic enzyme activities by appropriate commercial kits. Activities of ALT, AST, and ALP were determined spectrophotometrically based on special kits.

2-10-2-1 Estimation of Alanine Aminotransferase Activity

- **Principle**

ALT catalyzes the transamination reaction of alanine and α -ketoglutarate to generate pyruvate and glutamic acid according to the following reaction:

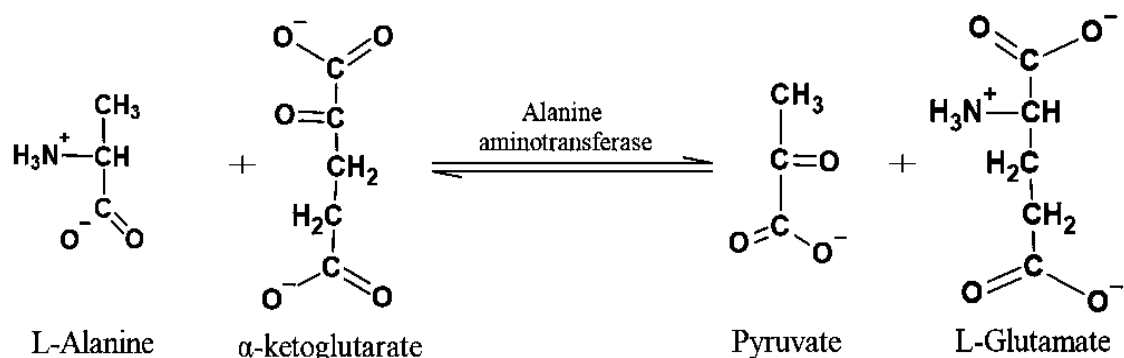


Figure 2-7: The chemical reaction to determination of ALT

The addition of 2,4-dinitrophenylhydrazine solution not only terminates the above reaction but also increases into phenyl pyrene pyruvate; which shows brownish red in alkaline conditions, the activity of ALT enzyme activity can be calculated by measuring the absorbance of 540 nm.

- **Reagents**

Reagent I: Pyruvate standard

Reagent II: Phosphate buffer, L-Alanine and α -ketoglutarate.

Reagent III: 2,4-dinitrophenylhydrazine.

Reagent IV: Sodium hydroxide (NaOH).

- **Preparation of Standard Curve**

1- The spectrophotometer was run for 30 minutes, then the wavelength was adjusted at 540 nm and set the counter to zero with de-ionized water.

2- Standard solutions were obtained by the following table operation.

Table 2-7: Preparation of standard solutions to determination of ALT

Pyruvate Standard (mL)	De-ionized water (mL)	Reagent II (mL)	Concentration of standard ($\mu\text{mol/mL}$)
0	0.5	2.00	0.00
0.1	0.5	1.9	0.05
0.2	0.5	1.8	0.1
0.3	0.5	0.7	0.2
0.4	0.5	1.6	0.4
0.5	0.5	1.5	0.6
0.6	0.5	1.4	0.8
0.7	0.5	1.3	0.1
0.8	0.5	1.2	1.5

Note: 0 $\mu\text{mol/mL}$ standard tube as a blank tube.

3- The standard curve was plotted the standard concentration as the X-axis, and the absorbance as the Y-axis. The absorbances of the increasing amount of pyruvate standard correspond to transaminase activities. Take ($A_{\text{Specimen}} - A_{\text{Control}}$) into the equation $y=kx+b$ to find the x value.

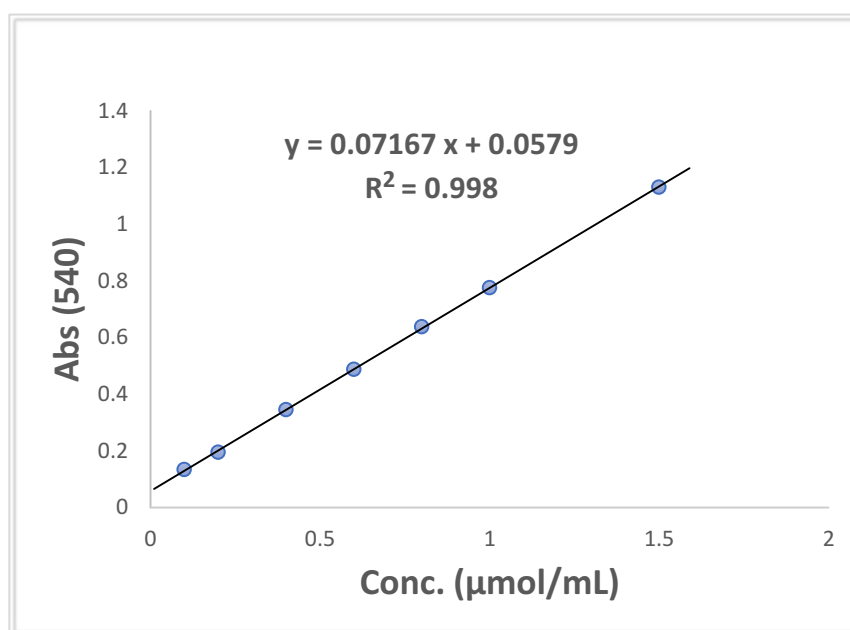


Figure 2-8: Standard curve of ALT

- **Procedure**

Reagents were mixed as the following table:

Table 2-8: Mixing of reagents to determination of ALT

Reagent Name (mL)	Specimen tube (A _{Specimen})	Blank tube (A _{Blank})
Reagent II	0.5	0.5
Mixed, incubated in a water bath at 25°C for 10 min		
Specimen	1	-----
De-ionized water	-----	1
Mixed exactly at 25°C in water bath for 30 min.		
Reagent III	0.5	0.5
The mixture was shaken thoroughly, and placed for 20 min at room temperature.		
Reagent IV	0.5	0.5
The mixture was mixed and the net absorbance was detected at 540 nm of specimen tube against blank tube after 10 minutes.		

- **Calculations**

The standard concentration as the X-axis, and the ΔA ($A_{\text{Specimen}} - A_{\text{Blank tube}}$) as the Y-axis, was obtained the standard curve $y=kx+b$.

$$\text{ALT (U/mL)} = \frac{x \times (V_s + V_{\text{Reagent I}})}{V_s} \times \frac{1}{T} = 12x$$

Where, V_s : Specimen volume=1 mL, $V_{\text{Reagent I}}$: Reagent I volume=0.1 mL,

T: Reaction time=30 minutes.

2-10-2-2 Estimation of Aspartate Aminotransferase Activity

- **Principle**

AST catalyzes α -ketoglutaric acid react with aspartate to produce glutamate and oxaloacetate according to the following reactions:

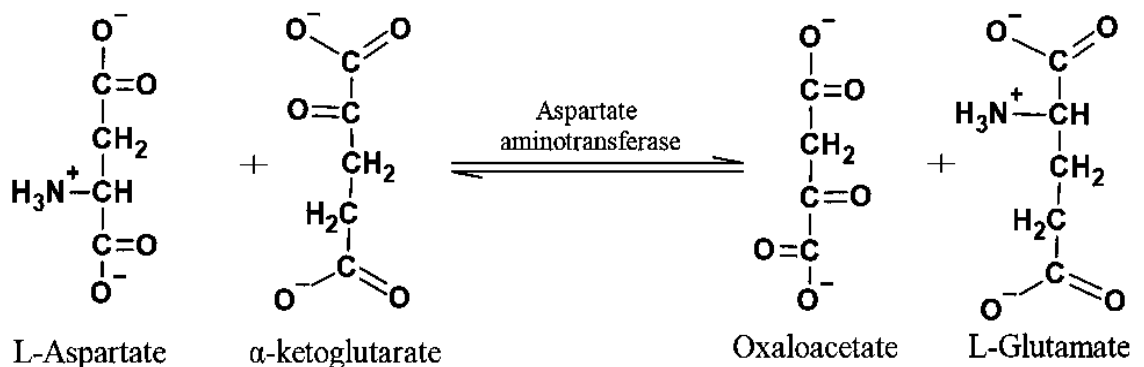


Figure 2-9: The chemical reaction to determination of AST

Oxaloacetic acid is further de-carboxylated to form pyruvate, pyruvate can react with 2,4-dinitrophenylhydrazine to produce 2,4-dinitrophenylhydrazone, which shows brownish red in alkaline conditions. The AST activity can be calculated by measuring the absorbance of 540 nm.

- **Reagents**

Reagent I: Pyruvate standard

Reagent II: Phosphate buffer, L-Aspartate and α -ketoglutarate.

Reagent III: 2,4-dinitrophenylhydrazine.

Reagent IV: Sodium hydroxide (NaOH).

- **Preparation of Standard Curve**

1- The spectrophotometer was run for 30 minutes, then the wavelength was adjusted at 540 nm, and set the counter to zero with de-ionized water.

2- Standard curve detection

Firstly, the standard was diluted to 2 $\mu\text{mol/mL}$ with de-ionized water, and the corresponding concentration standard tube is obtained by mixing the pyruvate standard and reagent II according to the table below:

Table 2-9: Preparation of standard solutions to determination of AST

Pyruvate Standard (mL)	De-ionized water (mL)	Reagent II (mL)	Concentration of standard ($\mu\text{mol/mL}$)
0	0.5	2.00	0.00
0.1	0.5	1.9	0.05
0.2	0.5	1.8	0.1
0.3	0.5	0.7	0.2
0.4	0.5	1.6	0.4
0.5	0.5	1.5	0.6
0.6	0.5	1.4	0.8
0.7	0.5	1.3	0.1
0.8	0.5	1.2	1.5

Note: 0 $\mu\text{mol/mL}$ standard tube as a blank tube.

3- The standard curve was plotted the standard concentration as the X-axis, and the absorbance as the Y-axis. Absorbances of the increasing

amount of pyruvate standard correspond to ALT activities. ($A_{\text{Specimen}} - A_{\text{Control}}$) were taken into the equation $y=kx+b$ to find the x value.

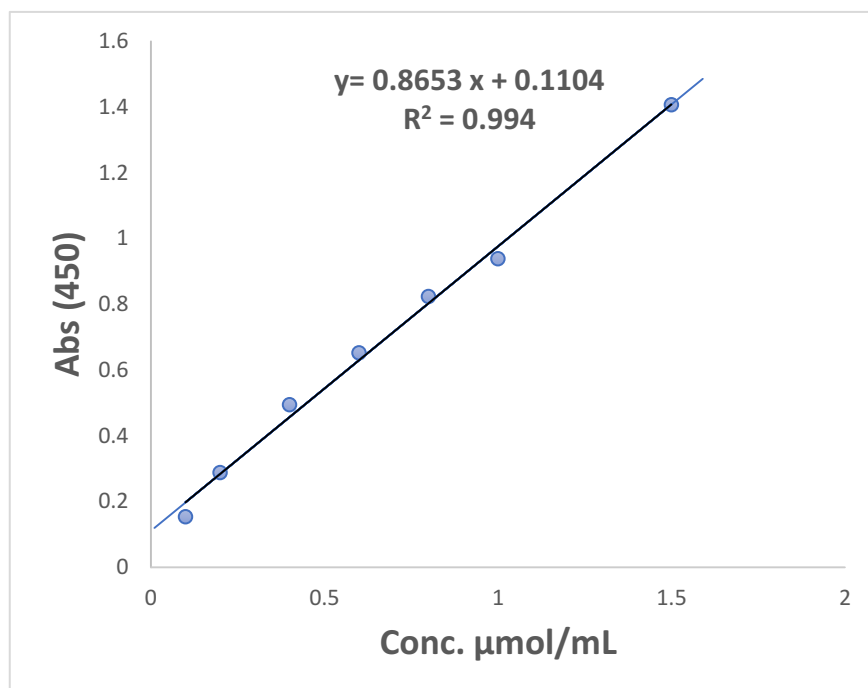


Figure 2-10: Standard curve of AST

- **Procedure**

Reagents were mixed as the following table:

Table 2-10: Mixing of reagents to determination of AST

Reagent Name (mL)	Specimen tube (A_{Specimen})	Blank tube (A_{Blank})
Reagent II	0.5	0.5
Mixed, incubated in a water bath at 25°C for 10 min		
Specimen	1	-----
De-ionized water	-----	1
Mixed exactly at 25°C in water bath for 30 min.		
Reagent III	0.5	0.5
The mixture was shaken thoroughly, and placed for 20 min at room temperature.		
Reagent IV	0.5	0.5
The mixture was mixed and then the absorbance was detected at 540 nm of specimen tube against blank tube after 10 minutes.		

- **Calculations**

$$\text{AST (U/mL)} = \frac{x \times (V_S + V_{R1})}{V_S} \times \frac{1}{T} = 12x$$

Where, V_S : Specimen volume = 1 ml, V_{R1} : Reagent I volume = 0.1 mL,

T: Reaction time = 30 minutes.

2-10-2-3 Estimation of Alkaline Phosphatase Activity

• Principle

In alkaline conditions, ALP catalyzes hydrolysis of disodium phenyl phosphate to phenol and phosphate. The produced phenol reacts with 4-Aminoantipyrine and potassium ferricyanide to form a red quinone derivative, whose absorbance at 510 nm is directly proportional to the ALP activity in the specimen.

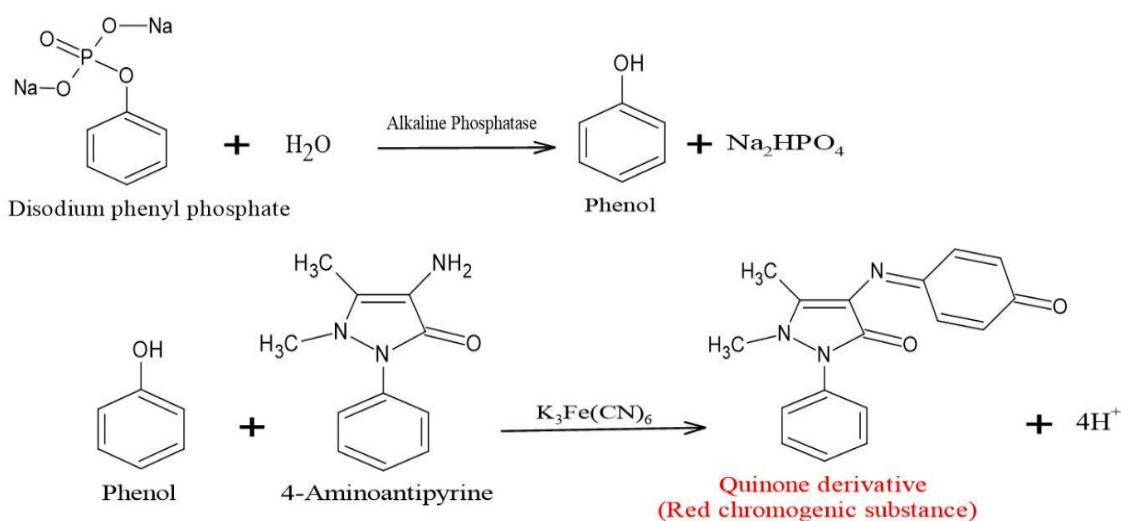


Figure 2-11: The chemical reaction to determination of ALP

• Reagents

Reagent I: standard (Phenol)

Reagent II: Carbonate-bicarbonate buffer disodium phenyl phosphate

Reagent III: 4-Aminoantipyrine and sodium arsenate

Reagent IV: Potassium ferricyanide ($K_3Fe(CN)_6$).

• Procedure

1-The spectrophotometer was run for 30 minutes, then the wavelength was adjusted at 510 nm, and set the counter to zero with de-ionized water.

2-The reagents were added in 5 mL test tube as the following:

Table 2-11: Addition of reagents to determination of ALP

Reagent Name (mL)	Specimen tube (A_{Specimen})	Control tube (A_{Control})	Blank tube (A_{Blank})	Standard tube (A_{Standard})
Reagent II	2	2	2	2
Mixed, incubated for 10 minutes at 25°C				
Standard	-----	-----	-----	0.2

Specimen	0.2	-----	-----	-----
The mixture was mixed thoroughly, staying in 25°C for 15 minutes.				
Reagent III	0.5	0.5	0.5	0.5
Mixed well, incubated at 25°C for 5 minutes.				
Reagent VI	0.5	0.5	0.5	0.5
Specimen	-----	0.2	-----	-----
De-ionized water	-----	-----	0.2	-----
The mixture was mixed thoroughly, incubated in dark for 10 minutes, and measured the absorbance at 510 nm of specimen (A_{Specimen}), control (A_{Control}), standard (A_{Standard}) and (A_{Blank}).				

- **Calculation:**

$$\text{ALP (U/mL)} = \left[\frac{C_s \times (A_{\text{Specimen}} - A_{\text{Control}})}{(A_{\text{Standard}} - A_{\text{Blank}}) \times V_s} \right] \times \frac{1}{T} = 0.167 \times (A_{\text{Specimen}} - A_{\text{Control}}) \times (A_{\text{Standard}} - A_{\text{Blank}})$$

Where, C_s : Standard concentration = 2.5 $\mu\text{mol/ml}$, V_s : Specimen volume = 0.2 ml, T : Reaction time = 15 minutes.

2-10-3 Estimation of Antioxidant Statuses

The antioxidants statuses which included total antioxidant capacity (TAC), catalase (CAT), superoxide dismutase (SOD), reduced glutathione (GSH), oxidative stress parameters malondialdehyde (MDA) as a marker for lipid peroxidation, and nitric oxide (NO) were determined spectrophotometrically using a commercial assay kits.

2-10-3-1 Estimation of Total Antioxidant Capacity Assay

- **Principle**

The principal assay was based on the reduction of Fe^{3+} -TPTZ (2,4,6-tris(2-pyridyl)-1,3,5-triazine) by antioxidant substances in acidic medium to form of the blue Fe^{2+} -TPTZ that absorbed at 593 nm. Amount of iron reduced was correlated with the concentration of the total antioxidant capacity.

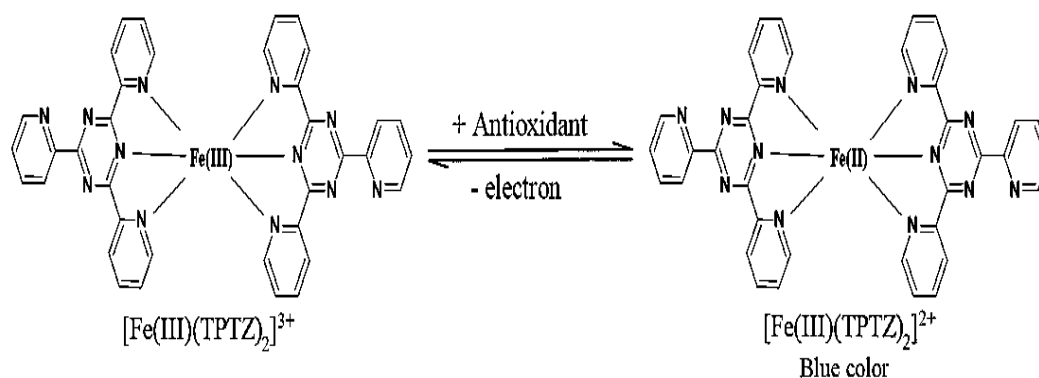


Figure 2-12: The chemical reaction to determination of TAC

- **Reagents**

Reagent I: Ferrous sulfate heptahydrate ($\text{FeSO}_4 \cdot 7\text{H}_2\text{O}$) standard

Reagent II (Diluent): 2,4,6-tris(2-pyridyl)-1,3,5-triazine (TPTZ)

Reagent III (Solution): 2,4,6-tris(2-pyridyl)-1,3,5-triazine (TPTZ)

Reagent IV: Assay buffer concentrate

- **Preparation of Standard Curve**

1- The freshly FeSO_4 solution was prepared by dissolved 0.00139 mg of $\text{FeSO}_4 \cdot 7\text{H}_2\text{O}$ in 1 mL phosphate-buffer saline (PBS), the solution was diluted 10 times to make the concentration of 5 $\mu\text{mol/mL}$.

2- The following Standard solutions of Fe^{2+} 0.5, 0.25, 0.125, 0.0625, 0.03125, 0.0156 $\mu\text{mol/mL}$ were prepared as describe in the following table:

Table 2-12: Preparation of standard solutions to determination of TAC

[FeSO_4] ($\mu\text{mol/mL}$)	FeSO_4 solution (mL)	De-ionized water (mL)
0.5	1	9
0.25	0.5	9.5
0.125	0.25	9.75
0.0625	0.125	9.875
0.0315	0.063	9.973
0.0156	0.0312	9.9688
0	0	10

3- The spectrophotometer was run for 30 minutes, then the wavelength was adjusted at 593 nm, used the de-ionized water to set the counter to zero, and measured the absorbance.

4- Standard curve were created by taken standard concentrations of Fe^{2+} as X-axis, absorbances as Y-axis, to get linear regression equation $y=kx+ b$.

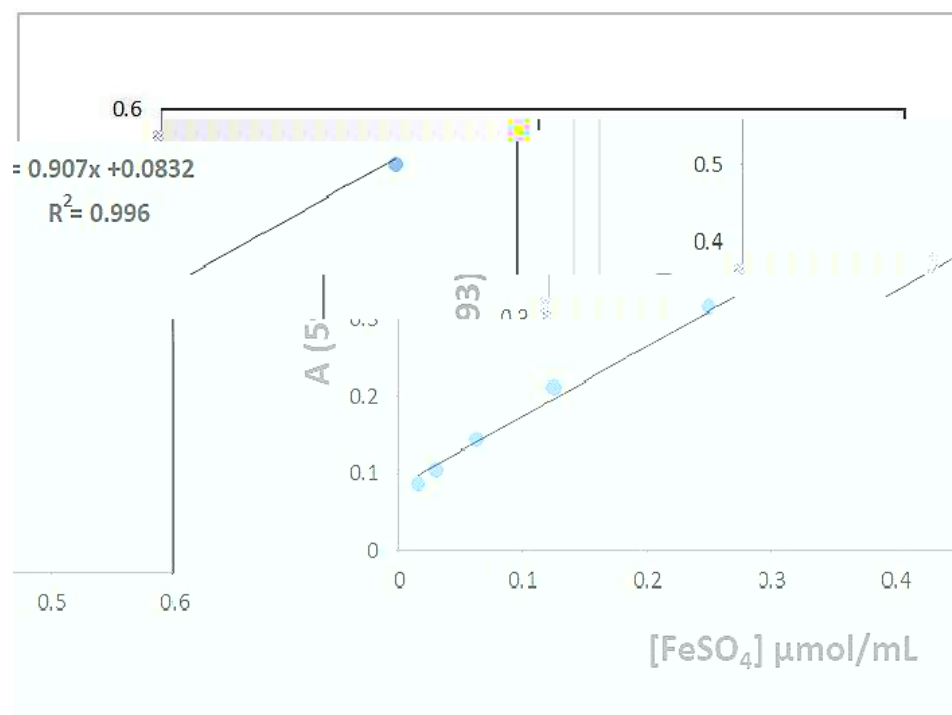


Figure 2-13: Standard curve of TAC

- **Procedure**

- 1- Solutions of TBTZ Diluent, TBTZ solution and assay buffer with ratio of 10:1:1 were mixed to make the assay solution, were prepared and direct used, operated on ice.
- 2- A 50 μL of specimen were added, positive control and de-ionized water (blank solution) to test tube.
- 3- A 150 μL of assay solution were added to each test tube.
- 4- The mixture was mixed thoroughly and incubated at 25°C for 10 min.
- 5- The absorbance was measured at 593nm.

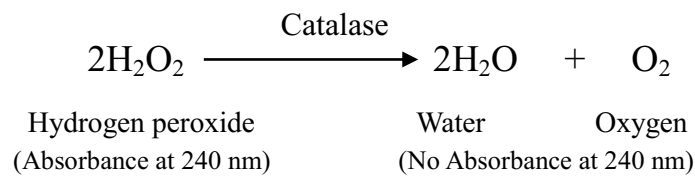
- **Calculations**

The total antioxidant capacity ($\mu\text{mol/mL}$) of the specimen was calculated according to the standard curve using linear regression fitting ($y = mx + b$) to get x value.

2-10-3-2 Estimation of Catalase Activity Assay

- **Principle**

Catalase is the main enzyme of clearing H_2O_2 , which plays an important role in the active oxygen scavenging system. The principle test of catalase based on the rapid detection of catalase presence, which becomes evident by the formation of copious gas bubbles. H_2O_2 has a characteristic absorption peak at 240 nm. It can be decomposed into H_2O and O_2 by catalase which makes the absorbance of reagent at 240 nm decrease.



The height of the foam is an indication of the amount of catalase present and can be calculated according to the change rate of absorbance.

- **Reagents:** Sample dilution buffer, assay buffer, hydrogen peroxide (H_2O_2) and catalase standard.

The spectrophotometer was run for 30 minutes, then the wavelength was adjusted at 240 nm and set the counter to zero with de-ionized water.

- **Procedure**

1- The working reagent of CAT was heated in water bath at 25°C for 10 minutes.

2- One mL of CAT working reagent and 35 μ L of specimen were added in 1 mL quartz cuvette, mixed for 5 seconds. Immediately detected the absorbance at 240 nm at the initial time (A_1) and the absorbance after reaction for 1 minute (A_2), $\Delta A = A_1 - A_2$ was calculated.

- **Calculations:**

$$\text{CAT activity (U/mL)} = \left[\frac{\Delta A \times V_{rv}}{(\epsilon \times d) \times 10^6} \right] \times \frac{1}{V_s} = 678 \times \Delta A$$

Where, V_{rv} : Total reaction volume = 1.035×10^{-3} L, ϵ : Molar extinction coefficient = 43.6 L/mol/cm, d : Length path of cuvette = 1 cm, V_s : Sample volume = 0.035 mL, V_{sv} : Extraction volume = 1 mL, T : Reaction time = 1 minute, 10^6 : Unit conversion factor, 1 mol = 10^6 μ mol.

2-10-3-3 Estimation of Superoxide Dismutase Activity Assay

- **Principle**

Superoxide dismutase (SOD) catalyzes the superoxide anion (O_2^-) to form H_2O_2 and O_2 . It is not only the superoxide anion scavenging enzyme, but also the main H_2O_2 producing enzyme, which plays an important role in the biological antioxidant system. Superoxide anion (O_2^-) is produced by the xanthine and xanthine oxidase reaction system. O_2^- can reduce the tetrazole (WST-1) to form blue formazan (WST-1), which has an absorbance in of 450 nm. SOD can remove O_2^- and inhibit the formation of methionine. The darker blue color of the reaction solution, the lower activity of SOD. The lighter blue color of the reaction solution, the higher activity of SOD.

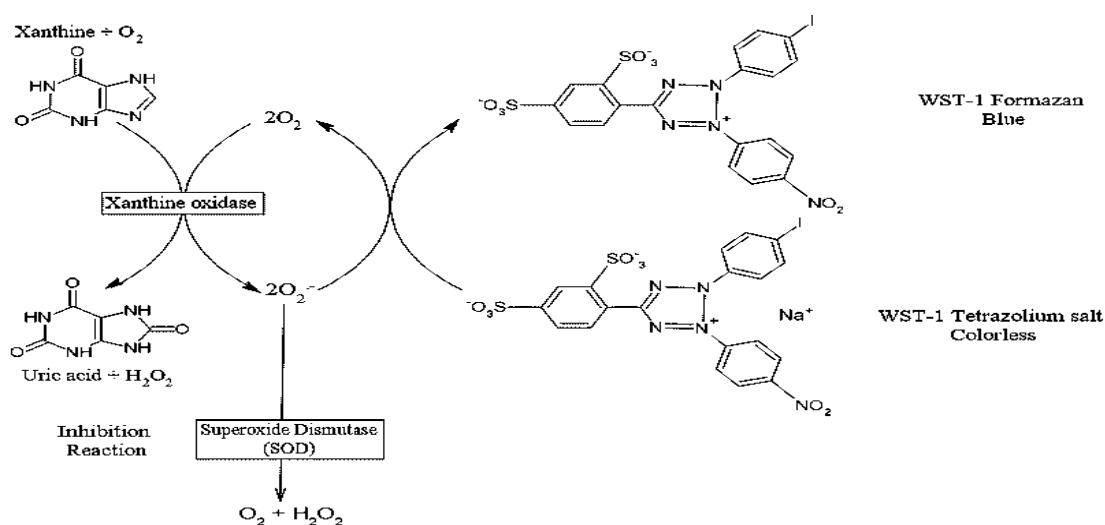


Figure 2-14: The chemical reaction to determination of SOD

- **Reagents**

Reagent I: Superoxide dismutase standard

Reagent II: Xanthine oxidase enzyme

Reagent III: WST-1 (working solution)

Reagent IV: SOD assay buffer

Reagent V: Xanthine solution

The spectrophotometer was run for 30 minutes, then the wavelength was adjusted at 450 nm, and set the counter to zero with de-ionized water.

- **Producer**

Reagents were added as the following table:

Table 2-13: Addition of reagents to determination of SOD

Reagent (μL)	Specimen tube (A _{Specimen})	Control tube (A _{Control})	Blank1 tube (A _{Blank1})	Blank2 tube (A _{Blank2})
Specimen	40	40	-	-
De-ionized water	40	40	80	80
Reagent I	100	100	100	100
Reagent II	40	40	-	-
Reagent III	200	200	200	200
Reagent IV	30	30	70	70
Reagent V	50	50	50	50

The mixture was mixed thoroughly and incubated at room temperature for 30 minutes, then the mixture was added into a 1mL glass cuvette and detected the absorbance value of each tube at 450 nm.

$$\Delta A_{\text{Specimen}} = A_{\text{Specimen}} - A_{\text{Control}}, \quad \Delta A_{\text{Blank}} = A_{\text{Blank1}} - A_{\text{Blank2}}$$

- **Calculations:**

$$\text{Inhibition percentage} = \left[\frac{\Delta A_{\text{Blank}} - \Delta A_{\text{Specimen}}}{\Delta A_{\text{Blank}}} \right] \times 100\%$$

$$\text{SOD activity (U/mL)} = \left[\frac{P}{(1-P) \times V_{\text{rv}}} \right] = \frac{11.4 \times P}{(1-P) \times F}$$

Where, V_{rv}: Total reaction volume=1.026 mL, V_s: Sample volume = 0.09 mL, P: Inhibition percentage=%, F: Sample dilution multiple.

2-10-3-4 Estimation of Reduced Glutathione Assay

- Principle

Glutathione can react with 5,5'-dithiobis-(2-nitrobenzoic acid) (DTNB) to form 2-nitro-5-thiobenzoic acid (TNB) and mixed disulfide. 2-nitro-5-mercaptobenzoic acid (TNB) is a yellow product with the maximum absorption at 412 nm. The rate of TNB formation is proportional to the concentration of GSH in the serum.

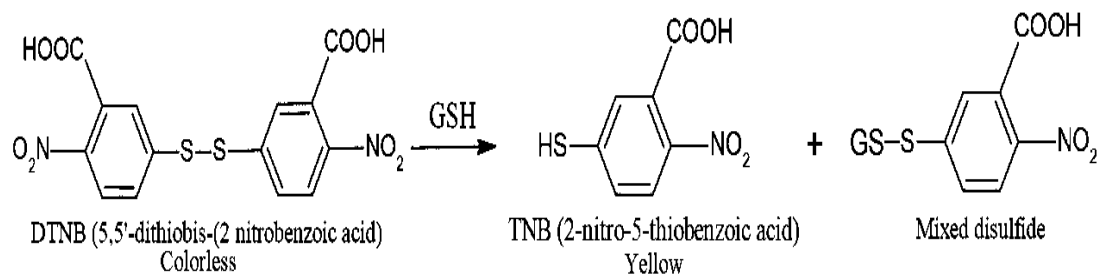


Figure 2-15: The chemical reaction to determination of GSH

- Reagents

Reagent I: Acid reagent

Reagent II: Reduced glutathione (GSH) standard solution

Reagent III: Phosphate buffer

Reagent IV: DTNB solution

Reagent V: Salt reagent

- Procedure

1- Pretreatment of the specimen: 0.5 ml of the sample was added to 0.5 ml of reagent I, then centrifugated at 4000 g for 10 min and collected the supernatant for measurement.

2- Reagents were added as the following table:

Table 2-14: Addition of reagents to determination of GSH

Reagent name (mL)	Specimen tube (A_{Specimen})	Standard tube (A_{Standard})	Blank tube (A_{Blank})
Reagent I	---	---	1
Reagent II	---	1	---
Specimen	1	---	---
Reagent III	1.25	1.25	1.25
Reagent IV	0.25	0.25	0.25
Reagent V	0.05	0.05	0.05

The mixture in each tube was mixed fully and stand for 15 minutes at room temperature. The spectrophotometer was adjusted to zero with de-ionized water at the wavelength 412 nm, and measured absorbances, A_{Specimen} , A_{Standard} and A_{Blank} . Then recorded, $\Delta A_1 = (A_{\text{Specimen}} - A_{\text{Blank}})$ and $\Delta A_2 = (A_{\text{Standard}} - A_{\text{Blank}})$

- **Calculation:**

$$[\text{GSH}] (\mu\text{mol/mL}) = \frac{\Delta A_1}{\Delta A_2} \times C \times M \times 2 \times F$$

Where, C = Concentration of standard, 20×10^{-3} $\mu\text{mol/mL}$, M = Molecular weight of GSH, 307 gm/mol, 2 = Dilution factor of sample pretreatment, 2 times and F = Dilution factor of sample before test.

2-10-3-5 Estimation of Malondialdehyde Assay

- **Principle**

The level of lipid peroxidation can be shown by detecting the level of malondialdehyde (MDA). Under acidic and high temperature conditions, MDA in the sample was reacted with thiobarbituric acid (TBA) to produce the pinked color MDA-TBA adduct which can be easily measured at the wavelength 532 nm.

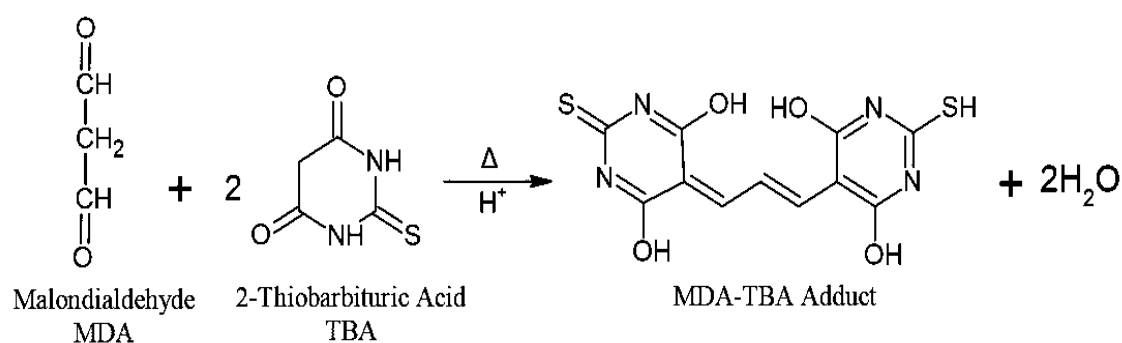


Figure 2-16: The chemical reaction to determination of MDA

Increasing levels of MDA or other reactive aldehydes cause a linear increase in the color. The content of lipid peroxidation can be estimated after colorimetric. But the soluble sugar will disturb the detection, the production (color reaction of soluble sugar with TBA) as absorption wavelength of 450 nm and 532 nm. In this kit, the MDA content is calculated by the difference between the absorbance at 532 nm, 450 nm, and 600 nm. Because of sucrose in plant tissues and glucose in animal tissues, this kit has two computational formulas for sucrose and glucose. The two formulas are suited for fat.

- **Reagents**

Reagent I: Malondialdehyde (MDA) standard

Reagent II: Sample diluent (diluted hydrochloric acid)

Reagent III: TBA (2-Thiobarbituric acid)

The spectrophotometer was run for 30 minutes, and set the counter to zero with de-ionized water.

- **Procedure**

The reagents were added as the following table:

Table 2-15: Addition of reagents to determination of MDA

Reagent (ml)	Specimen tube (A _{Specimen})	Blank tube (A _{Blank})
Reagent I	0.3	0.3
Specimen	0.2	-
De-ionized water	-	0.2
Reagent II	0.2	0.2
Reagent III	0.3	0.3

The mixture was incubated at 25 °C for 60 minutes with shaking tightly closed to prevent moisture loss, then centrifuged at 10000 g for 10 minutes at room temperature to remove insoluble materials. The produced supernatant was taken and transferred to 1 mL glass cuvette, and then the absorbance was measured at 450 nm, 532 nm, and 600 nm.

$$\Delta A_{450} = A_{450}(\text{Specimen}) - A_{450}(\text{Blank})$$

$$\Delta A_{532} = A_{532}(\text{Specimen}) - A_{532}(\text{Blank})$$

$$\Delta A_{600} = A_{600}(\text{Specimen}) - A_{600}(\text{Blank})$$

The blank tube needs to test once or twice.

- **Calculation:**

$$[\text{MDA}] (\mu\text{mol/mL}) = \left[\frac{(6.45 \times (\Delta A_{532} - \Delta A_{600}) - 1.29 \times \Delta A_{450}) \times V_{rv}}{V_s} \right]$$

$$= 5 \times (6.45 \times (\Delta A_{532} - \Delta A_{600}) - 1.29 \times \Delta A_{450})$$

Where, V_{rv}: Total reaction volume=1 mL, V_s: Sample volume=0.2 mL.

2-10-3-6 Estimation of Nitric Oxide Scavenging Assay

- **Principle**

Nitric Oxide (NO) is easily oxidized to form (NO₂⁻) and (NO₃⁻) in the body or an aqueous solution. This method uses the nitrate reductase to reduce (NO₃⁻) to (NO₂⁻) specifically. Under acidic conditions, NO₂⁻ and Diazonium sulfonamide produce diazo compounds. The compounds could further couple with naphthyl ethylenediamine. The product has a characteristic absorption peak at 540 nm, and its absorbance value can be measured to calculate the NO content.

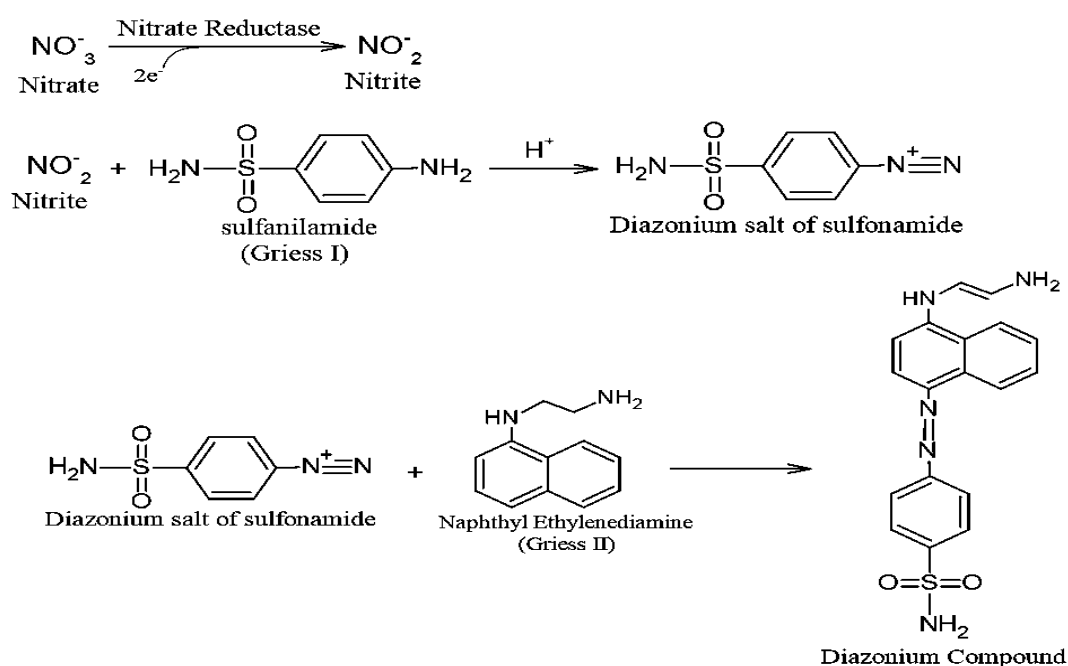


Figure 2-17: The chemical reaction to determination of NO

- **Reagents**

Reagent I: Sodium nitrite (NaNO₂) standard

Reagent II: Griess I (Sulfanilamide)

Reagent III: Griess II (Naphthyl ethylenediamine)

Reagent IV: VCl₃ reagent

Reagent V: ZnSO₄

- **Preparation of Standard Curve**

- 1- Using 10 μmol/mL of NaNO₂ standard to prepare standard curve as describe in the following table.

Table 2-16: Preparation of standard solutions to determination of NO

Volume of 10 (μmol/mL) NaNO ₂ Standard (mL)	Volume De-ionized water (mL)	Standard solution concentration (μmol/mL)
10	0	10
5	5	5
2.5	7.5	2.5
1.25	8.75	1.25
0.625	9.375	0.625
0.3125	9.6875	0.3125
0.1562	9.8438	0.1562
0	10	0

- **Procedure**

1- Working reagent: The freshly working reagent was prepared by mixing 2 mL VCl₃ reagent, 4 mL Griess I reagent and 4 mL Griess II reagent.

2- A 0.2 mL of diluted standard solution and sample were added to separate Eppendorf tube, then added 0.3 mL of working reagent to each standard and sample tube.

3- The mixture was mixed well and incubated the reaction at 25°C for 30 minutes.

4- The reaction tubes were briefly centrifuged to pellet any condensation, then transferred 0.25 mL of each reaction to new separate Eppendorf tube.

5- The spectrophotometer was run for 30 minutes, then set the counter to zero with de-ionized water at the wavelength 540 nm.

6- Absorbances were measured as A_{Standard}, A_{Specimen} and A_{Blank} (de-ionized water)

- **Calculations:**

1- The standard curve was created by plotted $\Delta A_{1(540)}$ as Y-axis and prepared standard concentration as X-axis, then determined the slope using linear regression fitting ($y = mx + b$).

2- The NO concentration of specimen was calculated as:

$$[\text{NO}] (\mu\text{mol/ml}) = \frac{(\Delta A_{2(540)} - b)}{a \times f}$$

Where, $\Delta A_{1(540)}$: absolute ($A_{\text{Standard}} - A_{\text{Blank}}$), $\Delta A_{2(540)}$: absolute ($A_{\text{Specimen}} - A_{\text{Blank}}$), a: the slope of standard curve and f: dilution factor of sample before test.

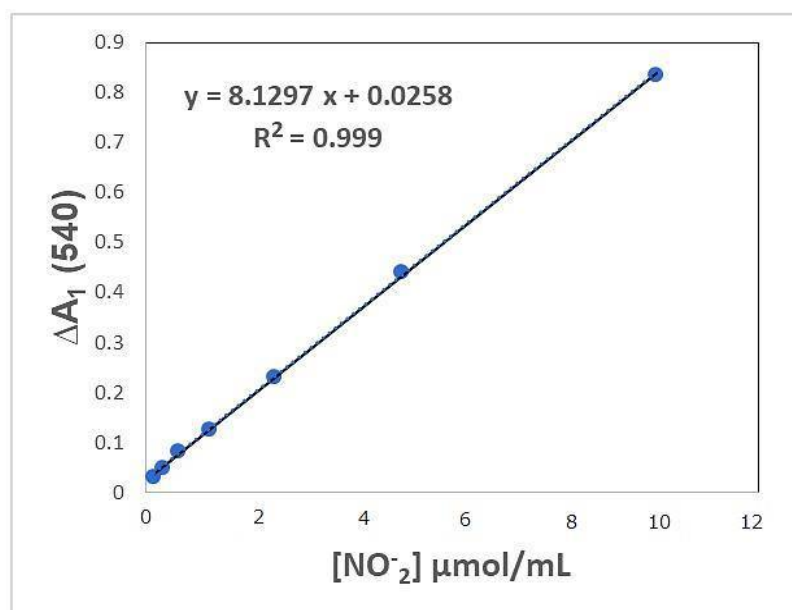


Figure 2-18: Standard curve of NO

2-11 Histological Study

- **Histological Technique (E & H) stain**

The kidneys and livers of rats were histological examination with a light microscope for assessment of histological alterations [181], as the following steps:

1-Fixation

The specimen fixated in the formalin 10 % for 24 – 48 hours.

2-Washing and Dehydration

After fixation, the specimens were washed with water to remove the fixative to avoid the interaction between the fixative and staining materials used later. By dehydration, the water had been completely extracted from fragments by bathing them successively in a graded series of ethanol and water (70 %, 80 %, 90 %, and 100 % ethanol).

3-Clearing

Bathing the dehydrated fragments in solvent (xylene) for 30 – 60 minutes, this step was repeated 3 times. As the tissues cleared, they generally became transparent.

4-Infiltration and Embedding

Once the tissue fragments were impregnated with the solvent, they were placed in melted paraffin in an oven, typically at 52 °C. The heat

causes the solvent to evaporate, and the space within the tissues becomes filled with paraffin.

5-Sectioning

After cooling from the oven, the specimen left at room temperature to be solid and removed from their containers to section. They were put in the rotary microtome and were sliced by the microtome, a steel blade into sections 5 micrometers thick. The sections were floated on a water bath (50-55 °C), then transferred into glass slides coated with Mayer's albumin as an adhesive substance and left to dry.

6-Staining

The histological sections of the studied organs were stained with Hematoxylin - Eosin stain.

2-12 Statistical Analysis

The results were expressed as mean \pm standard deviation (SD) of studied groups using the analysis of variance test (one way-ANOVA) followed by Tukey post hoc test to determine the differences between the averages with statistical significance at $P \leq 0.05$. All statistical analyses were performed by Statistical Package for the Social Sciences Software (Version 26, SPSS Inc., Chicago, IL, USA).

Chapter Three

Results and Discussion

3 Results and Discussion

3-1 Qualitative Analysis of the Phytochemicals in the *Ziziphus-spina christi* Leaves Aqueous and Alcohol Extracts.

The present study screening of phytochemicals from some selected *Z.-spina christi* leaves extract were carried out. Phytochemicals were extracted by organic solvents, including ethanol and aqueous extract. The result was showed that the presence of phytochemical constituents. The presence of mentioned components in these plants clearly confirm that these plant species are rich indigenous sources for pharmaceutical industries.

Investigation of the crude phytochemical compounds presented in the *Z.-spina christi* leaves extract is shown in table 3-1. *Ziziphus-spina christi* leaves are rich in chemical constituents. Flavonoids, alkaloids, terpenoids, phenolic compounds, steroids, saponins, tannins, proteins, amino acids, quinines, and carbohydrates have been documented in this study, that was helped to know biological effect of these constituents in the plant extracts.

Phytochemicals in *Z.-spina christi* leaves have a significant role in reductant, capping, and stabilizing the nanoparticles. Flavonoids and phenolic compounds play a principal role in the reductant of metal precursor salts. As flavonoids have various functional groups, which are capable of reductant metal ions to nanoparticles, the OH groups present in phenols and flavonoids can reduce and stabilize the zinc compounds into ZnO-NPs. Also, tannins and saponins may act as the capping agents [182], [183].

Table 3-1: Qualitative analysis of the phytochemicals in the *Ziziphus-spina christi* leaves aqueous and alcohol extracts.

	Phytochemical Screening	Reagents Used	Detection indicator	Results
Aqueous Extract	Proteins and amino acids	Xant oproteic	Yellow color	++
		Biuret	Violet color	++
	Alkaloids	Dragendorff's	Orange-brown spots	-
	Flavonoids	50% Et anol+ 50% NaOH	Dirty yellowis	++
	Saponins	Distilled water	Foam	+
	P enolic Compounds	2% Ferric c loride	Brownis color	++
	Carbo ydrates	Benedict	Orange red color	+++
	Terpenoids and Steroids	C loroform and H ₂ SO ₄	Terpenoids Reddis -brown color	+
			Steroids	-
	Coumarins	10% NaOH	Yellow color fluorescence	+
	Tannins	10% KOH	Dirty w ite precipitate	++
	Resins	4% HCl	Strong turbidity	+
	Quinines	Alco olic KOH	Red to blue color	+
	Fats and Oils	Stain test	Oil stain	++
Alcohol Extract	Proteins and amino acids	Xant oproteic	Yellow color	+
		Biuret	Violet color	+
	Alkaloids	Dragendorff's test	Orange-brown spots	+++
	Flavonoids	50% Et anol+ 50% NaOH	Dirty yellowis	++
	Saponins	Distilled water	Foam	++
	P enolic Compounds	2% Ferric c loride	Brownis color	++
	Carbo ydrates	Benedict	Orange red color	++
	Terpenoids and Steroids	C loroform and H ₂ SO ₄	Terpenoids Reddis -brown color	++
			Steroids green-blue color	+
	Coumarins	10% NaOH	Yellow color fluorescence	+
	Tannins	10% NaOH	Formation of emulsion	++
	Resins	4% HCl	Strong turbidity	++
	Quinines	Alco olic KOH	Red to blue color	+
	Fats and Oils	Stain test	Oil stain	+

Source: Experimental results

(+) Presences of constituents, (++) moderate presences of constituents,

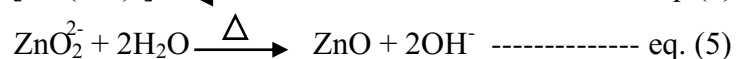
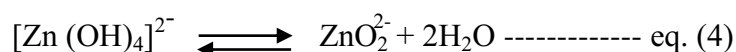
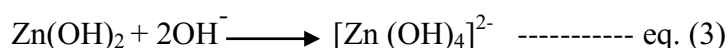
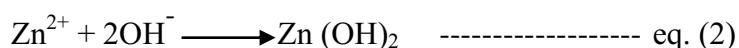
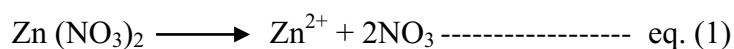
(+++) ig presence of constituents, (-) Absence of constituents.

3-2 Biosynthesis of Zinc Oxide Nanoparticles

T e synt esis of ZnO-NPs using biological tec niques as received a lot of interest recently, mainly to its safety, eco-friendliness, and low cost, in addition to t e removal of ig energy or armful c emical by-products utilized in c emical met ods [184].

The color change was the first indication for synthesis ZnO-NPs, and this change was observed after 15 minutes when mixed the solution of zinc nitrate hexahydrate salt with the aqueous extract of *Z.-spina christi* leaves. The principal behind nanoparticle production was the reduction of zinc nitrate hexahydrate ($Zn(NO_3)_2 \cdot 6H_2O$) into ZnO-NPs by the phytochemicals involved in the plant extract. The color of the solution was changed from yellow into deep yellow and the intensity of color increased with time until the solution was changed into a brownish yellow colored pellet (Figure 3-1a). The nanoparticle synthesis process was detected by UV-visible spectroscopy. Finally, the pellet of ZnO NPs was dried after the completion of the process, and a yellowish-white color ZnO-NPs powder was obtained (Figure 3-1b).

The synthesis of ZnO-NPs involved a redox process. The crude extract solution was added to act as a reducing agent that reduced Zn^{2+} into Zn and stabilizer for ZnO-NPs, which maintains the size of particles formed on a nano scale by capping them from coming into contact with each other. The first indication for ZnO-NPs construction the cloudy solution was formed that the occurrence of reduction reaction. Addition of sodium hydroxide NaOH act as an accelerant to enhance the rate of reduction and nucleation process by direct precipitation of Zn^{2+} to zinc hydroxide $Zn(OH)_2$ in alkaline condition (pH 9) followed by loss of water. ZnO molecules were accumulated to form ZnO-NPs [185], [186]. The related chemical reactions are shown in the equations below and the change of color gradually was followed by UV-visible spectroscopy with time.



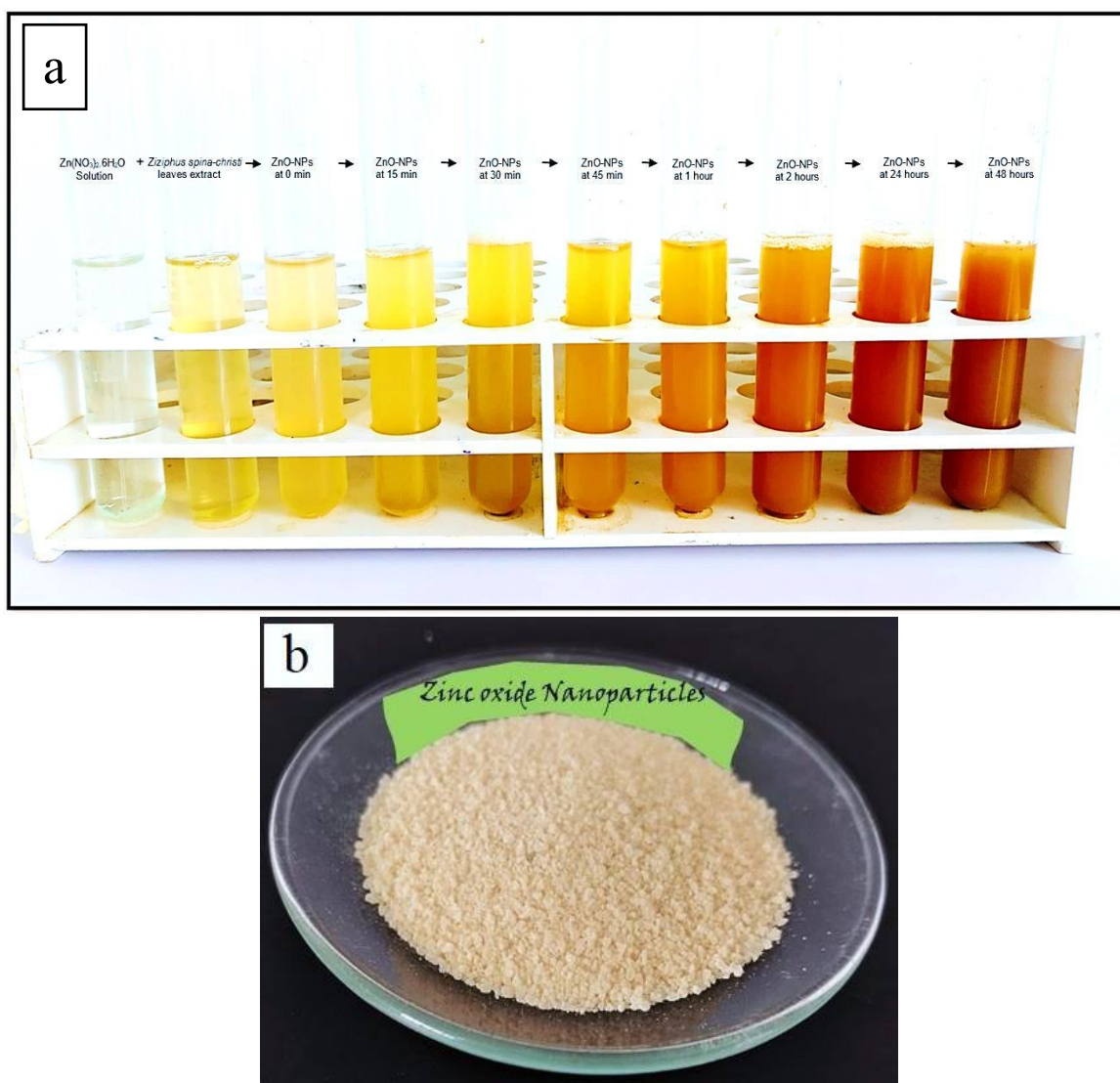


Figure 3-1: (a) The gradual change in the color of the synthesized ZnO-NPs from *Z.-spina christi* leaves and zinc nitrate hexahydrate with time (0 min-48 hours). (b) Yellowish-white powder of the synthesized ZnO-NPs.

Reaction time is also considered as the significant factor, where the reaction time is the period required for the complete reduction of the metal ions for the synthesis of ZnO-NPs. Results indicate that no absorption peak was observed at 15 minutes to 1 hour (Figure 3-2). The reaction time was processed until reacted 2 , A distinct absorption peak will be observed at this time at a wavelength of 362 nm, this result is consistent with previously published studies on *Catharanthus roseus* leaves where observation peak was also recorded at 2 [187], and on *C. roseus*, where observation peak was also recorded at 3 [188].

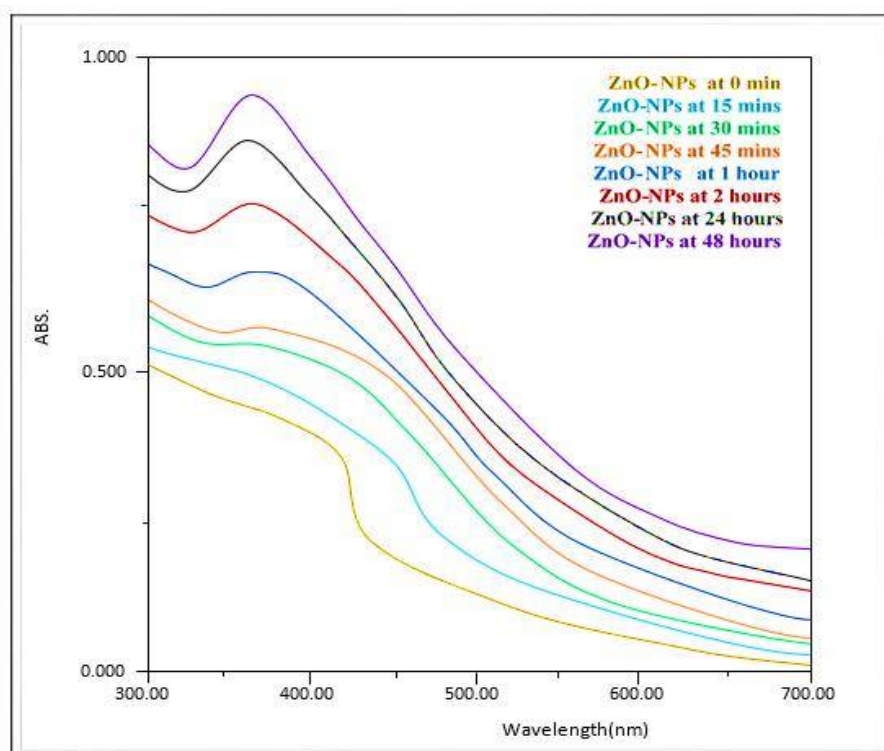


Figure 3-2: UV-Visible spectra of the synthesized ZnO-NPs at different times

strengt of t e absorption peak was increased as t e duration mixing of *Z.-spina christi* leaves extracts wit $Zn(NO_3)_2 \cdot 6H_2O$ solution. An increase in t e absorbance intensity wit t e time means t e nucleation and growt processes started to t e production of ZnO-NPs [189]. Even after 48 ours, t e absorbance remained constant, s owing t at t e reaction was complete and t e ZnO-NPs produced were stable at room temperature. T e gradual c anges in t e color of mixture were followed by measuring UV-visible absorption wit time, t is color c ange of mixture due to t e presence of bioactive compounds in t e aqueous extract of *Z.-spina christi* leaves. Various p ytochemicals are responsible for t e reduction of zinc ions Probably, flavonoids or p enolic compounds in aqueous extract, w ic possible, w ile saponins and tannins may act as t e capping agents. Furt ermore, because of OH groups are abundant in t e p enols and flavonoids, t ese act as stabilizing agents and bio-reducing of zinc compounds into ZnO-NPs [190].

3-3 Characterization of Synthesized Zinc Oxide Nanoparticles

3-3-1 Ultraviolet-Visible Spectroscopy (UV-Vis Spectroscopy)

The synthesized Zn-ONPs were analyzed using UV–vis spectra at room temperature and the scanning of the wavelength ranged between 200 and 700 nm (Figure 3-3). The results showed Surface Plasmon Resonance (SPR) absorption band was at 362 nm. At this wavelength, the absorption may be due to the band gap energy (E_{bg}) of the valence band (V_B) and conduction band (C_B) for ZnO-NPs based on the equation below, where was the bound electron in V_B for ZnO-NPs always trends to be raised to C_B by absorbing the energy from the ultraviolet light.

$$E_{bg} = \frac{c}{\lambda}$$

Where, h = Planck's constant (6.63×10^{-34} m² kg/s), c = speed of light (3.00×10^8 m/s), λ = absorption wavelength in UV region (362 nm).

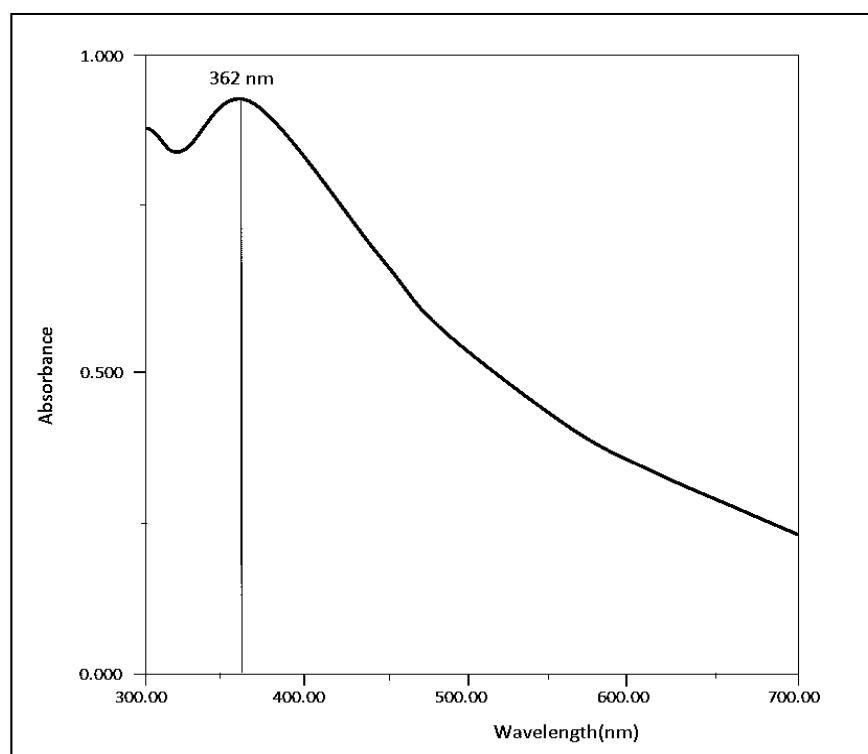


Figure 3-3: UV-Visible spectra of the synthesized ZnO-NPs.

To evaluate the effect of the boiling time to preparation of *Z. spina christi* leaves extract, the dry leaves were boiled for 10, 15, and

20 minute respectively. The UV-Vis spectrum of synthesized ZnO-NPs was measured at different times. Results noticed that the boiled time did not significantly impact on the yield of ZnO-NPs and they are very little difference in the formation of ZnO-NPs in 10 and 20 minutes boiling time. Whereas, 15 minutes boiling time increased the formation of ZnO-NPs (Figure 3-4). After 15 minutes of boiling, slightly declined the yield of ZnO-NPs due to the possibility of the dissociation of some phytochemical constituents. In addition, the longer boiling time causes more consumption of energy, therefore the suitable boiling time for preparation of the aqueous extract of *Z.s-spina christi* leaves was selected as 15 minute for the following experiments [191].

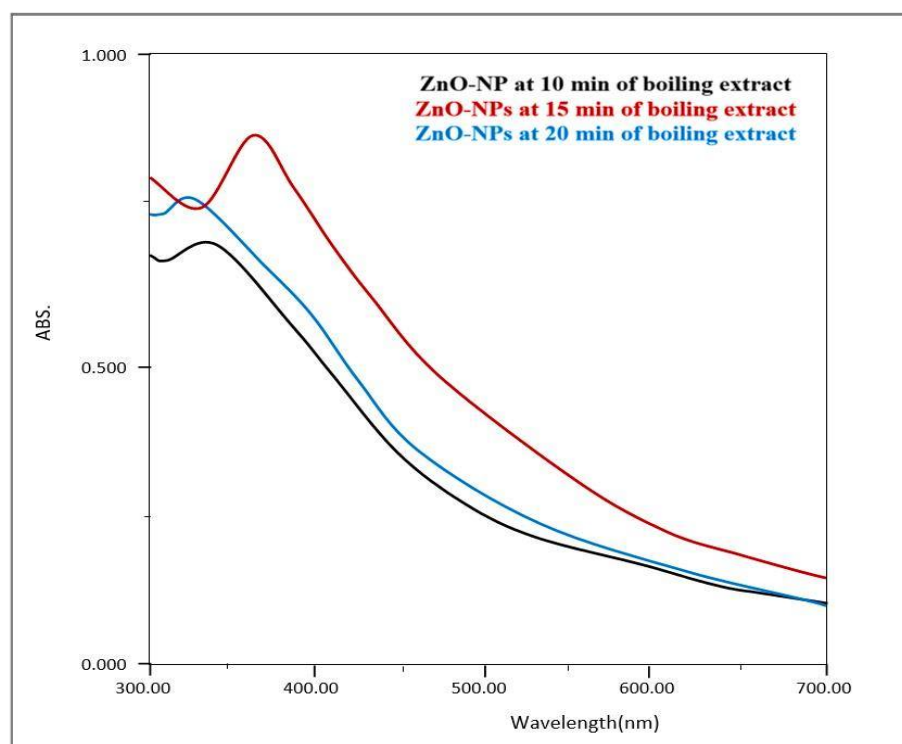


Figure 3-4; UV-Visible spectra of the synthesized ZnO-NPs at different boiling times of extract.

The different volume of 15 minutes boiled leaves extract (5, 10 and, 15 mL) respectively were added to 90 mL of 1 mM Zn (NO₃)₂.6H₂O solution. UV-visible spectra showed an increase in the absorbance intensity. UV-visible absorption spectra of ZnO-NPs were measured at different volume of *Z.-spina christi* leaves extract. Figure

3-5 shows the best volume was 10 mL of *Z.-spina christi* leaves extract than 5 and 15 mL and the nanoparticles synthesis occurred faster. Additionally, the maximum absorbance indicates the complete reducing of zinc ions and rapid synthesis of ZnO-NPs.

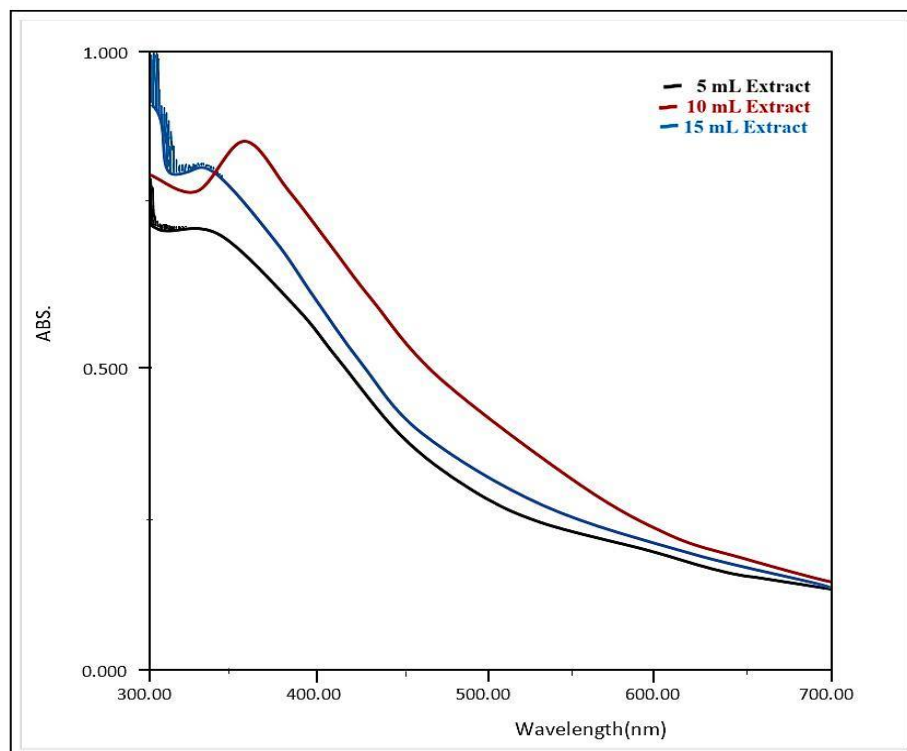


Figure 3-5: UV-Visible spectra of ZnO-NPs at different volumes of extract.

The quantity of phytochemicals present in the plant leaf extract as a significant role in the synthesis of metallic nanoparticles. Also, varying the amount of the leaf extract in the reaction medium might significantly affect on the shape of the prepared nanoparticles [192]. When the content of *Z.-spina christi* leaves was increased, the yield of ZnO-NPs gradually increased and preventing nanoparticles from aggregating as well as their stability was increased due to the increase in the flavonoid, phenolic, and other plant components [193]. Finally, when using a large amount of plant extract, phytochemicals strongly confirmed the reduction reaction and function as stabilizing and capping agents [194].

The concentration of $\text{Zn}(\text{NO}_3)_2 \cdot 6\text{H}_2\text{O}$ as a significant effect on the green synthesis of ZnO-NPs. If the concentration of Zn

$(\text{NO}_3)_2 \cdot 6\text{H}_2\text{O}$ increased the absorption would have increased. However, the concentration 1 mM is considered optimal for the ZnO-NPs synthesis. Also, increasing the $\text{Zn}(\text{NO}_3)_2 \cdot 6\text{H}_2\text{O}$ concentration resulted in an increase in the size of nanoparticles. Moreover, the 2 mM and 3 mM concentrations showed the lowest absorption intensity and no clear peaks (Figure 3-6). The morphology and crystal size of ZnO-NPs based on the concentration of metallic salt precursors, and capping agents (plant extracts) used. So, these parameters play the principal role in the synthesis of ZnO-NPs and other nanostructured compounds [195]. These results confirmed that concentrations of $\text{Zn}(\text{NO}_3)_2 \cdot 6\text{H}_2\text{O}$ and plant extract largely affect the crystallite size and the morphology of the ZnO-NPs [196]. Various researchers were reported that the synthesis of nanoparticles utilizing low concentration of metallic precursor always result in the formation of nanoparticles with smaller crystallite size [197], [198].

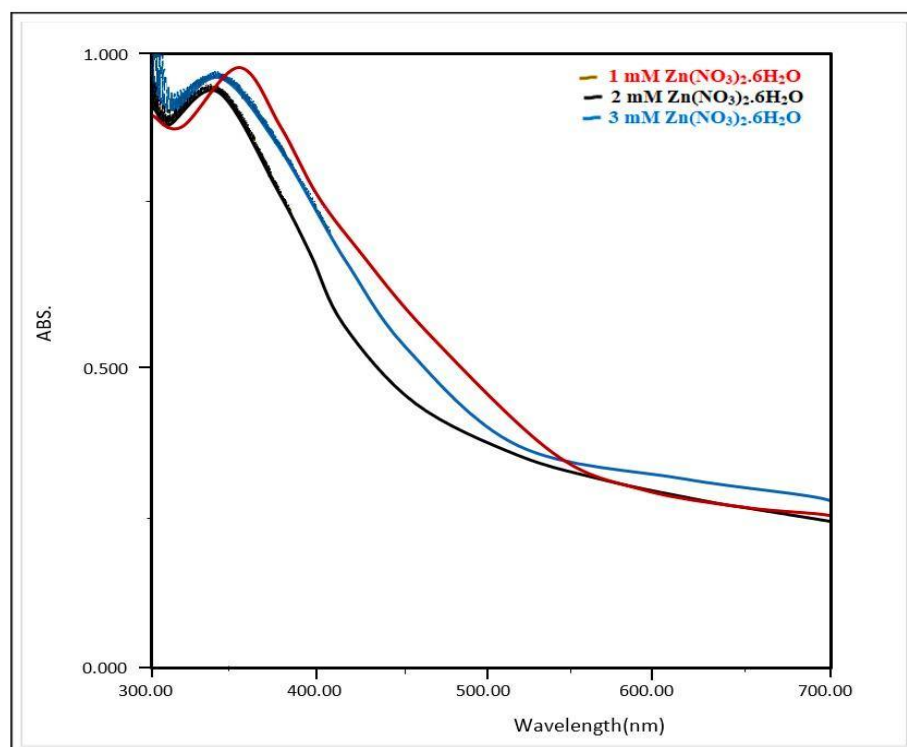


Figure 3-6: UV-Visible spectra of ZnO-NPs at different concentrations of $\text{Zn}(\text{NO}_3)_2 \cdot 6\text{H}_2\text{O}$.

The green synthesis of the ZnO-NPs from the *Z. spinosa* cristi leaf extract was performed at different pH (5-10) using litmus paper (a

strip of test paper is immersed in a solution whose pH is needed to be determined, if the strip is red (at any pH less than 5) and if blue (at any pH greater than 8), that assist of the laboratory technician to determine whether a solution is acidic or basic. So, pH of the reaction medium defines the structural types of the synthesized ZnO-NPs [199]. The findings showed that the absorbance of the formed ZnO-NPs was increased gradually from pH 8.0 to 9.0, while decreased between pH 9.0 and 10.0. It was found that at pH 9.0, the characteristic absorption peak of ZnO-NPs observed at 362 nm (Figure 3-7), suggested that at pH 9.0, which indicated the metal oxide reduction and zinc nitrate hexahydrate was converted to ZnO-NPs when be the reaction medium at alkaline condition that was more favorable to the synthesis of ZnO-NPs than acidic or neutral condition. Finally, when the pH was lower lead to the decreases in ZnO-NPS production.

The crystallite size and surface morphology strongly depended on the pH of reaction mixture throughout the synthesis process, due to the pH was changed the electrical charge of molecules and will be affect their reduction [200]. Throughout the synthesis of ZnO-NPs in an acidic medium (at pH 5 and 6), the hydroxyl ion (OH^-) is less in the solution which limits hydrolysis and condensation processes, resulting in the smaller aggregates [201]. The decrease in the crystallite size of ZnO-NPs in an acidic medium was due to the dissociation of the crystal structure of ZnO-NPs [202]. When the pH of the solution reached 7 (neutral), ions concentrations of hydrogen (H^+) and hydroxyl (OH^-) are

are high, causing a strong attraction between Zn^+ and OH^- ions; then,

OH^- is high in a solution leading to the formation of intermediate products such as zinc hydroxide

($\text{Zn}(\text{OH})_2$) (see eq. 2) and salt-containing tetra hydroxozincate ion ($[\text{Zn}(\text{OH})_4]^{2-}$) (see eq. 3). The drying of ZnO-NPs product in the oven, then calcination in the furnace lead to the formation of good crystallite sizes of ZnO-NPs [204]. Similar results were reported in the study effect of the pH (5.0–10.0) on the synthesis of ZnO-NPs using *Aloe vera* skin extract [205] and found that the optimum pH required for the biosynthesis of ZnO-NPs was 8.0. Therefore, in the following experiments, ZnO-NPs were synthesized at pH 9.0.

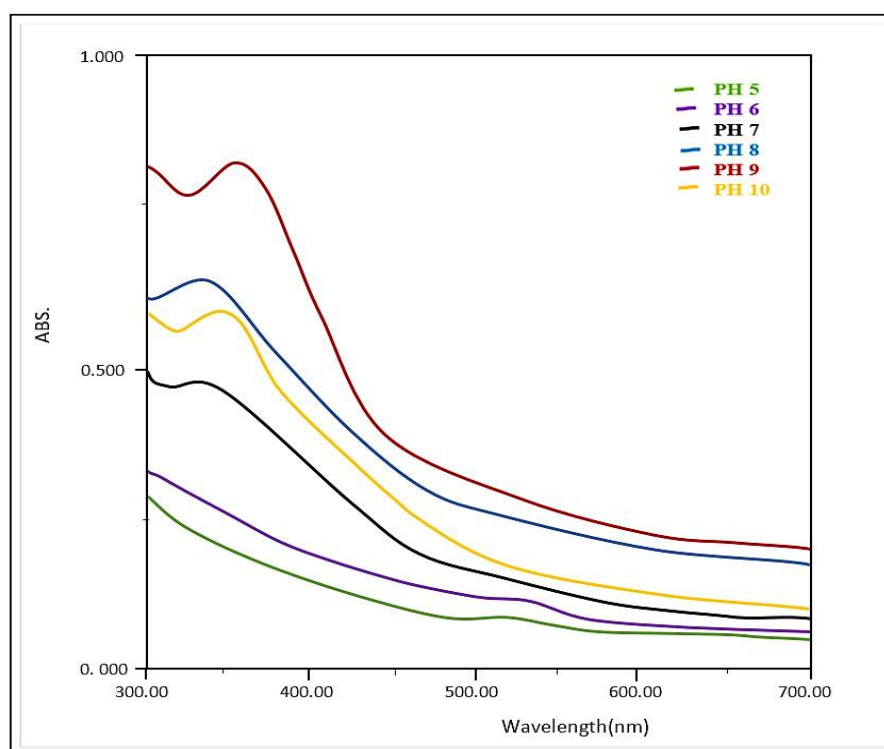


Figure 3-7: UV-Visible spectra of Zn-NPs at different pH.

The reaction temperature is critical in the synthesis of ZnO-NPs. The effect of varying temperatures on ZnO-NPs production is investigated at temperatures ranging from 40 to 70 °C. As shown in figure 3-8, no characteristic absorption peaks were observed at lower temperatures of 40 and 50 °C, whereas characteristic absorption peaks were observed at higher temperatures (60 and 70 °C). In comparison with other temperatures. The maximum synthesis of ZnO-NPs was observed at 60 °C, and a sharp peak was appeared by a UV-vis

spectrophotometer at 362 nm. On the other side, it is clear that with the rise in temperature from 60 °C, the absorption bands of ZnO-NPs showed similar patterns with slight and extremely broad peaks.

The reaction temperature had a considerable influence on the synthesis of ZnO-NPs. When the temperature was changed to 60°C, the typical absorption peak at 362 nm was detected. The higher the activation energy of molecules, the faster the reaction rate, resulting in a decrease in the size of the nanoparticles formation of monodispersed smaller-sized nanoparticles. UV-visible spectroscopy findings from the synthesized ZnO-NPs at various temperatures revealed peaks at 376 nm, 370 nm, 362 nm, and 348 nm for 40°C, 50°C, 60°C, 70°C respectively (Figure 3-8).

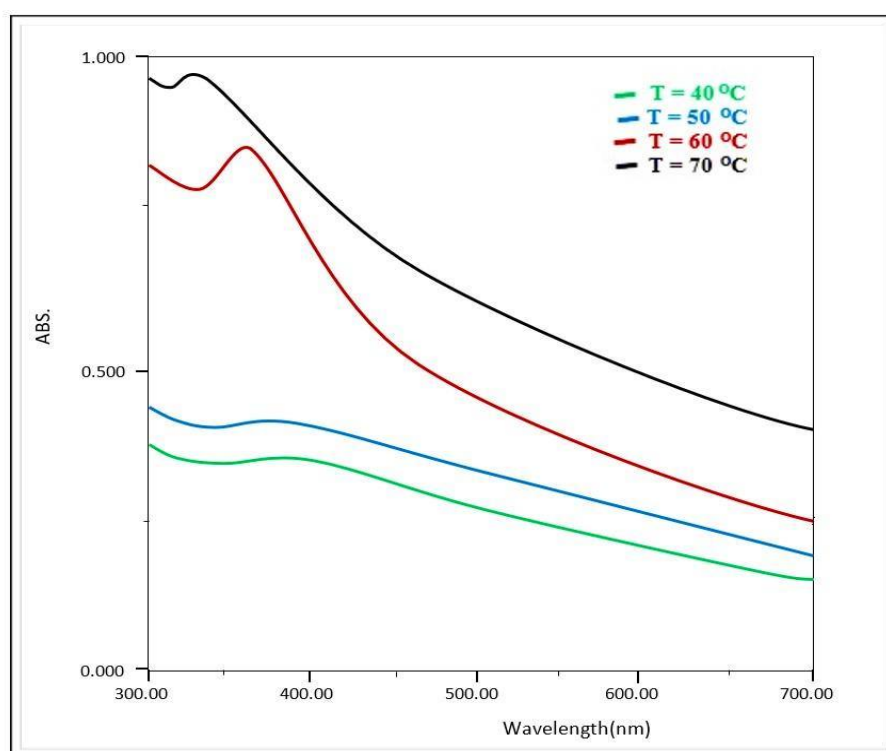


Figure 3-8: UV-Vis spectra of ZnO-NPs at different temperatures

The synthesized ZnO-NPs were optimized by several parameters, *Z.-spina christi* leaves were boiled with de-ionized water for 15 minutes, 10 mL leaves extract, the concentration of Zn (NO₃)₂.6H₂O solution was (1 mM), pH of the mixture adjusted at 9, and the

temperature of the mixture at 60 °C with magnetic stirrer for 2 hours, all these conditions were the best and selected for the biosynthesis of ZnO-NPs. These conditions were chosen due to the color change of the reaction mixture and increases of the absorbance intensity that indicated the increase of ZnO-NPs production.

In the present study, the absorption peak was observed in the UV-Visible spectroscopy at wavelength 362 nm (Figure 3-3), which was consistent with both [206], who found that ZnO-NPs have the absorption peak at 368 nm for the smaller size of crystals, and with [207], who revealed a blue shifted (13 nm) absorption wavelength than the bulk. Based upon these reports the absorption of the bulk-ZnO appeared near 375 nm and a blue shift (6 nm) could be observed for nanoparticles with a smaller size around 369 nm. Therefore, the characterization by UV-visible spectroscopy strongly supported the green synthesis of ZnO-NPs using the *Z.-spina christi* leaves extract.

3-3-2 Fourier Transform Infrared Spectroscopy (FT-IR)

Identifying and comparison of functional groups between the synthesized ZnO-NPs using *Z.-spina christi* leaves extract and the *Z.-spina christi* leaves extract alone is shown in figure 3-9. FT-IR spectrum of *Z.-spina christi* leaves extract alone (Figure 3-9a) showed the broad band observed at 3412.15 cm^{-1} corresponds to O-H stretching of phenolic and alcoholic compounds as well as carbohydrates [208]. Besides, the peak at 2918.06 cm^{-1} related to the stretching vibrations of C-H of aliphatic hydrocarbons chains, 1642.34 cm^{-1} (C=O stretching vibration) related to flavonoid and amino acids or carboxylic acid (COO^-) [209]. Moreover, 1454.10 cm^{-1} (O-H bending vibrations), 1398.28 cm^{-1} (C-O stretching of the ester group), 1234.25 cm^{-1} (C-O asymmetric stretching in cyclic polyphenolic compounds), and 1083.05 cm^{-1} to 681.70 cm^{-1} indicating the presence of (C-N stretching) aromatic

amines and alkyl alides, respectively [210]. The vibrational bands above were mostly found in the *Z. spina-Christi* leaves extract. These peaks disappeared or shifted to lower frequency indicating the successful participation of phytochemicals compounds presented in the *Z. spina-Christi* leaves as reducing and stabilizing agents in the synthesis of ZnO-NPs, which facilitates the conversion of metal ions to metal-NPs. This is shown by the peak for the shifted carbonyl groups (C=O) at 1612.48 cm^{-1} . The shifted peaks were, 3412.15 cm^{-1} to 3385.38 cm^{-1} , 2918.06 cm^{-1} to 2784.26 cm^{-1} , 1642.34 cm^{-1} to 1630.45 cm^{-1} , 1454.10 cm^{-1} to 1446.92 cm^{-1} , 1398.28 cm^{-1} to 1352.71 cm^{-1} and 1083.05 cm^{-1} to 972.13 cm^{-1} . Furthermore, the significant vibration of stretching peaks appeared at 491.75 , 443.22 , and 428.07 cm^{-1} (Figure 3-9b), corresponding to the Zn-O vibrational stretching that further confirmed the formation of ZnO-NPs.

The FT-IR spectrum validates the production of ZnO-NPs by comparing the positions and intensities of peaks in *Z.-spina christi* leaf extract to those generated in ZnO-NPs. Results demonstrated that the band locations and absorption intensities from the plant extract peak had changed and that new peaks appeared in the FT-IR spectra of the produced ZnO-NPs. The observed spectra suggested that biological substances produced by *Z.-spina christi* leaf extract were involved in the reduction and capping of ZnO-NPs. In this work, Zn^{2+} is assumed to react with biological components found in *Z.-spina christi* leaves extract, such as flavonoids, phenolic compounds, alkaloids, amino acids, tannins, and carbohydrates, to stimulate the production of ZnO-NPs and act as a capping and stabilizing agent. Finally, peaks at 491.75 , 443.22 , and 428.07 cm^{-1} in spectrum of the synthesized ZnO-NPs match to the stretching vibration of Zn-O bond that are absent in *Z.-spina christi* leaf extract, strongly confirmed the formation of ZnO-NPs. This finding was consistent with previous research, which found

multiple Zn-O bands at 416.14, 515, and 618 cm^{-1} [211], [212]. As a result, biological synthesis does not require any chemical sources for stabilizers, which is an advantage over chemical synthesis.

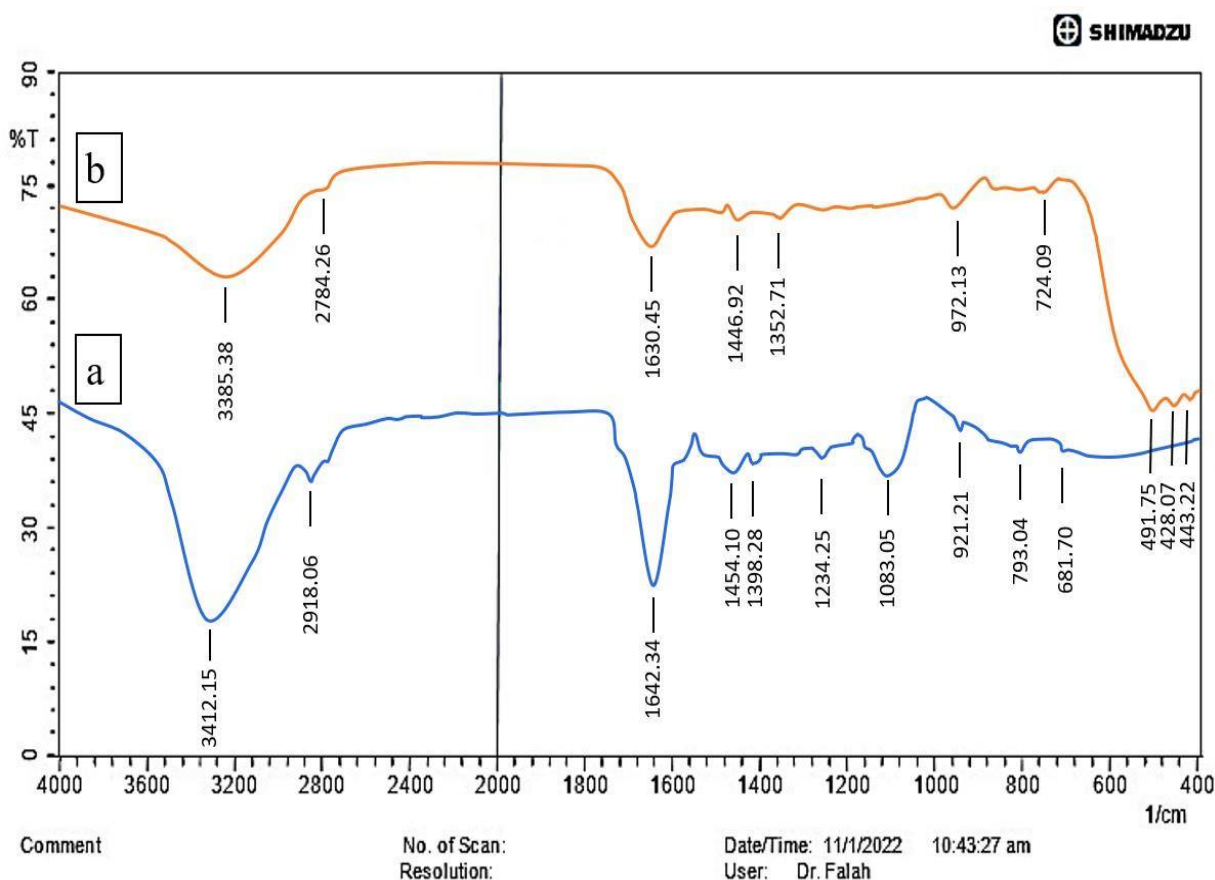


Figure 3-9: FT-IR spectrum, (a) *Z-spina christi* leaves extract (b) ZnO-NPs.

3-3-3 X-ray Diffraction (XRD)

The synthesized ZnO-NPs were studied and confirmed using the XRD technique to determine their phases, structures, and crystal size. The observed diffraction peaks of the biosynthesized ZnO-NPs in terms of intensities and positions were at 2θ 31.77° (100), 33.21° (002), 36.59° (101), 47.84° (102), 56.24° (110), 63.19° (103), 66.20° (200), 67.73° (112), 69.09° (201) 73.55° (004), and 76.67° (202) as shown in figure 3-10 which strongly detected the hexagonal wurtzite structure of ZnO-NPs. Based on the FWHM of most intense diffraction peaks (100%), (66%), and (41%) at 2θ with 36.59° (101), 33.21° (002), 31.77° (100) respectively. Using Debye-Scherrer equation, average

crystalline size was calculated to be 38.177 nm confirming the nano size for the synthesized ZnO-NPs.

As an X-ray passes through a particle crystal, a diffraction pattern is formed, which gives information on the atomic arrangement within the crystals. Peaks in the XRD diffractogram (Figure 3-10b) appeared to be broadening, revealing that perhaps the ZnO-NPs were formed on the nanoscale. When compared with the Joint Committee on Powder Diffraction Standards (JCPDS) card No. 36-1451 (Figure 3-10a), the most intense diffraction peaks found were indexed as the hexagonal wurtzite structure of ZnO-NPs with high crystallinity. As illustrated in Figure 3-10b, all of distinctive peaks were found to be ZnO-NPs, and no such impurities were found in produced ZnO-NPs. These findings were consistent with earlier research [213], [214].

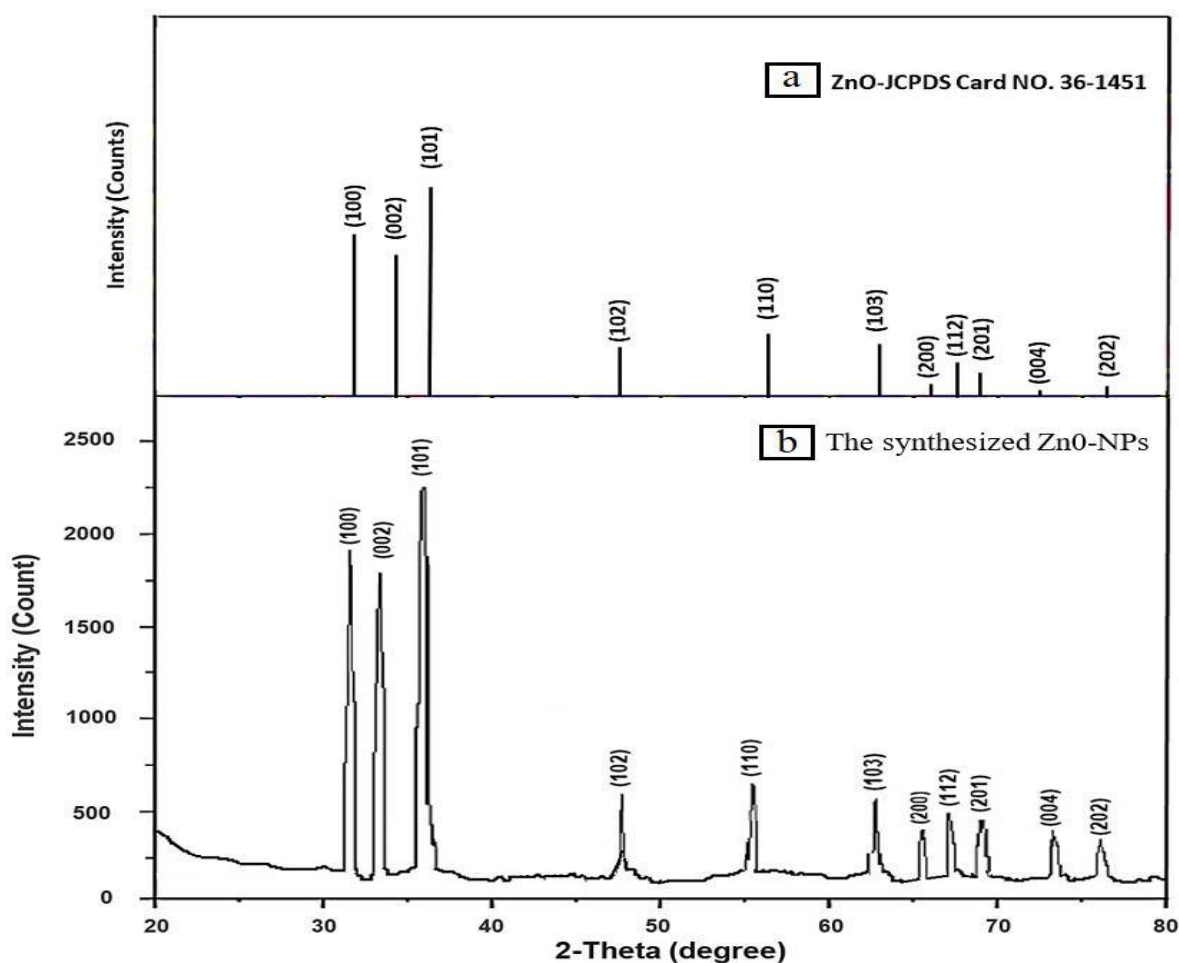


Figure 3-10: XRD diffractogram, (a) ZnO- card No. 36-1451. (b) the synthesized ZnO-NPs.

3-3-4 Transmission Electron Microscopy (TEM)

The size distribution and morphological characters of ZnO-NPs observed under TEM analysis (Figure 3-11a, b) were uniform in size. Agglomeration was common, due to the ultra-small size and high surface energy of ZnO-NPs. Also, TEM micrographs showed most of the ZnO-NPs were in a spherical shape. The histogram of the size distribution of ZnO-NPs was generated based on TEM data (Figure 3-11c). The majority of ZnO-NPs measured fell in the range of 35 - 45 nm in diameter.

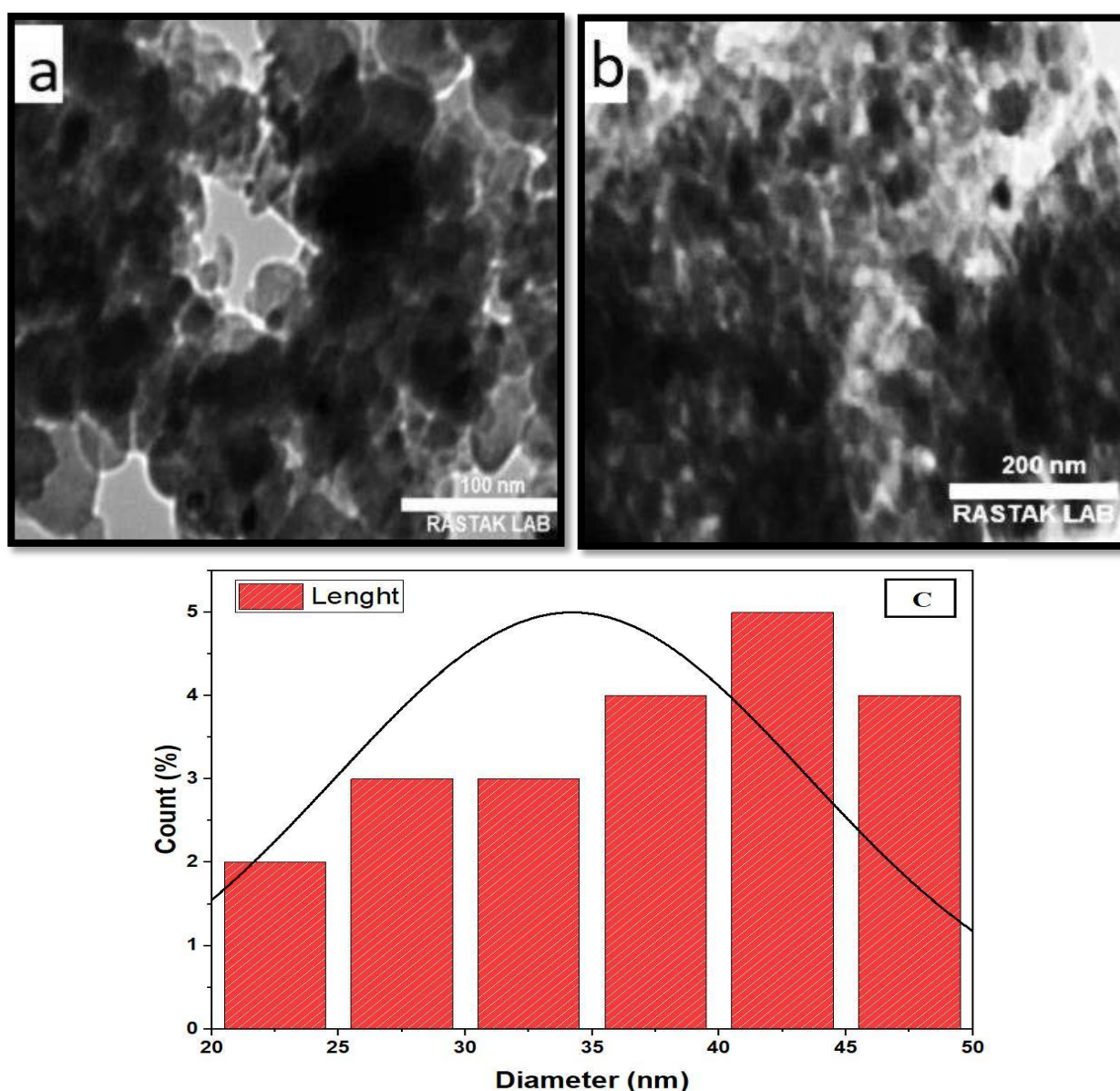


Figure 3-11: TEM micrograph of the synthesized ZnO-NPs. (a) Scale at 100 nm. (b) Scale at 200 nm. (c) The size distribution histogram of ZnO-NPs.

The TEM method was used to examine the biosynthesized ZnO-NPs. The acquired micrographs show that the biosynthesized ZnO-NPs were agglomerated particles that were spherical and hexagonal in shape. ZnO-NPs are capped by hexagonal molecules and biomolecules. Similar hexagonal molecules have been found in ZnO-NPs synthesis in *Euphorbia jatropha* plants [215]. The TEM pictures exhibit nanocrystalline of the synthesized ZnO-NPs, this is attributed to the biomolecules presented in *Z.-spina christi* leaf extract that strongly influenced the formation of ZnO-NPs. These findings are consistent with earlier publications [216], [217].

3-3-5 Scanning Electron Microscope (SEM)

Under SEM at varying magnifications, observations of images were made to study the surface morphology of the ZnO-NPs that were synthesized. The results of these observations can be found in Figure 3-12. In Figures 3-12a and b, it was observed that ZnO-NPs had a spherical shape and were tightly clustered together. Upon analysis of Figure 3-12c, particle diameters were noticed to have an average size in the following ranges: D_1 (39.74 nm), D_2 (42.25 nm), and D_3 (48.19 nm), with an average diameter size equal to be 43.39 nm.

The SEM image of ZnO-NPs (Figure 3-12) reveals spherical nanoparticles with high density. A large number of ZnO-NPs aggregated and formed nano-like morphology with agglomerated particles of various irregular shapes. Aggregation may be exacerbated by the high surface energy of ZnO-NPs as well as by the close distance between nanoparticles. These strongly confirm that the particles exist in a uniform form, and this uniformity plays an important role in the different activities of ZnO-NPs. SEM results in this study were in agreement with the previous studies [218], [219].

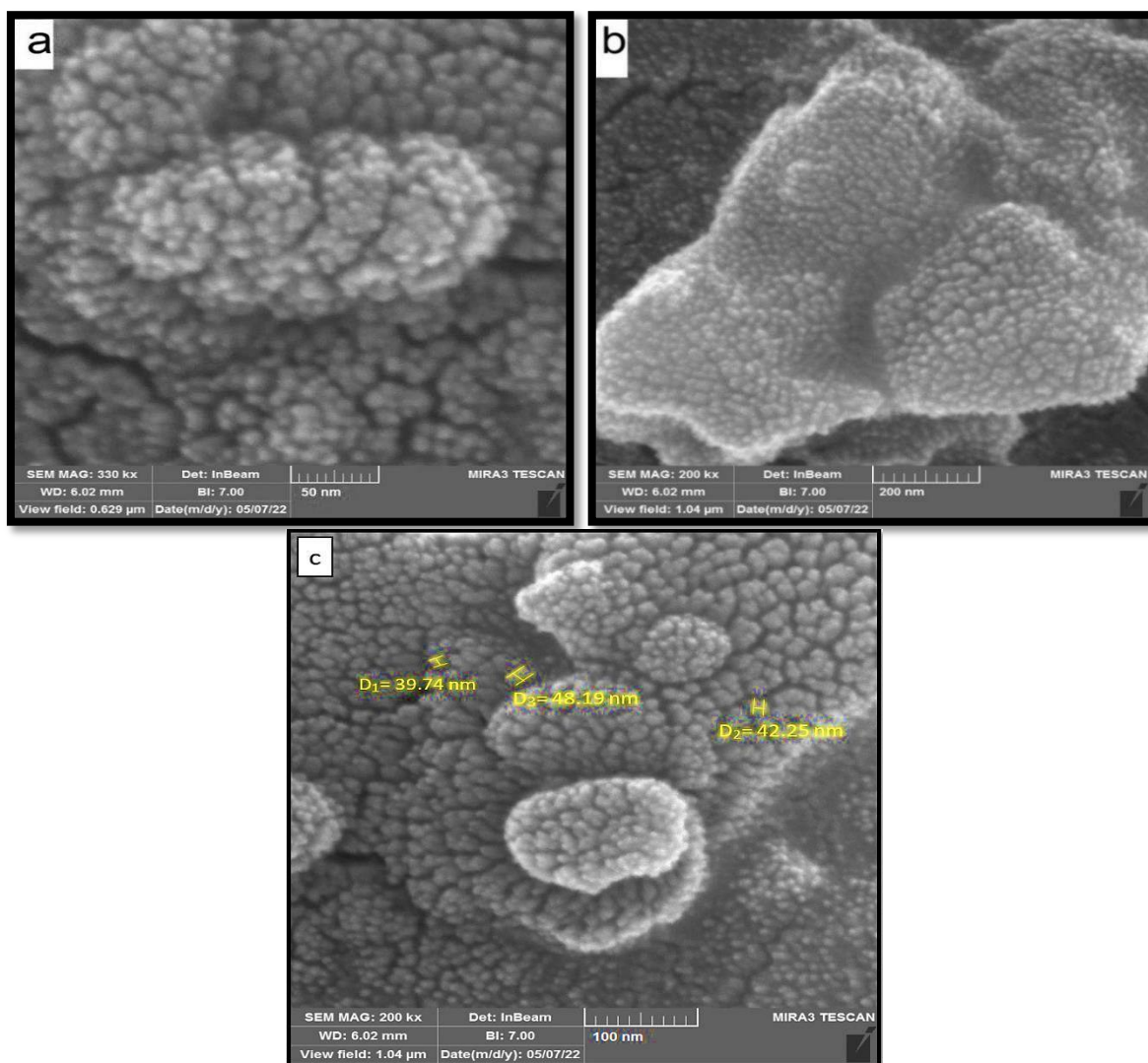


Figure 3-12: SEM images of synthesized ZnO-NPs at different magnifications (a) At 50 nm. (b) At 200 nm. (c) SEM images at 100 nm with the particle size at different average diameters D_1 , D_2 , and D_3 .

3-3-6 Atomic Force Microscopy (AFM)

Atomic force microscopy (AFM) analysis is a basic technique and inescapable for all nanoscopic studies was used to determine the topography surface of nanoparticles. Images of AFM for the synthesized ZnO-NPs (Figure 3-13a, b) showed the roughness and surface morphology features under AFM micrograph in two-dimension and three-dimension. The micrograph at (5.08x5.08 μ) scan (Figure 3-13b) display a uniform surface with cone like grains covering the surface of ZnO-NPs. In this study was determined the average surface roughness of the synthesized ZnO-NPs that found in the range of 42 to

45 nm due to the granularity distribution chart (Figure 3-13c). Moreover, AFM for the ZnO-NPs surface showed the three-dimension image that observed regularly in the composition of film and grains have a vertical structure on the crystal axis and are approximately equal. Figure 3-13c shows the granularity distribution chart of ZnO-NPs aggregates on the surface of the film. The surface roughness of ZnO-NPs was increased in the presence of capping agents due to the presence of various functional groups in *Z.-spina christi* leaves extract. These results were in agreement with the previous study [220].

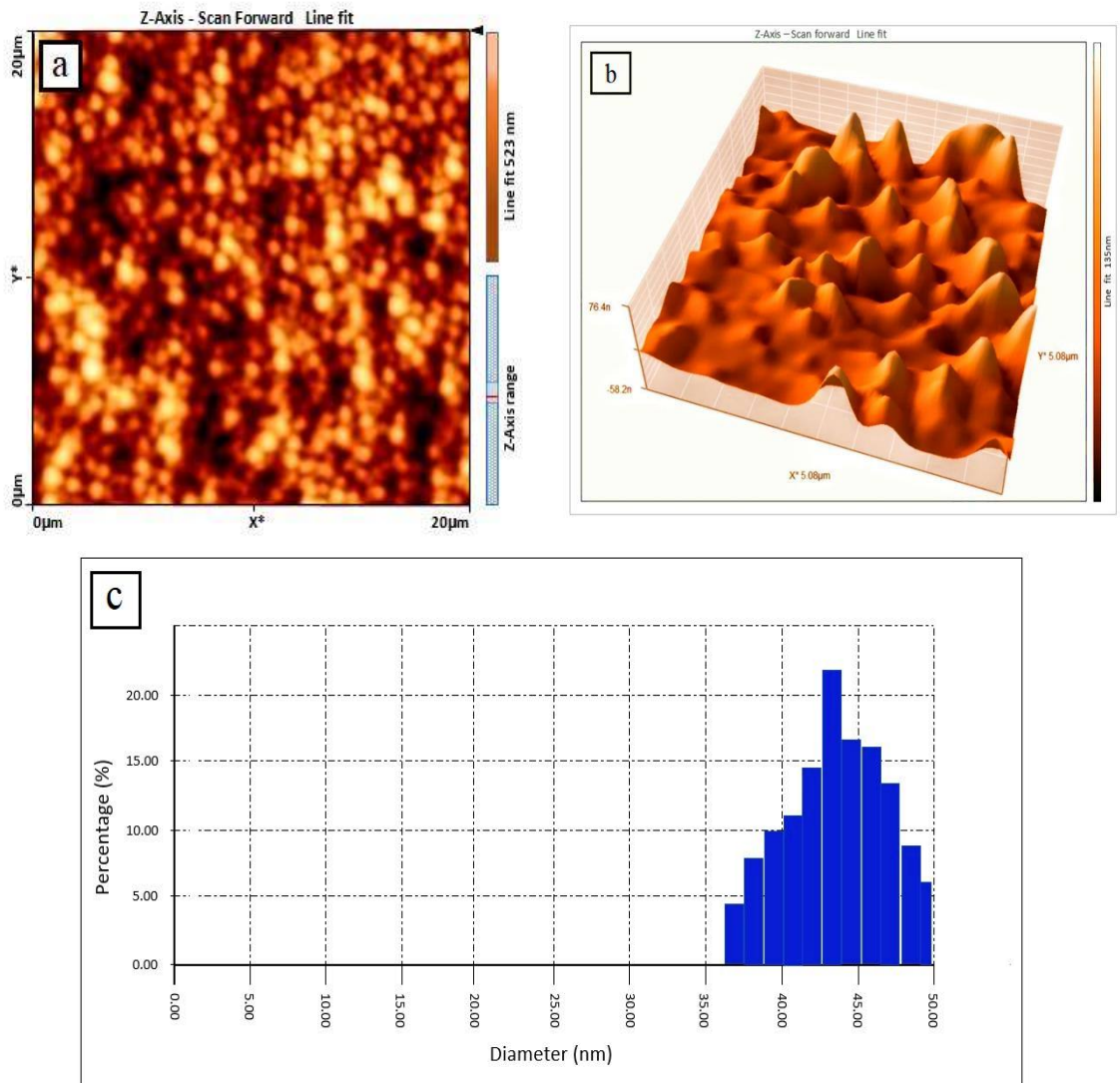


Figure 3-13: AFM analysis of synthesized ZnO-NPs (a) 2-Dimension image (b) 3-Dimension image (c) The granularity distribution chart.

3-4 Biochemical Analysis

This study evaluated the main effects of ZnO-NPs and *Z.-spina christi* leaves extract on body weight, kidney, and, liver biochemical parameters of male rats exposed to adenine. Healthy male rats were treated with ZnO-NPs and an aqueous extract of *Z.-spina christi* leaves for sequential 30 days and displayed some important changes in the biochemical parameter levels.

3-4-1 Body Weight Changes

As shown in Table 3-2, rats of the control group were grown by about (10 ± 2 gm) during the 30 days of giving diet only (G-I) whereas, the second group rats (G-II) that gavaged adenine (100 mg/kg.BW) for the same period showed a significant decrease ($P < 0.001$) in body weight about (20 ± 2 gm) in comparison to the control group. At the same time showed the administration of *Z.-spina christi* leaves extract for third group rats (G-III) at a dose (10 mg/kg B.W) significantly slightly decreased ($P = 0.04$) their body weights when compared to the control group, but these weights were high in comparison to adenine group. The same behavior for the body weight of fourth group rats (G-IV) after administered of ZnO-NPs (10 mg/kg B.W), which is high compared to the adenine group, but ZnO-NPs was significantly slightly decrease ($P = 0.04$) the body weight when compared to a control group. Finally, the fifth and sixth group rats (G-V and G-VI) after co-administration of adenine plus *Z.-spina christi* leaves extract or adenine plus ZnO-NPs at a dose (10 mg/kg B.W) respectively, mitigated significantly the decreasing in body weights of rats by compared to adenine group rats, but they still lower when compared with control group rats ($P < 0.001$).

Table 3-2: Effect of ZnO-NPs and *Z.-spina christi* leaves extract on adenine-induced body weight changes.

Period time Groups	Day-0 Weight (gm)	Week-1 Weight (gm)	Week-2 Weight (gm)	Week-3 Weight (gm)	Week-4 Weight (gm)
G-I	204.19±0.32	206.98±0.35	209.74±1.29	212.16±0.96	215.85±0.48
G-II	204.23±0.05	197.52±0.06	193.03±0.26	187.54±0.73	182.38±1.13
G-III	204.27±0.06	205.14±0.46	207.65±0.57	209.85±0.59	211.50±0.67
G-IV	204.08±0.29	206.13±0.57	208.96±0.62	211.35±0.66	214.69±0.81
G-V	204.25±0.10	201.16±0.16	197.23±1.06	194.41±1.19	191.26±1.64
G-VI	204.36±0.43	203.26±0.64	199.51±0.91	196.84±0.38	194.35±0.59
Tukey Test	0.317	0.422	0.846	0.863	1.513

Notes: Values in the table are expressed as mean ± SD. n=6 male rats in each group, SD: Standard deviation.

G-I: Control group, G-II: Adenine group, G-III: *Z.-spina christi* leaves extract group, G-IV: ZnO-NPs group, G-V: Adenine + *Z.-spina christi* leaves extract group, G-VI: Adenine + ZnO-NPs group.

The first effect of ZnO-NPs and *Z.-spina christi* leaves extract was on the body weight of rats with renal failure caused by adenine that measured at the beginning every week until end experiment. Adenine administration to rats resulted in body weight loss due to the buildup of uremic toxins, which causes inflammation and activation of protein catabolic pathways, resulting in protein breakdown [221]. Rats after 30 days of treatment with ZnO-NPs at concentrations of (10 mg/kg BW) showed a slight decrease in body weight; the decreases may be due to ZnO-NPs at this dose causing instability in protein degradation and lipid metabolism, resulting in an increase or decrease in body weight [222], depending on the effect of dose and treatment period. Moreover, ZnO-NPs may accumulate in numerous animal organs such as the kidney and liver, causing alterations in tissue functioning and, as a result, altering metabolic rate. Another study found that giving rats ZnO-NPs at different dosages (5, 50, and 100 mg/kg.BW) for 14 days resulted in a considerable reduction in body weight [223]. In addition, research conducted by [224] on Wistar rats treated with ZnO-NPs at a concentration of (10 mg/kg.BW) revealed a non-significant influence

on body weight increase, indicating the absence of hazardous indicators and mortality in adult male rats exposed to ZnO-NPs. Table 3-2 shows that there was a less significant change in weights in all rats after treatment with aqueous leaf extract of *Z.-spina christi* at a level of (10 mg/kg.BW). The weight loss in these rats might be attributed to anti-nutritional bioactive components in the plant extract, such as tannin, flavonoids and phenolic compounds [225].

3-4-2 Estimation of Kidney Function Tests

Results in Table 3-3 showed a significant increase ($P<0.001$) in concentrations of uric acid, urea, and creatinine was observed in serums of the second group rats (G-I) after administered of adenine in comparison to control group rats. This increase was significantly reduced after administration of *Z.-spina christi* leaves extract at a dose (10 mg/kg B.W) (G-III) when compared to the adenine group, but not completely restored these changes as in the control group ($P=0.04$). At the same table, significant increases ($P=0.02$) also were showed in concentrations of uric acid, urea and creatinine in rats administered with ZnO-NPs (G-IV) when compared to control group. Moreover, results as shown in both groups (G-V and G-VI), co-administration of adenine plus *Z.-spina christi* leaves extract or adenine plus ZnO-NPs, resulted in a significant decrease in uric acid, urea, and creatinine concentrations when compared to adenine group, but their values still in raises by comparison to the control group rats ($P<0.001$).

As shown in table 3-3, when compared to the control group rats, there was an increase in serum levels of uric acid, urea, and creatinine in the second group (G-II). These findings were characterized by renal dysfunction, as evidenced by congestion and necrosis of the renal glomeruli, as well as degenerative changes and necrosis of the normal renal tubular epithelium lining renal tubules [226], because these

products accumulate in the bloodstream and formation of 2,8-dihydroxyadenine crystals, result in big accumulation of different guanidino compounds such as (guanidino uric acid and methyl-guanidine) and nitrogenous compounds with renal failure [227]. The exposure of rats (G-III) and (G-IV) respectively to *Z.-spina christi* leaves extract or ZnO-NPs revealed a less significant difference in the levels of uric acid, urea, and creatinine in comparison to the control group, this indicates that dosage at the concentration (10 mg/kg B.W) for *Z.-spina christi* leaves extract and ZnO-NPs have no negative effect on the kidneys. However, serum levels of uric acid, urea, and creatinine showed a significant decrease after the administration of adenine plus ZnO-NPs (10 mg/kg B.W) or adenine plus *Z.-spina christi* leaves (10 mg/kg B.W) at the same time in both fifth and sixth groups rats (G-V and G-VI) by comparison to adenine group and a significant increase with comparison to control group rats, which evaluated that the synthesized ZnO-NPs and *Z.-spina christi* leaves might be able to avoid the damaged renal excretion, i.e., kidney alterations with adenine-induced renal failure. These results were in agreement with previous studies [228–230].

Table 3-3: Effect of ZnO-NPs and *Z.-Spina Christi* leaves extract on kidney function parameters in adenine-exposed male rats.

Parameters Groups	Uric acid mg/dL	Urea mg/dL	Creatinine mg/dL
G-I	1.24±0.08	13.66±1.10	0.26±0.03
G-II	3.22±0.19	105.88±1.96	0.84±0.05
G-III	1.31±0.09	14.05±1.37	0.29±0.03
G-IV	1.68±0.10	16.07±2.20	0.31±0.04
G-V	2.48±0.15	73.41±0.93	0.51±0.01
G-VI	2.73±0.14	87.03±1.60	0.68±0.01
Tukey Test	0.094	1.705	0.023

Notes: Values in the table are expressed as mean ± SD. n=6 male rats in each group, P ≤0.05 (One-Way ANOVA followed by Tukey post-hoc test). SD: Standard deviation. G-I: Control, G-II: Adenine, G-III: *Z.-spina christi* leaves extract, G-IV: ZnO-NPs, G-V: Adenine + *Z.-spina christi* leaves extract, G-VI: Adenine + ZnO-NPs.

3-4-3 Estimation of Liver Function Tests

The results of ALT, AST, and ALP were statistically significant increases ($P<0.001$) in their activities in the adenine group (G-II) compared with the control group (Table 3-4). The result of the third group rats (G-III) administered *Z.-spina christi* leaves extract (10 mg/kg B.W) showed a significant decrease in enzymes activities of ALT, AST, and ALP in compared to the adenine group but were slightly significant differences in comparison to the control group ($P=0.003$), while the fourth group of rats (G-IV) administered ZnO-NPs (10 mg/kg B.W) showed decreasing significantly in their enzymes activities compared to the adenine group but they were still high as compared to the control group ($P<0.001$). Furthermore, in both fifth and sixth group rats (G-V and G-IV) co-administration of adenine plus *Z.-spina christi* leaves extract (10 mg/kg B.W) or adenine plus ZnO-NPs (10 mg/kg B.W) caused a considerable decrease in activities of ALT, AST, and ALP when compared with adenine group, but still higher when compared to the control group ($P<0.001$).

Table 3-4: Effect of *Z.-spina christi* leaves extract and ZnO-NPs on liver function parameters in adenine-exposed male rats.

Parameters Groups	ALT (U/ml)	AST (U/ml)	ALP (U/ml)
G-I	33.94±1.15	103.28±2.17	122.36±2.64
G-II	91.60±3.57	179.46±3.89	213.55±4.18
G-III	36.35±1.23	108.03±2.36	125.14±2.79
G-IV	44.71±1.26	117.67±2.51	132.80±2.85
G-V	60.44±2.28	144.53±2.92	183.49±3.92
G-VI	72.11±2.63	158.80±3.27	197.03±4.05
Tukey Test	2.735	3.189	4.096

Notes: Values in the table are expressed as mean±SD. n=6 male rats in each group, SD: Standard deviation.

ALT= Alanine aminotransaminase, AST= Aspartate aminotransaminase, ALP= Alkaline phosphatase. G-I: Control group, G-II: Adenine group, G-III: *Z.-spina christi* leaves extract group, G-IV: ZnO-NPs group, G-V: Adenine + *Z.-spina christi* leaves extract group, G-VI: Adenine + ZnO-NPs group.

The measurement of enzyme activities ALT, AST, and ALP play a significant role in diagnosis, disease investigation, and the assessment of the plant extracts or nanoparticles for safety and toxicity risk. These enzymes considered in this study are useful markers to damage liver tissues. The ALT is found in many organs, particularly in the liver for diagnostic use, when its elevation indicates hepatocyte damage and release into the plasma. The AST is not a specific enzyme for the liver only but is also found in several organs such as the kidney, heart, brain, and skeletal muscle, these organs when are destroyed, AST is released. ALP is the indication enzyme for the plasma membrane and is elevated in a variety of tissues. It is often used to estimate the safety of plasma membranes and as a marker for hepatobiliary diseases [231]. Tissue damage is usually associated with the release of enzymes from the affected organ or tissue into circulation. Exposure of rats to adenine led to cytotoxicity in a time and dose dependent as a consequence of the oxidative stress, the peroxidation of lipids, and the damage of carbohydrates, proteins, and cell membranes. Adenine caused a significant increase in serum levels of ALT, AST, and ALP (Table 3-4). Increases in serum ALT and AST activities have been indicated in conditions involving necrosis of hepatocytes, while increases in serum ALP activity have been implicated in hepatobiliary diseases. The decrease in activities of ALT, AST, and ALP in the liver of rats were administrated with *Z.-spina christi* leaves extract or ZnO-NPs (Table 3-5) when compared to the adenine group might be according to the inactivation of these enzymes by the extract or its metabolites, which could have suppressed the synthesis of the enzymes, also suggested that ZnO-NPs might be interaction with key molecules in membranes (enzymes inclusive) and then inhibited or denature them. Furthermore, in both the treated groups (fifth and sixth) after co-administration of adenine plus *Z.-spina christi* leaves extract or adenine plus ZnO-NPs

showed a significant decrease in serum ALT, AST, and ALP activities indicating the strong evidence of the protective effect by the plant extract and ZnO-NPs. The results showed a significant decrease in ALT, AST, and ALP enzymes activities in the fifth group rats who were treated with *Z.-spina christi* leaves extract at a dose (10 mg/kg B.W), and sixth group rats were treated with ZnO-NPs at a dose (10 mg/kg B.W), these when comparison with adenine group rats, and these results agree with [232]. The alteration in the activities of the enzymes in this study might be due to the biological activity of ZnO-NPs and phytochemicals (main components of *Z.-spina christi* leaves) in the doses given for 30 days are capable to decreasing serum ALT, AST, and ALP.

3-4-4 Effect on antioxidants statuses

Table 3-5 showed the results of antioxidant levels, SOD, CAT, TAC, GSH, MDA, and NO. Administration of adenine to the second group rats (G-II) lead to a significant reduction in levels of SOD, CAT, TAC, and GSH, this reduction was accompanied by a significant elevation in MDA and NO levels in comparison to the control group ($P < 0.001$). As shown in Table 3-5, for both third and fourth groups rats (G-III and G-IV) after administration of *Z.-spina christi* leaves extract (10 mg/kg B.W) and ZnO-NPs (10 mg/kg B.W) respectively, there are significant increases in SOD, CAT, TAC and GSH levels when compared to adenine group rats (G-II), but significantly less decreased in comparison to the control group rats (G-I) ($P = 0.003$), while levels of MDA and NO significantly reduced when compared to the adenine group rats, but still less significant in comparison to control group rats ($P < 0.001$). Finally, rats of the both fifth and sixth groups (G-V and G-VI) were co-administrated adenine plus *Z.-spina christi* leaves extract (10 mg/kg B.W) and adenine plus ZnO-NPs (10 mg/kg B.W)

respectively, resulted in a significant increase in SOD, CAT, TAC and GSH levels when compared to an adenine group rats (G-II), but still lower when compared to the control group ($P=0.04$), this increase was accompanied with a significant reduction in MDA and NO levels when compared to adenine group, but were significantly increased in comparison to control group rats ($P<0.001$).

Table 3-5: The Effect of *Z.-spina christi* leaves extract and ZnO-NPs on the antioxidant levels in adenine-exposed male rats.

Parameters Groups	SOD (U/ml)	CAT (U/ml)	TAC ($\mu\text{mol/ml}$)	GSH ($\mu\text{mol/ml}$)	MDA ($\mu\text{mol/ml}$)	NO ($\mu\text{mol/ml}$)
G-I	17.15 \pm 0.44	10.83 \pm 1.37	17.56 \pm 0.80	13.48 \pm 0.38	0.49 \pm 0.02	0.93 \pm 0.01
G-II	8.92 \pm 0.14	1.69 \pm 0.03	6.84 \pm 0.87	5.40 \pm 0.05	4.16 \pm 0.41	8.54 \pm 0.21
G-III	15.23 \pm 0.41	9.15 \pm 0.69	15.45 \pm 0.17	11.35 \pm 0.29	0.62 \pm 0.10	1.47 \pm 0.02
G-IV	13.08 \pm 0.33	10.13 \pm 1.25	16.94 \pm 0.84	9.74 \pm 0.26	0.54 \pm 0.06	1.95 \pm 0.02
G-V	10.73 \pm 0.28	2.74 \pm 0.25	9.71 \pm 0.07	7.55 \pm 0.10	3.53 \pm 0.37	4.52 \pm 0.04
G-VI	9.51 \pm 0.24	6.75 \pm 0.33	13.52 \pm 0.61	6.19 \pm 0.08	2.29 \pm 0.30	6.31 \pm 0.10
Tukey Test	0.479	0.917	0.642	0.355	0.238	0.294

Notes: Values in the table are expressed as mean \pm SD. n=6 male rats in each group, $P \leq 0.05$ (One-Way ANOVA followed by Tukey post-hoc). SD: Standard deviation, SOD: superoxide dismutase, CAT: catalase, TAC: total anti-oxidant capacity, GSH: reduced glutathione, MDA: malonaldehyde and NO: nitric oxide.

G-I: Control group, G-II: Adenine group, G-III: *Z.-spina christi* leaves extract group, G-IV: ZnO-NPs group, G-V: Adenine + *Z.-spina christi* leaves extract group, G-VI: Adenine + ZnO-NPs group.

The results obtained from antioxidant status as shown in table 3-5, rats were exposed to adenine, the levels of SOD, CAT, TAC, and GSH were significantly decreased in serum, this is associated with the significant elevation of MDA and NO levels. Therefore, an increase in MDA and NO is considered a marker of oxidative damage that reveals excess of free radical production, which is consistent with the view that adenine induces lipid peroxidation. The antioxidant defense mechanism fails due to the decreased activities of the scavenging enzymes, or both. Increased MDA and NO levels, lipid peroxidation, also decreased SOD, CAT, TAC, and GSH levels are associated with cell damage. These results supported [233] and [234] who reported that adenine

significantly increased oxidative stress markers and decreased the activities of antioxidant enzymes in serum.

Rats were treated with an aqueous extract of *Z.-spina christi* leaves was ameliorated the change in antioxidant statuses. This amelioration appeared by the increase in serum levels of SOD, CAT, TAC, and GSH levels are associated with decreasing MDA and NO levels, which further confirms their role against adenine-induced liver damage. The given of ZnO-NPs showed approximately a similar activity (Table 3-5), to that of an aqueous extract of *Z.-spina christi* leaves in adenine-treated rats. Finally, ZnO-NPs protected rats against oxidative damage and liver injury induced by adenine which may be due to the anti-inflammatory and antioxidant properties that protect cell membranes against oxidative stress, decrease free radicals and increase the antioxidant enzyme activity as superoxide dismutase (SOD) and CAT levels [233]. Moreover, as shown in table 3, *Z.-spina christi* leaves extract and ZnO-NPs were able to significantly decrease renal failure induced by adenine, but observed that co-administration of adenine plus *Z.-spina christi* leaves extract (G-V) gave better results when compared to the adenine plus ZnO-NPs (G-VI). This study noted that an aqueous extract of *Z.-spina christi* leaves improved adenine-induced oxidative injury in the kidney and liver by its antioxidant and free radical-scavenging properties. These results were consistent with the previous research of [236] who suggested that the main mechanism for the beneficial action of gum acacia in adenine-induced kidney disease via its antioxidant properties. Furthermore, the kidney and liver were protected by the aqueous extract of *Z.-spina christi* leaves against adenine-induced toxicity due to its important contents of flavonoids, phenolic compounds, saponins, and triterpenes, these were confirmed by the previous study [237].

3-4-5 Histological Study

Results of the histological study of kidney and liver tissues for all groups of rats after 30 days of exposure were performed using two dyes called hematoxylin and eosin (H&E staining), which make it easy to see different parts of the tissues under the light microscope (Figures 3-14 and 3-15).

3-4-5-1 Kidney Section

Figure 3-14 showed the results of the histological study of the renal tissue from rats for six groups. The kidneys of control rats (G-I) showed no marker of damage, normal renal cortexes, normal renal architecture, and normal nephritic tubules (Figure 3-14-K1). Histological markers of group rats (G-II) with adenine-administered showed significant acute damage of the renal tissue. Their kidneys showed renal vein congestion and hypertrophy of renal glomeruli, besides necrosis and dilation of normal renal tubular (Figure 3-14-K2). Rats in the group (G-III) with the administration of *Z.-spina christi* leaves extract (10 mg/kg B.W) showed histological changes that involves: the normal structure of the renal cortex except the less degradation of some renal tubules (Figure 3-14-K3). Also, in the group rats (G-IV) after administered of ZnO-NPs (10 mg/kg B.W) showed that slightly inflammatory around blood vessels, but no significant glomerular changes (Figure 3-14-K4). The kidneys of rats (G-V) that co-administered adenine plus *Z.-spina christi* leaves extract and rats (G-VI) after co-administered of adenine plus ZnO-NPs (10 mg/kg B.W) resulted in significant lowered the markers and histological features were improved to normal in comparison with adenine group rats (Figure 3-14-K5 and K6).

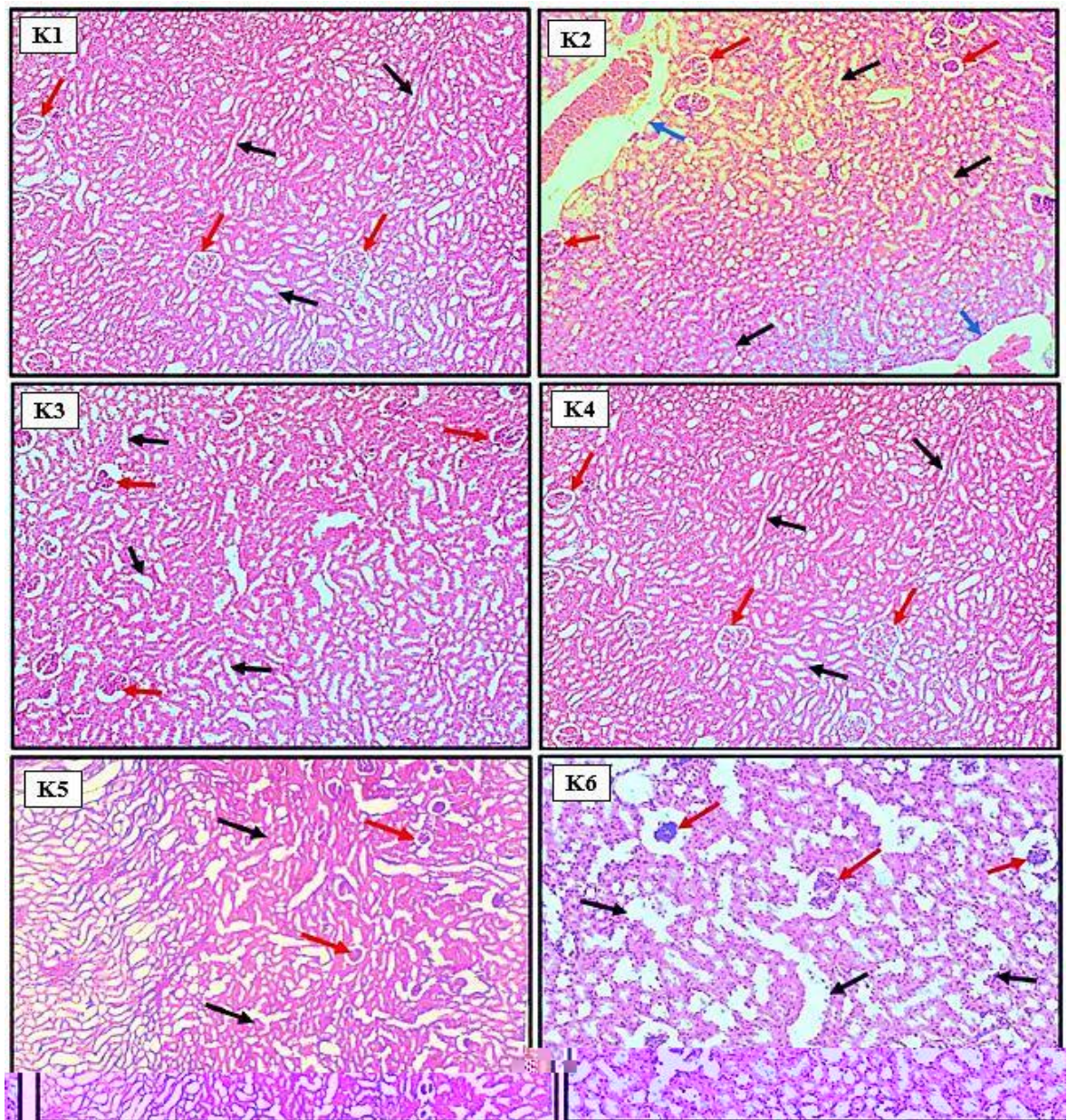


Figure (3-14): Effects of ZnO-NPs and *Z.-spina christi* leaves extract on the histological appearance of kidney tissues in male rats with renal failure induced by adenine. The view is captured using digital camera and light microscope at 10X magnification scale. **K1:** Kidneys of male rats in control group were treated with DMSO only that showed normal renal glomerulus (black arrows) and normal renal tubules (red arrows) without any significant occupied lesion. **K2:** Kidney of male rats were treated with Adenine showed acute renal glomerular hypertrophy (Black arrows) with expansion in tubular lumen and the renal glomeruli show severe atrophied lesion in some area of section (Red arrows) and clear renal vein congestion (Blue arrow). **K3:** Kidney of male rats were treated with *Z.-spina christi* leaves extract showed less significant change in renal glomerulus (Red arrows), but there very less narrowing in tubular lumen without any significant occupied lesion (Black arrows). **K4:** Kidney of male rats were treated with ZnO-NPs showed normal renal glomerulus (Red arrows) except slight degeneration and cystic extension of normal renal tubules (Black arrow) without any significant occupied lesion (SOL). **K5:** Kidney of male rats were treated with (Adenine + *Z.-Spina Christi* leaves extract) showed renal tubular hypertrophy or many intact tubules (Black arrows) with less narrowing in tubular lumen and the renal glomerular tufts show very mild atrophied lesion in some area of section (Red arrows). **K6:** Kidney of male rats were treated with (Adenine + ZnO-NPs) showed renal glomerular hypertrophy (Red arrows) with very slight narrowing in tubular lumen (Black arrows).

The histological changes of kidney tissues of rats were consistent with those results observed in antioxidants studies. In the kidney section, detected that adenine caused stripping of the epithelium of the renal tubules because its metabolite, 2,8-dihydroxyadenine (2,8-DHA), which has low solubility and can precipitate in the renal tubules leading to their obstruction and development of uremia with exudate of inflammatory cells and glomeruli, significant dilation and necrosis of renal tubules as shown in (Figure 3-14-K2) [238], and is capable of oxidative stress in renal tissue causing histological damage in the kidney [239]. The kidney of group rats when received adenine plus ZnO-NPs (10 mg/kg B.W) or adenine plus *Z.-spina christi* leaves extract (10 mg/kg B.W) showed improvement in the glomerular and renal tubules in comparison to adenine group rats (Figure 3-14-K5 and K6).

3-4-5-2 Liver Section

Figure 3-15 showed results of the histological study of the hepatic tissue from rats for six groups. Control group rats (G-I) showed the normal central vein, normal arrangement of hepatic cell and normal sinusoids, without any vacuolated of the cytoplasm (Figure 3-15-L1). The histopathological section in the liver of adenine group rats (G-II) showed a clear alteration including cytoplasm vacuolization, necrosis of hepatocytes, and amyloid like substance precipitation in the wall of liver sinusoids (Figure 3-15-L2). Group rats (G-III) were administered *Z.-spina christi* leaves extract (10 mg/kg B.W) and showed normal architecture of the liver, and normal hepatocytes with some areas around the periportal region appear to be mildly dilated (Figure 3-15-L3). Liver tissue of group rats (G-IV) after administered of ZnO-NPs (10 mg/kg B.W) exhibited a similar liver cytoarchitecture compared with the group rats (G-III) but the portal areas show mild to moderate

round cell inflammatory infiltrate (Figure 3-15-L4). Finally, in both groups rats (G-V and G-VI) were co-administered adenine plus aqueous extract of *Z.-spina christi* leaves (10 mg/kg B.W) or adenine plus ZnO-NPs (10 mg/kg B.W) showed reduced congestion of the hepatic central vein, the cytoplasm not vacuolated. Sinusoids are well protected with reduced inflammation hepatocytes (Figure 3-15-L5 and L6).

The liver section of rats demonstrates adenine-induced periportal inflammation, sinusoidal congestion hemorrhage, and hepatic necrosis in the liver of rats (Figure 3-15-7-L2). These results were in agreement with [240]. Liver damage is possible due to indirect renal failure or directly by the toxic effects of adenine-mediated oxidative stress on the hepatic cell. Administration of *Z.-spina christi* leaves extract alone or ZnO-NPs alone displayed approximately similar results as that showed in the control group (Figure 3-15- L3 and L4). These results were in agreement with previous studies [179], [241]. On the other hand, group rats that were co-administered adenine plus aqueous extract of *Z.-spina christi* leaves appeared significant improvement compared with adenine-treated rats as indicated by the contrary periportal decreased inflammatory hepatic cells, reduced vacuolization, and sinusoidal congestion in the liver cells (Figure 3-15-L5). Finally, co-administration of adenine plus ZnO-NPs enhanced the hepatic necrosis, central vein, and sinusoidal congestion compared to adenine-exposed rats (Figure 3-15-L6). The ameliorative roles of the synthesized ZnO-NPs and *Z.-spina christi* leaves in their doses used can scavenge free radicals and active oxygen species such as singlet oxygen, free radicals, and hydroxyl radicals, and save the renal and hepatic tissues to natural structure due to their antioxidant and anti-inflammatory properties [242], [243].

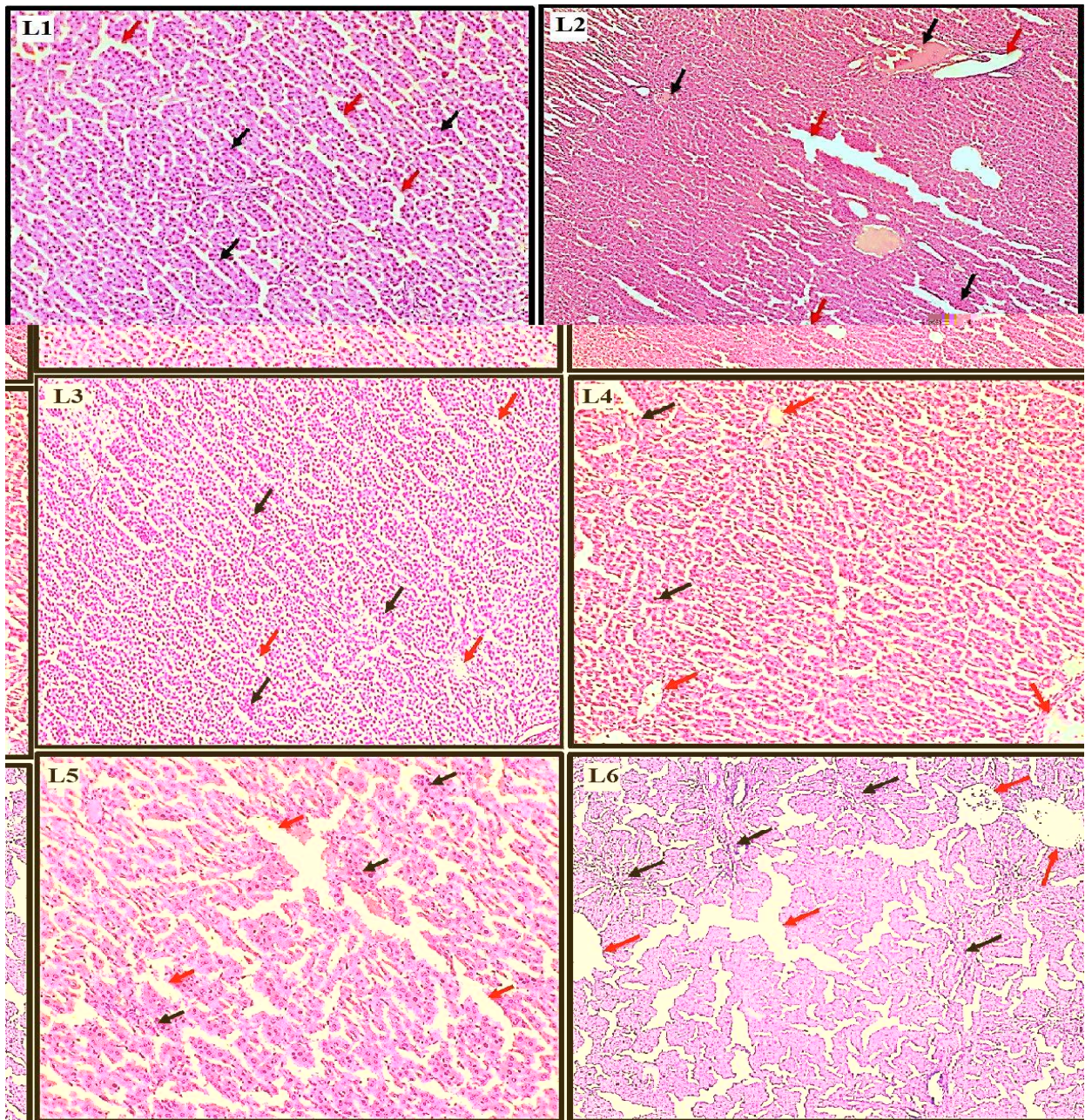


Figure (3-15): Effects of ZnO-NPs and *Z.-spina christi* leaves extract on the histological appearance of liver tissues in male rats with renal failure induced by adenine. The view is captured using digital camera and light microscope at 10X magnification scale. **L1:** Liver of control group rats were gavaged with DMSO only showed the normal hepatocytes (black arrows) and normal central vein (Red arrows), without any significant occupied lesion (SOL). **L2:** Liver of adenine group rats showed clear damage in the hepatocytes (Black arrows) and clear thrombi formation can be seen in the hepatic central vein in section (Red arrows). **L3:** Liver of male rats were administered with aqueous extract of *Z.-spina christi* leaves extract (10 mg/kg B.W) showed a normal hepatocyte (Black arrows) and normal radial arrangement around central vein (Red arrows). **L4:** Liver of male rats were administered with ZnO-NPs (10 mg/kg B.W) showed slightly thrombi of hepatocytes in some areas (Black arrows) and central vein (Red arrows). **L5:** The liver of male rats was treated with (Adenine + *Z.-spina christi* leaves extract (10 mg/kg B.W)) showed infiltration and necrosis in the hepatocytes (Black arrows) and clear damage of the central vein in some areas (Red arrows). **L6:** The liver of male rats treated with (Adenine + ZnO-NPs (10 mg/kg B.W)) showed infiltration in hepatic tissue and coagulative necrosis of the hepatocytes (Black arrows) and clear damage in the wall of the central vein (Red arrows).

Conclusions and Future Studies

Conclusions and Future Studies

Conclusions

- 1- Zinc oxide nanoparticles were successfully synthesized from the aqueous leaf extract of *Ziziphus-spina christi* and zinc nitrate hexahydrate.
- 2- Phytochemicals presented in *Ziziphus-spina christi* leaves extract could potentially be used as an effective reducing, capping, and stabilizing agent for the green synthesis of ZnO-NPs.
- 3- Adenine-exposed male rats lead to a decrease in body weight, and caused harmful defects in kidney and liver tissues by measuring levels of (uric acid, urea creatinine, ALT, AST, and ALP).
- 4- The synthesized ZnO-NPs have good antioxidant activity against oxidative stress and free radicals.
- 5- Both the synthesized ZnO-NPs and aqueous leaf extract of *Ziziphus-spina christi* at a dose (10 mg/kg B.W) respectively, have ameliorative effects against adenine-exposed male rats, implying that they may be used safely against kidney and liver damage at this concentration; slightly significant effects were observed in renal and liver tissues in comparison to adenine group rats, implying that they may be powerful antioxidant, anti-inflammatory, and antitoxic agents for biomedical applications.

Conclusions and Future Studies

Future Studies

- 1- Studying the green synthesis of another metal oxides nanoparticles using different medicinal plants.
- 2- Study the effect of the synthesized zinc oxide nanoparticles from *Ziziphus-spina christi* anticoagulant, anticancer antibacterial and antifungal.
- 3- Evaluating the effect of the synthesized zinc oxide nanoparticles from *Ziziphus-spina christi* as anti-anemia related with renal failure in male rats.
- 4- Evaluating the effect of the synthesized zinc oxide nanoparticles from *Ziziphus-spina christi* as anti-diabetic activity caused the renal failure in male rats.
- 5- Study the effect of the synthesized zinc oxide nanoparticles from *Ziziphus-spina christi* on the parathyroid hormone levels.

References

References

1. Santilli CV, Tokumoto MS, Briois V, Santilli C v, Pulcinelli SH. Preparation of ZnO nanoparticles: Structural study of t e molecular precursor Cite t is paper Preparation of ZnO Nanoparticles: Structural Study of t e Molecular Precursor. Vol. 26, Journal of Sol-Gel Science and Tec nology. 2003. <https://doi.org/10.1021/jp0217381>
2. Bec eri A, Dürr M, lo Nostro P, Baglioni P. Synt esis and c aracterization of zinc oxide nanoparticles: Application to textiles as UV-absorbers. Journal of Nanoparticle Researc . 2008 Apr;10(4):679–689. <https://doi.org/10.1007/s11051-007-9318-3>
3. S a M, Fawcett D, S arma S, Tripat y SK, Poinern GEJ. Green synt esis of metallic nanoparticles via biological entities. Materials. 2015;8(11):7278–308. <https://doi.org/10.3390/ma8115377>
4. Ja n W. Review: C emical Aspects of t e Use of Gold Clusters in Structural Biology [Internet]. 1999. Available from: <http://www.idealibrary.com>. <https://doi.org/10.1006/jsbi.1999.4123>
5. S a RK, Borua F, Parween N. Synt esis and c aracterization of ZnO nanoparticles using leaf extract of *Camellia Sinesis* and evaluation of t eir antimicrobial efficacy. Int J Curr Microbiol App Sci. 2015;4(8):444–450. <http://www.ijcmas.com/vol-4-8/Rajesh%...>
6. Oladeji OS, Adelowo FE, Ayodele DT, Odelade KA. P ytoce mistry and p harmacological activities of *Cymbopogon citratus*: A review. Vol. 6, Scientific African. Elsevier B.V.; 2019. <https://doi.org/10.1016/j.sciaf.2019.e00137>
7. Abdulra man MD, Zakariya AM, Hama HA, Hamad SW, Al-Rawi SS, Bradosty SW, et al. Et nop harmacology, Biological Evaluation, and C emical Composition of *Ziziphus spina - Christi* (L.) Desf.: A Review. Advances in P harmacological and P harmaceutical Sciences. Hindawi Limited. 2022; 2022:4495688. <https://doi.org/10.1155/2022/4495688>

References

8. Mars all AT, Haverkamp RG, Davies CE, Parsons JG, Gardea-Torresdey JL, van Agterveld D. Accumulation of gold nanoparticles in *Brassica juncea*. *Int J Phytoremediation*. 2007;9(3):197–206. <https://doi.org/10.1080/15226510701376026>
9. Sanchez-Moreno P, Ortega-Vinuesa JL, Peula-Garcia JM, Morales JA, Boulaiz H. Smart drug-delivery systems for cancer nanotherapy. *Curr Drug Targets*. 2018;19(4):339–359. [Doi: 10.2174/1389450117666160527142544](https://doi.org/10.2174/1389450117666160527142544)
10. Negrescu A, Killian M, Vakamulla Raghu SN, Scamuki P, Mazare A, Cimpean A. Metal Oxide Nanoparticles: Review of Synthesis, Characterization and Biological Effects. *J Funct Biomater*. 2022 Dec 5;13:274. <https://doi.org/10.3390/jfb13040274>
11. Biswas S, Bellare J. Bioactivity, biocompatibility, and toxicity of metal oxides. In: *Metal Oxides for Biomedical and Biosensor Applications*. Elsevier; 2022. p. 3–33. <https://doi.org/10.1016/B978-0-12-823033-6.00001-6>
12. Samsuzzaman AA, Asif M, Masrafi A, Khanam H. Green Synthesis of ZnO Nanoparticles Using *Bacillus Subtilis* and Their Catalytic Performance in the One-Pot Synthesis of Steroidal Topones. *European Chemical Bulletin*. 2014;3(9):939–45. [Doi: 10.17628/ECB.2014.3.939](https://doi.org/10.17628/ECB.2014.3.939)
13. Afifi M, Almaghrabi OA, Kadasa NM. Ameliorative effect of zinc oxide nanoparticles on antioxidant and sperm characteristics in streptozotocin-induced diabetic rat testes. *Biomed Res Int*. 2015;2015. <https://doi.org/10.1155/2015/153573>
14. Asghar MS, Qureshi NA, Jabeen F, Khan MS, Sakeel M, Chaudhry AS. Ameliorative effects of selenium in ZnO NP-induced oxidative stress and hematological alterations in *Catla catla*. *Biol Trace Elem Res*. 2018;186:279–87. [Doi: 10.1007/s12011-018-1299-9](https://doi.org/10.1007/s12011-018-1299-9)

References

15. El-Ba r SM, S ous a S, Albok adaim I, S e ab A, K attab W, A med-Farid O, et al. Impact of dietary zinc oxide nanoparticles on selected serum biomarkers, lipid peroxidation and tissue gene expression of antioxidant enzymes and cytokines in Japanese quail. BMC Vet Res. 2020;16(1):1–12.
<https://doi.org/10.1186/s12917-020-02482-5>
16. Aitken RJ, Roman SD. Antioxidant systems and oxidative stress in t e testes. Molecular mec anisms in spermatogenesis. 2008;154–71.
https://doi.org/10.1007/978-0-387-09597-4_9
17. Ma moud SM, Kassab RB, Moneim AEA. Zinc oxide nanoparticles ameliorate aluminum c loride-induced epato-renal oxidative stress and inflammation in rats. Lab Anim. 2020;15:16.
[Doi: 10.22159/ijpps.2020v12i1.35956](https://doi.org/10.22159/ijpps.2020v12i1.35956)
18. Augustine Amalraj, Sreeraj Gopi. Medicinal properties of Terminalia arjuna (Roxb.) Wig t & Arn.: A review. Journal of Traditional and Complementary Medicine. 2017;1(7):65–78.
<https://doi.org/10.1016/j.jtcme.2016.02.003>
19. Organization WH. Regulatory situation of erbal medicines: a worldwide review. 1998. <https://apps.w o.int/iris/ andle/10665/63801>
20. Oluyemisi F, Henry O, Peter O. Standardization of erbal medicines-A review. Int J Biodivers Conserv. 2012;4(3):101–112.
[Doi: 10.5897/IJBC11.163](https://doi.org/10.5897/IJBC11.163)
21. Saxena M, Saxena J, Nema R, Sing D, Gupta A. P yto c emistry of medicinal plants. J. of P armacognosy and P yto c emistry. 2013;1(6):168–182. https://dx.doi.org/10.22271/p_yto
22. Saied AS, Gebauer J, Hammer K, Buerkert A. *Ziziphus spina-christi* (L.) Willd.: a multipurpose fruit tree. Genet Resour Crop Evol. 2008;55:929–37. <https://doi.org/10.1007/s10722-007-9299-1>

References

23. Bukar AM, Kyari MZ, Gwaski PA, Gudusu M, Kuburi FS, Abadam YI. Evaluation of phytochemical and potential antibacterial activity of *Ziziphus spina-christi* L. against some medically important pathogenic bacteria obtained from University of Maiduguri Teaching Hospital, Maiduguri, Borno State Nigeria. *J. of Pharmacognosy and Phytochemistry*. 2015;3(5):98–101. https://dx.doi.org/10.22271/p_yto
24. Srinivasan A. Handbook of precision agriculture: principles and applications. CRC press; 2006.
25. Farooqi MIH. Cedar or lote-tree in the light of Al-Quran-a scientific study. 2016.
26. Amin A, Saad S, Andaleeb S, Khan MM, Khan MA. Studies on Antimicrobial and Antifungal Activities of *Ziziphus mauritiana* Against Human Clinical Bacterial and Fungal Pathogens. *Pakistan Journal of Scientific & Industrial Research*. 2012;55(1): 35–39. <https://doi.org/10.52763/PJSIR.BIOL.SCI.55.1.2012.35.39>
27. Sudersan C, Hussain J. In vitro Clonal Propagation of a Multipurpose Tree, *Ziziphus spina-christi* (L.) Desf. *Turk J Botany*. 2003;27(3):167–172. <https://journals.tubitak.gov.tr/botany/vol27/iss3/2>
28. Longbap, B.D, Usie, O A1, Oga, E., Kendenson, A. C, Nyikyaa, J. T. Phytochemical Screening and Quantitative Determination of Phytochemicals in Leaf Extracts of *Hannoa undulata*. *IJMPNP*. 2018;4(2): 32–38. <http://dx.doi.org/10.20431/2454-7999.0402005>
29. Wali AF, Pillai JR, Beig S, Mushtaq A, Arafat A, Reiman MU, et al. Ethnopharmacological Uses, Phytochemistry, Pharmacological Properties and Clinical Trials of *Ziziphus Spina-Christi*: A Comprehensive Review. *Saudi Pharmaceutical Journal*. 2022;5(1). [Doi: 10.1016/j.jsps.2022.05.001](https://doi.org/10.1016/j.jsps.2022.05.001)
30. Hussein AS. *Ziziphus spina-christi*: Analysis of bioactivities and chemical composition. *Wild Fruits: Composition, Nutritional Value and Products*. 2019;175–197. [Doi: 10.1007/978-3-030-31885-7_15](https://doi.org/10.1007/978-3-030-31885-7_15)

References

31. Walaa Fikry Elbossaty. Potent Medicinal Influences of *Ziziphus Spina-Christi*. ACTA Scientific Medical Sciences. 2020;4(3):143–146.
32. Na ar L, Sarker SD. Chemistry for pharmacy students: general, organic and natural product chemistry. John Wiley & Sons; 2007. [Doi:10.1002/9781118687529](https://doi.org/10.1002/9781118687529)
33. Koffi CK, Lourme-Ruiz A, Djoudi H, Bouquet E, Dury S, Gautier D. The contributions of wild tree resources to food and nutrition security in sub-Saharan African drylands: a review of the pathways and beneficiaries. International Forestry Review. 2020;22(1):64–82. <https://doi.org/10.1505/146554820828671490>
34. Butt SZ, Hussain S, Munawar KS. Phytochemistry of *Ziziphus mauritiana*: An overview of its nutritional and pharmaceutical potential. Sci Inquiry Rev. 2021;5(2):01–15. <https://doi.org/10.32350/sir/52.01>
35. Gazanfar SA. Handbook of Arabian medicinal plants. CRC press; 1994; 1st Edition. <https://doi.org/10.1201/b14834>
36. Tang W, Eisenbrand G. Chinese drugs of plant origin: chemistry, pharmacology, and use in traditional and modern medicine. Springer Science & Business Media; 2013. <https://doi.org/10.1007/978-3-642-73739-8>
37. Al assan KA, Indabawa AS, Sa MM. Phytochemical analysis, proximate composition and antibacterial activities of *Ziziphus* species (*Z. jujube* and *Z. spina-christi*). 2019; 4(1): 42-46. <http://dx.doi.org/10.21839/jaar.2019.v4i1.262>
38. Sofowora A, Ogunbodede E, Onayade A. The role and place of medicinal plants in the strategies for disease prevention. African journal of traditional, complementary and alternative medicines. 2013;10(5):210–29. <http://dx.doi.org/10.4314/ajtcam.v10i5.2>
39. Owolarafe, T.A.; Salau, A.K.; Salawu, K. 2019: Phytochemical screening and toxicity study of aqueous-methanol extract of *Ziziphus*

References

- spina-christi* seeds in Wistar albino rats Comparative Clinical Pathology 29(1): 267-274. DOI: [10.1007/s00580-019-03043-5](https://doi.org/10.1007/s00580-019-03043-5)
40. Adzu B, Amos S, Wambebe C, Gamaniel K. Antinociceptive activity of *Zizyphus spina-christi* root bark extract. Fitoterapia. 2001;72(4):344–50. Doi: [10.1016/s0367-326x\(00\)00289-6](https://doi.org/10.1016/s0367-326x(00)00289-6)
41. Abdel-Wahab MA, Omara EA, Abdel-Galil MM, Hassan NS, Nada SA, Saeed A, et al. *Zizyphus spina-christi* extract protects against aflatoxin B1-initiated hepatic carcinogenicity. African Journal of Traditional, Complementary, and Alternative Medicines. 2007;4(3):248. Doi: [10.4314/ajtcam.v4i3.31216](https://doi.org/10.4314/ajtcam.v4i3.31216)
42. Setorki M, Hoosmandi Z. Neuroprotective effect of *Zizyphus spina-christi* on brain injury induced by transient global cerebral ischemia and reperfusion in rat. Bangladesh J Pharmacol. 2017;12(1):69–76. DOI: <https://doi.org/10.3329/bjp.v12i1.29964>
43. Adzu B, Haruna AK, Salawu OA, Sule A. Bioassay-guided evaluation of the antidiarrhoeal potentials of *Zizyphus spina-christi* root bark in rats. Int J Biol Chem Sci. 2007;1(1):15–20. Doi: [10.4314/ijbcs.v1i1.39693](https://doi.org/10.4314/ijbcs.v1i1.39693)
44. Saied AS, Gebauer J, Hammer K, Buerkert A. *Zizyphus spina-christi* (L.) Willd.: a multipurpose fruit tree. Genet Resour Crop Evol. 2008;55:929–37. <https://doi.org/10.1007/s10722-007-9299-1>
45. Ben-Porat T, Weiss-Sadan A, Rottenstreich A, Serfati-Dagan S, Schweiger C, Yosef-Levi IM, et al. Nutritional management for chronic kidney disease patients who undergo bariatric surgery: a narrative review. Advances in Nutrition. 2019;10(1):122–32. Doi: [10.1093/advances/nmy112](https://doi.org/10.1093/advances/nmy112)
46. Almeer RS, Albasir G, Alotibi F, Alarifi S, Ali D, Alkhatani S. *Zizyphus spina-christi* leaf extract suppressed mercury chloride-induced nephrotoxicity via Nrf2-antioxidant pathway activation and inhibition

References

- of inflammatory and apoptotic signaling. *Oxid Med Cell Longev*. 2019;2019. <https://doi.org/10.1155/2019/5634685>
47. Dk il MA, Kassab RB, Al-Qurais y S, Abdel-Daim MM, Zrieq R, Abdel Moneim AE. Zizip us spina-c risti (L.) leaf extract alleviates myocardial and renal dysfunction associated wit sepsis in mice. *Biomed Pharmacother*. 2018;102:64-75.
[Doi:10.1016/j.biop a.2018.03.032](https://doi.org/10.1016/j.biop a.2018.03.032)
48. El-Beltagy AEF, Abdelaziz BM, Abdelaziz KK, Elsayy MR, G anem RA. Adverse effects of cadmium on t e t yroid, kidneys, and testes in Wistar albino rats and t e possible modulatory role of *Zizyphus spina-christi* (Sidr) fruit extract (Histological and bioc emical studies). *Journal of Bioscience and Applied Researc* . 2019;5(4):551–75.
[Doi: 10.21608/jbaar.2019.248623](https://doi.org/10.21608/jbaar.2019.248623)
49. Basuny AM, Arafat SM, Farag HA. Utilization from Fruit and Leaves of Nabek (*Ziziphus-spina christi* l.) as a Source of Bioactive components. *Banats J Biotec nol*. 2013;4(7):16.
[Doi: 10.7904/2068-4738-IV\(07\)-16](https://doi.org/10.7904/2068-4738-IV(07)-16)
50. Hussein HM, El-Sayed EM, Said AA. Anti yperglycemic, anti yperlipidemic and antioxidant effects of *Zizyphus spina christi* and *Zizyphus jujuba* in alloxan diabetic rats. *Int J P armacal*. 2006;2(5):563–70. DOI: [10.3923/ijp.2006.563.570](https://doi.org/10.3923/ijp.2006.563.570)
51. Sud ersan C, Hussain J. In vitro Clonal Propagation of a Multipurpose Tree, *Ziziphus spina-christi* (L.) Desf. *Turk J Botany*. 2003;27(3):167–172. <https://journals.tubitak.gov.tr/botany/vol27/iss3/2>
52. Majuru S, Oyewumi MO. Nanotec nology in drug development and life cycle management. *Nanotec nology in drug delivery*. 2009;597–619. https://doi.org/10.1007/978-0-387-77668-2_20
53. Jain KK. T e Role of Nanobiotec nology in Drug Discovery. *P arm Biotec nol*. 2010;655:37. https://doi.org/10.1007/978-1-4419-1132-2_4

References

54. Oroojalian F, Carbgo F, Hasemi M, Amani A, Yazdian-Robati R, Moktarzade A, et al. Recent advances in nanotechnology-based drug delivery systems for the kidney. *Journal of controlled release*. 2020;321:442–462. Doi: [10.1016/j.jconrel.2020.02.027](https://doi.org/10.1016/j.jconrel.2020.02.027)
55. Seidi F, Jenjob R, Pakkeeree T, Crespy D. Saccharides, oligosaccharides, and polysaccharides nanoparticles for biomedical applications. *Journal of controlled release*. 2018;284:188–212. Doi: [10.1016/j.jconrel.2018.06.026](https://doi.org/10.1016/j.jconrel.2018.06.026)
56. Jain A, Sing SK, Arya SK, Kundu SC, Kapoor S. Protein nanoparticles: promising platforms for drug delivery applications. *ACS Biomater Sci Eng*. 2018;4(12):3939–61. Doi: [10.1021/acsbiomaterials.8b01098](https://doi.org/10.1021/acsbiomaterials.8b01098)
57. Liu Y, Miyoshi H, Nakamura M. Nanomedicine for drug delivery and imaging: a promising avenue for cancer therapy and diagnosis using targeted functional nanoparticles. *Int J Cancer*. 2007;120(12):2527–37. Doi: [10.1002/ijc.22709](https://doi.org/10.1002/ijc.22709)
58. Riemann K, Schneider SW, Luger TA, Godin B, Ferrari M, Fuchs H. Nanomedicine—challenge and perspectives. *Angewandte Chemie International Edition*. 2009;48(5):872–97. Doi: [10.1002/anie.200802585](https://doi.org/10.1002/anie.200802585)
59. McMillan J, Batrakova E, Gendelman HE. Cell Delivery of Therapeutic Nanoparticles. *Prog Mol Biol Transl Sci*. 2011; 104: 563–601. Doi: [10.1016/b978-0-12-416020-0.00014-0](https://doi.org/10.1016/b978-0-12-416020-0.00014-0)
60. Hirsch L, Drezek R, Halas N, West J. Diagnostic and Therapeutic Applications of Metal Nanoparticles. *BioMEMS and Biomedical Nanotechnology*. 2006; pp 157-169. https://doi.org/10.1007/978-0-387-25844-7_9
61. Boudad H, Legrand P, Lebas G, Ceron M, Duchêne D, Poncel G. Combined hydroxypropyl- β -cyclodextrin and poly(alkylcyanoacrylate)

References

- nanoparticles intended for oral administration of saquinavir. *Int J Pharm.* 2001 Jun 1;218:113–24. [Doi: 10.1016/s0378-5173\(01\)00622-6](https://doi.org/10.1016/s0378-5173(01)00622-6)
62. Paramasivam G, Palem VV, Sundaram T, Sundaram V, Kisore SC, Bellucci S. Nanomaterials: Synthesis and Applications in Theranostics. *Nanomaterials.* 2021; 11(12):3228. <https://doi.org/10.3390/nano11123228>
63. Baroum A, García-Betancourt ML, Raier H, Van Assche G. Physicochemical characterization of nanomaterials: Polymorph, composition, wettability, and thermal stability. In: *Emerging applications of nanoparticles and architecture nanostructures.* Elsevier; 2018. p. 255–278. [Doi: 10.1016/B978-0-323-51254-1.00009-9](https://doi.org/10.1016/B978-0-323-51254-1.00009-9)
64. Sannino D. Types and Classification of Nanomaterials. *Nanotechnology: Trends and Future Applications.* 2021;15–38. https://doi.org/10.1007/978-981-15-9437-3_2
65. Gugulotu D, Baroum A, Afzal SM, Venkateswarlu B, Uludag H. Structural multifunctional nanofibers and their emerging applications. *Handbook of Nanofibers;* Springer: Berlin/Heidelberg, Germany. 2019; 693–732. https://doi.org/10.1007/978-3-319-53655-2_16
66. Abraham J, Arunima R, Nimita KC, George SC, Thomas S. One-dimensional (1D) nanomaterials: Nanorods and nanowires; nanoscale processing. In: *Nanoscale Processing.* Elsevier; 2021. p. 71–101. <https://doi.org/10.1016/B978-0-12-820569-3.00003-7>
67. Youssef AM, Moustafa HA, Baroum A, Hakim AEAA, Dufresne A. Evaluation of the Morphological, Electrical and Antibacterial Properties of Polyaniline Nanocomposite Based on Zn/Al-Layered Double Hydroxides. *ChemistrySelect.* 2017;2(27):8553–66. <https://doi.org/10.1002/slct.201701513>
68. Cimene D, Alge DL, Garwar AK. Two-dimensional nanomaterials for biomedical applications: emerging trends and future prospects. *Advanced Materials.* 2015;27(45):7261–7284.

References

- <https://doi.org/10.1002/adma.201502422>
69. Mefta i A, Samyn P, Geravand SA, K ajavi R, Alibk s i S, Bec elany M, et al. Nanocelluloses as skin biocompatible materials for skincare, cosmetics, and ealt care: Formulations, regulations, and emerging applications. *Carbo ydr Polym.* 2022;278:118956.
<https://doi.org/10.1016/j.carbpol.2021.118956>
70. El-Bes lawy MM, Abdel-Haleem FM, Bar ousm A. Molecularly imprinted potentiometric sensor for nanomolar determination of pioglitazone ydroc loride in p armaceutical formulations. *Electroanalysis.* 2021;33(5):1244–1254.
<https://doi.org/10.1002/elan.202060141>
71. Patra JK, Baek KH. Green nanobiotec nology: factors affecting synt esis and c aracterization tec niques. *J Nanomater.* 2015;2014:219. <https://doi.org/10.1155/2014/417305>
72. T. Cele, ‘Preparation of Nanoparticles’, *Engineered Nanomaterials - Healt and Safety. Intec Open*, Jul. 08, 2020.
[Doi: 10.5772/intec-open.90771.](https://doi.org/10.5772/intec-open.90771)
73. Haris V, Ansari MM, Tewari D, Gaur M, Yadav AB, García-Betancourt ML, et al. Nanoparticle and Nanostructure Synt esis and Controlled Growt Met ods. *Nanomaterials.* 2022;12(18):3226.
<https://doi.org/10.3390/nano12183226>
74. Prasad Yadav T, Mano ar Yadav R, Pratap Sing D. Mec anical milling: a top down approac for t e synt esis of nanomaterials and nanocomposites, *Nanosci Nanotec nol* 2 (2012): 22–48. 2012.
[Doi: 10.5923/j.nn.20120203.01](https://doi.org/10.5923/j.nn.20120203.01)
75. Kumar, K. Sant os , Kumar, Vijay B oos an, Paik, Pradip. Recent Advancement in Functional Core-S ell Nanoparticles of Polymers: Synt esis, P ysical Properties, and Applications in Medical Biotec nology. *Journal of Nanoparticles.* 2013. Vol. 2013, no. 2013, pp.1-24. <https://doi.org/10.1155/2013/672059>

References

76. Isaacoff BP, Brown KA. Progress in top-down control of bottom-up assembly. Vol. 17, Nano Letters. ACS Publications; 2017. p. 6508–10. <https://doi.org/10.1021/acs.nanolett.7b04479>
77. Ranjan S, Dasgupta N, Rajendran B, Avad ani GS, Ramalingam C, Kumar A. Microwave-irradiation-assisted hybrid chemical approach for titanium dioxide nanoparticle synthesis: microbial and cytotoxicological evaluation. Environmental Science and Pollution Research . 2016;23:12287–302. <https://doi.org/10.1007/s11356-016-6440-8>
78. Patil N, Baskar R, Vyavare V, Dudge R, Kaire V, Patil Y. Overview on Methods of Synthesis of Nanoparticles. Int J Curr Pharm Res. 2021;13(2):11–6. <https://doi.org/10.22159/ijcpr.2021v13i2.41556>
79. Si F, Xu J, Hu Z, Ren C, Xue Y, Zhang Y, et al. Bird nest-like zinc oxide nanostructures for sensitive electrochemical glucose biosensor. Chinese Chemical Letters. 2021;32(10):3185–8. <https://doi.org/10.1016/j.ccllet.2021.03.012>
80. Peng H, Fangli Y, Liuyang B, Jinlin L, Yunfa C. Plasma synthesis of large quantities of zinc oxide nanorods. The Journal of Physical Chemistry C. 2007;111(1):194–200. <https://doi.org/10.1021/jp065390b>
81. Fouad OA, Ismail AA, Zaki ZI, Mohamed RM. Zinc oxide thin films prepared by thermal evaporation deposition and its photocatalytic activity. Appl Catal B. 2006;62(1–2):144–9. <https://doi.org/10.1016/j.apcatb.2005.07.006>
82. Khan FA. Synthesis of nanomaterials: methods & technology. Applications of nanomaterials in human health . 2020;15–21. https://doi.org/10.1007/978-981-15-4802-4_2
83. Król A, Pomastowski P, Rafińska K, Railean-Plugaru V, Buszewski B. Zinc oxide nanoparticles: Synthesis, antiseptic activity and toxicity mechanism. Adv Colloid Interface Sci. 2017;249:37–52. [Doi: 10.1016/j.cis.2017.07.033](https://doi.org/10.1016/j.cis.2017.07.033)

References

84. Maryanti E, Damayanti D, Gustian I. Synthesis of ZnO nanoparticles by hydrothermal method in aqueous rinses extracts of *Sapindus rarak* DC. *Mater Lett*. 2014;118:96–8.
<https://doi.org/10.1016/j.matlet.2013.12.044>
85. Santos L, Nunes D, Calmeiro T, Branquinho R, Salgueiro D, Barquinha P, et al. Solvothermal synthesis of gallium–indium–zinc-oxide nanoparticles for electrolyte-gated transistors. *ACS Appl Mater Interfaces*. 2015;7(1):638–46. <https://doi.org/10.1021/am506814t>
86. Agarwal H, Menon S, Kumar SV, Rajes Kumar S. Mechanistic study on antibacterial action of zinc oxide nanoparticles synthesized using green route. *Chem Biol Interact*. 2018;286:60–70.
<https://doi.org/10.1016/j.cbi.2018.03.008>
87. Carrapiço A, Martins MR, Caldeira AT, Mirão J, Dias L. Biosynthesis of Metal and Metal Oxide Nanoparticles Using Microbial Cultures: Mechanisms, Antimicrobial Activity and Applications to Cultural Heritage. *Microorganisms*. 2023;11(2):378.
[Doi: 10.3390/microorganisms11020378](https://doi.org/10.3390/microorganisms11020378)
88. Parsons JG, Peralta-Videa JR, Gardea-Torresdey JL. Use of plants in biotechnology: synthesis of metal nanoparticles by inactivated plant tissues, plant extracts, and living plants. *Developments in environmental science*. 2007;5:463–85.
[https://doi.org/10.1016/S1474-8177\(07\)05021-8](https://doi.org/10.1016/S1474-8177(07)05021-8)
89. Król A, Railean-Plugaru V, Pomastowski P, Buszewski B. Phytochemical investigation of *Medicago sativa* L. extract and its potential as a safe source for the synthesis of ZnO nanoparticles: The proposed mechanism of formation and antimicrobial activity. *Phytochemistry Letters*. 2019;31:170–180.
<https://doi.org/10.1016/j.phytol.2019.04.009>
90. Iswarya R, Vaseeran B, Kalyani S, Banumathi B, Govindarajan M, Alarbi NS, et al. Facile green synthesis of zinc oxide nanoparticles

References

- using *Ulva lactuca* seaweed extract and evaluation of their photocatalytic, antibiofilm and insecticidal activity. *J Photocatal Photobiol B*. 2018;178:249–58. [Doi: 10.1016/j.jphotobiol.2017.11.006](https://doi.org/10.1016/j.jphotobiol.2017.11.006)
91. Bloc K, Pardesi K, Satriano C, Gos S. Bacteriogenic platinum nanoparticles for application in nanomedicine. *Front Chem*. 2021;9:624344. <https://doi.org/10.3389/fchem.2021.624344>
92. Sing J, Dutta T, Kim KH, Rawat M, Samddar P, Kumar P. Green synthesis of metals and their oxide nanoparticles: applications for environmental remediation. *J Nanobiotechnology*. 2018;16(1):1–24. [Doi: 10.1186/s12951-018-0408-4](https://doi.org/10.1186/s12951-018-0408-4)
93. Mittal AK, Chisti Y, Banerjee UC. Synthesis of metallic nanoparticles using plant extracts. *Biotechnol Adv*. 2013;31(2):346–356. <https://doi.org/10.1016/j.biotechadv.2013.01.003>
94. Meer B, Andleeb A, Iqbal J, Asraf H, Meer K, Ali JS, et al. Bio-Assisted Synthesis and Characterization of Zinc Oxide Nanoparticles from *Lepidium Sativum* and Their Potent Antioxidant, Antibacterial and Anticancer Activities. *Biomolecules*. 2022;12(6):855. <https://doi.org/10.3390/biom12060855>
95. Ramesh P, Saravanan K, Manogar P, Johnson J, Vinot E, Mayakannan M. Green synthesis and characterization of biocompatible zinc oxide nanoparticles and evaluation of its antibacterial potential. *Sens Biosensing Res*. 2021;31:100399. [Doi: 10.1016/j.sbsr.2021.100399](https://doi.org/10.1016/j.sbsr.2021.100399)
96. Liu YC, Li J, An J, Pu J, Rupa EJ, Huo Y, et al. Biosynthesis of zinc oxide nanoparticles by one-pot green synthesis using fruit extract of *Amomum longiligulare* and its activity as a photocatalyst. *Optik (Stuttg)*. 2020;218:165245. <https://doi.org/10.1016/j.ijleo.2020.165245>
97. Naser R, Abu-Huwaij R, Al-kateeb I, Abbas MM, Atoom AM. Green synthesis of zinc oxide nanoparticles using the root air extract of *Poenix dactylifera*: Antimicrobial and anticancer activity. *Appl Nanosci*. 2021;11:1747–57. <https://doi.org/10.1007/s13204-021-01837-0>

References

98. T akkar KN, M atre SS, Parik RY. Biological synt esis of metallic nanoparticles. *Nanomedicine*. 2010;6(2):257–262.
<https://doi.org/10.1016/j.nano.2009.07.002>
99. Rónavári A, Igaz N, Adamecz DI, Szerencsés B, Molnar C, Kónya Z, et al. Green silver and gold nanoparticles: Biological synt esis approaches and potentials for biomedical applications. *Molecules*. 2021;26(4):844. <https://doi.org/10.3390/molecules26040844>
100. Mourdikoudis S, Pallares RM, Tan NTK. Characterization techniques for nanoparticles: comparison and complementarity upon studying nanoparticle properties. *Nanoscale*. 2018;10(27):12871–934.
<https://doi.org/10.1039/C8NR02278J>
101. Co EJ, Holback H, Liu KC, Abouelmagd SA, Park J, Yeo Y. Nanoparticle characterization: state of the art, challenges, and emerging technologies. *Mol Pharm*. 2013;10(6):2093–110.
<https://doi.org/10.1021/mp300697>
102. Unger W, Hodoroaba V. D, & S ard A. Characterization of Nanoparticles: Measurement Processes for Nanoparticles. Elsevier, 2019. <https://doi.org/10.1016/C2017-0-00312-9>
103. A. C inec erem Nkele and F. I. Ezema, ‘Diverse Synt esis and Characterization Techniques of Nanoparticles’, *T in Films*. *Intec Open*, Nov. 17, 2021. [Doi: 10.5772/intec_open.94453](https://doi.org/10.5772/intec_open.94453)
104. Kumar A, Dixit CK. Methods for characterization of nanoparticles. In: *Advances in nanomedicine for the delivery of therapeutic nucleic acids*. Elsevier; 2017. p. 43–58.
<https://doi.org/10.1016/B978-0-08-100557-6.00003-1>
105. Jiang J, Pi J, Cai J. The advancing of zinc oxide nanoparticles for biomedical applications. *Bioinorg Chem Appl*. 2018;2018.
<https://doi.org/10.1155/2018/1062562>
106. A, H., Fouad, W., Wasly, H., El-Deeb, B., Abd El-sadek, M. Zinc oxide nanoparticles: green synt esis, characterization, photocatalysis, and

References

- antibacterial activity. *Egyptian Journal of Physics*, 2023; 51(1): 57-71.
Doi: 10.21608/ejp_ysics.2022.157467.1084
107. Mal otra SPK. Applications of zinc oxide nanoparticles as an antimicrobial agent in t e food packaging industry. In: Zinc-Based Nanostructures for Environmental and Agricultural Applications. Elsevier; 2021: 125–137.
<https://doi.org/10.1016/B978-0-12-822836-4.00021-5>
108. Ali, Attarad, P ull, Abdul-Re man and Zia, Mu ammad. "Elemental zinc to zinc nanoparticles: is ZnO NPs crucial for life? Synt esis, toxicological, and environmental concerns" *Nanotechnology Reviews*, vol. 7, no. 5, 2018, pp. 413-441.
<https://doi.org/10.1515/ntrev-2018-0067>
109. Díez-Pascual AM. Biodegradable food packaging nanocomposites based on ZnO-reinforced poly ydroxy alkanoates. In: Food packaging. Elsevier; 2017. p. 185–221.
<https://doi.org/10.1016/B978-0-12-804302-8.00006-6>
110. Mutukwa D, Taziwa R, K otseng LE. A Review of t e Green Synt esis of ZnO Nanoparticles Utilizing Sout ern African Indigenous Medicinal Plants. *Nanomaterials*. 2022;12(19):3456.
<https://doi.org/10.3390/nano12193456>
111. Awwad AM, Amer MW, Salem NM, Abdeen AO. Green synt esis of zinc oxide nanoparticles (ZnO-NPs) using Ailant us altissima fruit extracts and antibacterial activity. *C em Int*. 2020;6(3):151–9.
Doi:10.5281/Zenodo.3559520
112. Balogun SW, James OO, Sanusi YK, Olayinka OH. Green synt esis and c aracterization of zinc oxide nanoparticles using bas ful (*Mimosa pudica*), leaf extract: A precursor for organic electronics applications. *SN Appl Sci*. 2020;2:1–8. <https://doi.org/10.1007/s42452-020-2127-3>
113. Mo amed HYG, Ismael E, Elaasser MM, K alil MMH. Green synt esis of zinc oxide nanoparticles using portulaca oleracea (regla

References

- seeds) extract and its biomedical applications. Egypt J Chem. 2021;64(2):661–72. [Doi: 10.21608/EJCHEM.2020.45592.2930](https://doi.org/10.21608/EJCHEM.2020.45592.2930)
114. Saleemi MA, Alallam B, Yong YK, Lim V. Synthesis of Zinc Oxide Nanoparticles with Bioflavonoid Rutin: Characterisation, Antioxidant and Antimicrobial Activities and In Vivo Cytotoxic Effects on Artemia Nauplii. Antioxidants. 2022;11(10):1853. <https://doi.org/10.3390/antiox11101853>
115. Saba EY, Jacob JO, Tijani JO, Suleiman MAT. A critical review of synthesis parameters affecting the properties of zinc oxide nanoparticle and its application in wastewater treatment. Appl Water Sci. 2021;11(2):1–41. <https://doi.org/10.1007/s13201-021-01370-z>
116. Puspitanan K, Satya S, Citra MJ, Gowtami S, Santia R. Influence of Reaction Temperature on Crystal Structure and Band Gap of ZnO Nanoparticles. Materials and Manufacturing Processes [Internet]. 2012 Dec 1;27(12):1334–42. Available from: <https://doi.org/10.1080/10426914.2012.700163>
117. Rifaie HA, Samat NA, Nor RM. Effect of pH on the growth of zinc oxide nanorods using *Citrus aurantifolia* extracts. Mater Lett. 2014;137:297–9. <https://doi.org/10.1016/j.matlet.2014.09.033>
118. Phan CM, Nguyen HM. Role of capping agent in wet synthesis of nanoparticles. J Phys Chem A. 2017;121(17):3213–9. <https://doi.org/10.1021/acs.jpca.7b02186>
119. Mogri Moazzen MA, Borghei SM, Talebi F. Change in the morphology of ZnO nanoparticles upon changing the reactant concentration. Appl Nanosci. 2013;3(4):295–302. [Doi: 10.1007/s13204-012-0147-z](https://doi.org/10.1007/s13204-012-0147-z)
120. Manzoor U, Zaira FT, Rafique S, Moin MT, Mujaid M. Effect of synthesis temperature, nucleation time, and postsynthesis treatment

References

- treatment of ZnO nanoparticles and its sensing properties. *J Nanomater.* 2015;16(1):9. <https://doi.org/10.1155/2015/189058>
121. Que M, Lin C, Sun J, Chen L, Sun X, Sun Y. Progress in ZnO nanosensors. *Sensors.* 2021;21(16):5502. <https://doi.org/10.3390/s21165502>
122. Jiang J, Pi J, Cai J. The advancing of zinc oxide nanoparticles for biomedical applications. *Bioinorg Chem Appl.* 2018;2018. <https://doi.org/10.1155/2018/1062562>
123. Wu T, Tang M. Review of the effects of manufactured nanoparticles on mammalian target organs. *Journal of Applied Toxicology.* 2018;38(1):25–40. [Doi: 10.1002/jat.3499](https://doi.org/10.1002/jat.3499)
124. Lin Z, Monteiro-Riviere NA, Riviere JE. Pharmacokinetics of metallic nanoparticles. *Wiley Interdiscip Rev Nanomed Nanobiotecnol.* 2015;7(2):189–217. [Doi: 10.1002/wnan.1304](https://doi.org/10.1002/wnan.1304)
125. Baek M, Chung HE, Yu J, Lee JA, Kim TH, Oh JM, et al. Pharmacokinetics, tissue distribution, and excretion of zinc oxide nanoparticles. *Int J Nanomedicine.* 2012;3081–3097. [Doi: 10.2147/IJN.S32593](https://doi.org/10.2147/IJN.S32593)
126. Aamed MIN, Kalaivani K, Vinayaka K S, Sangeetha S, Srinivasan P, P. Tirumalai Vasan. Assessment on the Therapeutic Applications Zinc Oxide Nanoparticles. *Vegueta Anuario de la Facultad de Geografía e Historia.* 2022;22:12. <https://doi.org/10.5281/zenodo.7503603>
127. Zhao CY, Tan SX, Xiao XY, Qiu XS, Pan JQ, Tang ZX. Effects of dietary zinc oxide nanoparticles on growth performance and antioxidative status in broilers. *Biol Trace Elem Res.* 2014;160:361–7. [Doi: 10.1007/s12011-014-0052-2](https://doi.org/10.1007/s12011-014-0052-2)
128. Jan H, Sam M, Andleeb A, Faisal S, Khatkhat A, Rizwan M, et al. Plant-based synthesis of zinc oxide nanoparticles (ZnO-NPs) using aqueous leaf extract of aquilegia pubiflora: Their antiproliferative activity

References

- against HepG2 cells inducing reactive oxygen species and other in vitro properties. *Oxid Med Cell Longev*. 2021;2021.
<https://doi.org/10.1155/2021/4786227>
129. Moapatra S, Leelavathi L, Rajes Kumar S, Sakti DS, Jayasri P. Assessment of Cytotoxicity, Anti-Inflammatory and Antioxidant Activity of Zinc Oxide Nanoparticles Synthesized Using Clove and Cinnamon Formulation--An In-Vitro Study. *J Evol Med Dent Sci*. 2020;9(25):1859–65. Doi: [10.14260/jemds/2020/405](https://doi.org/10.14260/jemds/2020/405)
130. Popović D, Kocić G, Katić V, Jović Z, Zarubica A, Veličković LJ, et al. Protective effects of antocyanins from bilberry extract in rats exposed to nephrotoxic effects of carbon tetrachloride. *Chem Biol Interact*. 2019;304:61–72. <https://doi.org/10.1016/j.cbi.2019.02.022>
131. Moss R, Thomas SR. Hormonal regulation of salt and water excretion: a mathematical model of whole kidney function and pressure natriuresis. *American journal of physiology. Renal physiology*. 2014;306(2):F224-F248. Doi:[10.1152/ajprenal.00089.2013](https://doi.org/10.1152/ajprenal.00089.2013)
132. Kamisan FH, Yaya F, Ismail NA, Din SS, Mamat SS, Zabidi Z, et al. Hepatoprotective activity of methanol extract of *Melastoma malabathricum* leaf in rats. *J Acupunct Meridian Stud*. 2013;6(1):52-55. Doi: [10.1016/j.jams.2012.08.002](https://doi.org/10.1016/j.jams.2012.08.002)
133. Lee BM, Lee WC, Jang JY, An P, Kim JN, Jeong SW, et al. Clinical features of drug-induced liver injury according to etiology. *J Korean Med Sci*. 2015;30(12):1815–20. Doi: [10.3346/jkms.2015.30.12.1815](https://doi.org/10.3346/jkms.2015.30.12.1815)
134. Tévénod F, Lee WK. Toxicology of cadmium and its damage to mammalian organs. *Cadmium: from toxicity to essentiality*. 2013;415–90. Doi: [10.1007/978-94-007-5179-8_14](https://doi.org/10.1007/978-94-007-5179-8_14)
135. Cruickshank CC, Dyer KR. A review of the clinical pharmacology of methamphetamine. *Addiction*. 2009;104(7):1085–99.
[Doi: 10.1111/j.1360-0443.2009.02564.x](https://doi.org/10.1111/j.1360-0443.2009.02564.x)

References

136. Andrade RJ, Ait al GP, Björnsson ES, Kaplowitz N, Kullak-Ublick GA, Larrey D, et al. EASL clinical practice guidelines: drug-induced liver injury. *J Hepatol.* 2019;70(6):1222–61.
Doi: 10.1016/j.jep.2019.02.014
137. Akintelu SA, Folorunso AS. A review on green synthesis of zinc oxide nanoparticles using plant extracts and its biomedical applications. *Bionanoscience.* 2020;10(4):848–63.
<https://doi.org/10.1007/s12668-020-00774-6>
138. Xiong H. ZnO nanoparticles applied to bioimaging and drug delivery. *Advanced Materials.* 2013;25(37):5329–35.
<https://doi.org/10.1002/adma.201301732>
139. Hassan SA, Muja id H, Ali MM, Irs ad S, Naseer R, Saeed S, et al. Synthesis, characterization and protective effect of green tea-mediated zinc oxide nanoparticles against oc ratotoxin A induced hepatotoxicity and nephrotoxicity in albino rats. *Appl Nanosci.* 2021;11(8):2281–9.
<https://doi.org/10.1007/s13204-021-02006-z>
140. Rani V, Verma Y, Rana K, Rana SVS. Zinc oxide nanoparticles inhibit dimethylnitrosamine induced liver injury in rat. *Chem Biol Interact.* 2018;295:84–92. Doi: 10.1016/j.cbi.2017.10.009
141. Hassan I, Husain FM, Khan RA, Ebaid H, Al-Tamimi J, Al azza IM, et al. Ameliorative effect of zinc oxide nanoparticles against potassium bromate-mediated toxicity in Swiss albino rats. *Environmental Science and Pollution Research.* 2019;26:9966–80.
Doi: 10.1007/s11356-019-04443-4
142. Yogalakshmi B, Viswanathan P, Anuradha CV. Investigation of antioxidant, anti-inflammatory and DNA-protective properties of eugenol in acetaminophen-induced liver injury in rats. *Toxicology.* 2010;268(3):204–12. Doi: 10.1016/j.tox.2009.12.018
143. Basandy SAE, Alaamer A, Moussa SAA, Omara EA. Role of zinc oxide nanoparticles in alleviating hepatic fibrosis and nephrotoxicity

References

- induced by tioacetamide in rats. *Can J P ysiol P armacol.* 2018;96(4):337–344. [Doi: 10.1139/cjpp-2017-0247](https://doi.org/10.1139/cjpp-2017-0247)
144. C ung IM, Abdul Ra uman A, Marimut u S, Vis nu Kirt i A, Anbarasan K, Rajakumar G. An investigation of t e cytotoxicity and caspase-mediated apoptotic effect of green synt esized zinc oxide nanoparticles using *Eclipta prostrata* on uman liver carcinoma cells. *Nanomaterials.* 2015;5(3):1317–30. [Doi: 10.3390/nano5031317](https://doi.org/10.3390/nano5031317)
145. Barakat LAA, Barakat N, Zakaria MM, K iralla SM. Protective role of zinc oxide nanoparticles in kidney injury induced by cisplatin in rats. *Life Sci.* 2020;262:118503. [Doi: 10.1016/j.lfs.2020.118503](https://doi.org/10.1016/j.lfs.2020.118503)
146. Alomari G, Al-Trad B, Hamdan S, Aljabali AAA, Al Zoubi MS, Al-Batanye K, et al. Alleviation of diabetic nep ropat y by zinc oxide nanoparticles in streptozotocin-induced type 1 diabetes in rats. *IET Nanobiotec nol.* 2021;15(5):473–83. [Doi: 10.1049/nbt2.12026](https://doi.org/10.1049/nbt2.12026)
147. Anjum S, Has im M, Malik SA, K an M, Lorenzo JM, Abbasi BH, et al. Recent advances in zinc oxide nanoparticles (ZnO NPs) for cancer diagnosis, target drug delivery, and treatment. *Cancers (Basel).* 2021;13(18):4570. [Doi: 10.3390/cancers13184570](https://doi.org/10.3390/cancers13184570)
148. Yo anes Buang. Dietary adenine alleviates fatty liver induced by orotic acid. *Indo. J. C em.* 2010; 10 (3): 363 - 369. [ttps://doi.org/10.22146/ijc.21444](https://doi.org/10.22146/ijc.21444)
149. Moffatt BA, As i ara H. Purine and pyrimidine nucleotide synt esis and metabolism. *Arabidopsis Book.* 2002;1:e0018. [Doi:10.1199/tab.0018](https://doi.org/10.1199/tab.0018)
150. Bot am KM, Mayes PA. Bioenergetics: T e Role of ATP. *Harper's Illustrated Bioc emistry*, 30e Eds. Rodwell VW, et al. McGraw Hill, 2016, [ttps://accessmedicine.m medical.com/Content.aspx?bookid=1366§ionid=73243196](https://accessmedicine.m medical.com/Content.aspx?bookid=1366§ionid=73243196).

References

151. Fred olm BB. Adenosine, an endogenous distress signal, modulates tissue damage and repair. *Cell Deat Differ.* 2007;14(7):1315–23.
Doi: 10.1038/sj.cdd.4402132
152. Tang J, Jiang X, Z ou Y, Xia B, Dai Y. Increased adenosine levels contribute to isc emic kidney fibrosis in t e unilateral ureteral obstruction model. *Exp T er Med.* 2015;9(3):737–43.
Doi: 10.3892/etm.2015.2177
153. Ulbric t T. L. V. Purines, Pyrimidines and Nucleotides: And t e Chemistry of Nucleic Acids. Elsevier, 2013; v(25).
<https://doi.org/10.1016/C2013-0-06579-6>
154. Jia T, Olauson H, Lindberg K, Amin R, Edvardsson K, Lind olm B, et al. A novel model of adenine-induced tubulointerstitial nep ropat y in mice. *BMC Nep rol.* 2013;14(1):1–8.
<https://doi.org/10.1186/1471-2369-14-116>
155. Mis ima E, Fukuda S, S ima H, Hirayama A, Akiyama Y, Takeuc i Y, et al. Alteration of t e intestinal environment by lubiprostone is associated wit amelioration of adenine-induced CKD. *Journal of t e American Society of Nep rology.* 2015;26(8):1787–94.
Doi: 10.1681/ASN.2014060530
156. Kumakura S, Sato E, Sekimoto A, Has izume Y, Yamakage S, Miyazaki M, et al. Nicotinamide attenuates t e progression of renal failure in a mouse model of adenine-induced c ronic kidney disease. *Toxins (Basel).* 2021;13(1):50. Doi: 10.3390/toxins13010050
157. Nasir O, Umbac AT, Rex epaj R, Ackermann TF, B andaru M, Ebra im A, et al. Effects of gum arabic (*Acacia senegal*) on renal function in diabetic mice. *Kidney Blood Press Res.* 2012;35(5):365–72.
Doi: 10.1159/000336359
158. Fox BA, Bzik DJ. Bioc emistry and metabolism of *Toxoplasma gondii*: Purine and pyrimidine acquisition in *Toxoplasma gondii* and ot er Apicomplexa. *Toxoplasma gondii.* 2020;397–449.

References

<https://doi.org/10.1016/B978-0-12-815041-2.00009-8>

159. Pey J, San José-Eneriz E, Ochoa MC, Apaolaza I, de Atauri P, Rubio A, et al. In-silico gene essentiality analysis of polyamine biosynthesis reveals APRT as a potential target in cancer. *Sci Rep.* 2017;7(1):14358.
[Doi: 10.1038/s41598-017-14067-8](https://doi.org/10.1038/s41598-017-14067-8)
160. Kaartinen K, Hemmilä U, Salmela K, Räisänen-Sokolowski A, Kouri T, Mäkelä S. Adenine phosphoribosyltransferase deficiency as a rare cause of renal allograft dysfunction. *Journal of the American Society of Nephrology.* 2014;25(4):671–4. [Doi: 10.1681/ASN.2013090960](https://doi.org/10.1681/ASN.2013090960)
161. Rasheed I, Verma A, Tiwari P, D'Cruz S. Adenine phosphoribosyltransferase deficiency leads to renal allograft dysfunction in kidney transplant recipients: a systematic review. *J Bras Nefrol.* 2022;44(3):403-416. [Doi:10.1590/2175-8239-JBN-2021-0283en](https://doi.org/10.1590/2175-8239-JBN-2021-0283en)
162. Pandya D, Nagrajappa AK, Ravi KS. Assessment and Correlation of Urea and Creatinine Levels in Saliva and Serum of Patients with Chronic Kidney Disease, Diabetes and Hypertension- A Research Study. *J Clin Diagn Res.* 2016;10(10):ZC58-ZC62.
[Doi:10.7860/JCDR/2016/20294.8651](https://doi.org/10.7860/JCDR/2016/20294.8651)
163. Zaidan M, Palsson R, Merieau E, Cornec-Le Gall E, Garstka A, Maggiore U, et al. Recurrent 2, 8-dihydroxyadenine nephropathy: a rare but preventable cause of renal allograft failure. *American Journal of Transplantation.* 2014;14(11):2623–32. [Doi: 10.1111/ajt.12926](https://doi.org/10.1111/ajt.12926)
164. Junaid R Saik, MK Patil. Qualitative tests for preliminary phytochemical screening: An overview. *Int J Chem Stud* 2020;8(2):603-608. [Doi: 10.22271/chemi.2020.v8.i2i.8834](https://doi.org/10.22271/chemi.2020.v8.i2i.8834)
165. Kalpna R, Mital K, Sumitra C. Phytochemical and Phytochemical Analysis of Different Parts of Indian Kesar Mango—A unique variety from Saurashtra Region of Gujarat. *Pharmacognosy Journal.* 2016;8(5):502-506. [Doi:10.5530/pj.2016.5.16](https://doi.org/10.5530/pj.2016.5.16)

References

166. Mace ME. Histoc emical localization of p enols in ealt y and diseased banana roots. *Physiol Plant*. 1963;16(4):915–25. <https://doi.org/10.1111/j.1399-3054.1963.tb08367.x>
167. Santos M K, S aila D, C andrakumar T, Rajyalaks mi I, Sanjeeva Rao I. P ysicoc emical and P ytoc emical Examination of Medicinal Plants Used in Indigenous System of Medicine. *Journal of Chemistry*. 2005;2(2):142-151. <https://doi.org/10.1155/2005/589869>
168. Gupta M, T akur S, S arma A, Gupta S. Qualitative and Quantitative Analysis of P ytoc emicals and P armacological Value of Some Dye Yielding Medicinal Plants. *Oriental journal of chemistry*. 2013;29(2): 475-481. [Doi:10.13005/OJC/290211](https://doi.org/10.13005/OJC/290211)
169. Suman Kumar Ratnampally, Venkates war C inna. Quantitative Analysis of P ytoc emicals in t e Bark Extracts of Medicinally Important Plant Cassia fistula, Linn. *Int. J. Curr. Microbiol. App. Sci*. 2017;6(4):1073-1079. [Doi: https://doi.org/10.20546/ijcmas.2017.604.133](https://doi.org/10.20546/ijcmas.2017.604.133)
170. S arma V, C aud ary U. P armacognostic and p ytoc emical screening of *Helicteres isora* roots. *Asian J P arm Clin Res*. 2016;9(2):96–101. [Doi: 10.22159/ajpcr.2016.v9s2.12178](https://doi.org/10.22159/ajpcr.2016.v9s2.12178)
171. Faisal S, Jan H, S a SA, S a S, K an A, Akbar MT, et al. Green synt esis of zinc oxide (ZnO) nanoparticles using aqueous fruit extracts of *Myristica fragrans*: t eir c aracterizations and biological and environmental applications. *ACS Omega*. 2021;6(14):9709–9722. <https://doi.org/10.1021/acsomega.1c00310>
172. Cullity BD. Elements of X-Ray Diffraction. Second ed. Reading MA: Addison-Wesley Publis ing Company; 1978.
173. National Researc Council (US) Committee for t e Update of t e Guide for t e Care and Use of Laboratory Animals. Guide for t e Care and Use of Laboratory Animals. 8t ed., National Academies Press (US), 2011. [Doi:10.17226/12910](https://doi.org/10.17226/12910)

References

174. Al Za'abi M, Ali B, Yasin J, Scupp N, Nemmar A. Development of a new model for the induction of chronic kidney disease via intraperitoneal adenine administration, and the effect of treatment with gum acacia terebinth. *The FASEB Journal*. 2015;29(1): 938.3.
https://doi.org/10.1096/fasebj.29.1_supplement.938.3
175. Yokozawa T, Zeng PD, Oura H, Koizumi F. Animal model of adenine-induced chronic renal failure in rats. *Nephron*. 1986;44(3):230–234.
<https://doi.org/10.1159/000183992>
176. Basandy SAE, Ahmed-Farid OAH, Abdelmottaleb-Moussa S, Omara EA, Abdel-Jaleel GA, Ibrahim FAA. Efficacy of zinc oxide nanoparticles on hepatocellular carcinoma induced biochemical and trace element alterations in rats. *J Appl Pharm Sci*. 2021;11:108–17.
[Doi: 10.7324/JAPS.2021.110515](https://doi.org/10.7324/JAPS.2021.110515)
177. Awadalla A, Hamam ET, El-Senduny FF, Omar NM, Madi MR, Barakat N, et al. Zinc oxide nanoparticles and spironolactone-enhanced Nrf2/HO-1 pathway and inhibited Wnt/ β -catenin pathway in adenine-induced nephrotoxicity in rats. *Redox Report*. 2022;27(1):249–258.
[Doi: 10.1080/13510002.2022.2139947](https://doi.org/10.1080/13510002.2022.2139947)
178. Hafiz TA, Mubarak MA, Diab MSM, Dkhal MA, Al-Quraisy S. Ameliorative role of Ziziphus spina-cristi leaf extracts against hepatic injury induced by Plasmodium cabaudi infected erythrocytes. *Saudi J Biol Sci*. 2019;26(3):490-494. [Doi:10.1016/j.sjbs.2017.10.012](https://doi.org/10.1016/j.sjbs.2017.10.012)
179. Abd Elmonem HA, Mahmoud AH, Abbas MM. Ameliorative Effect of Zinc Oxide Nanoparticles and vitamin E on some Biochemical and Histological changes in Irradiated Albino Rats. *Egyptian Journal of Radiation Sciences and Applications*, 2021; 34(1): 1-10.
[Doi: 10.21608/ejrsa.2021.63788.1116](https://doi.org/10.21608/ejrsa.2021.63788.1116)
180. Mescher Antony L. Junqueira's Basic Histology: Text and Atlas. 16th ed. New York: McGraw Hill Medical Publishing Division; 2021.
<https://www.accessscience.com/content/book/9781260462982>

References

181. Drury RAB, Wallington EA. *Histological technique*. 4th ed. New York, Oxford University Press, 1967. <https://lccn.loc.gov/67004351>
182. Weng X, Guo M, Luo F, Chen Z. One-step green synthesis of bimetallic Fe/Ni nanoparticles by eucalyptus leaf extract: Biomolecules identification, characterization and catalytic activity. 2017;308, 904-911. <https://doi.org/10.1016/j.cej.2016.09.134>
183. Demissie MG, Sabir FK, Edossa GD, Gonfa BA. Synthesis of Zinc Oxide Nanoparticles Using Leaf Extract of *Lippia adoensis* (Koseret) and Evaluation of Its Antibacterial Activity. *Journal of Chemistry*. 2020;2020, 1-9. <https://doi.org/10.1155/2020/7459042>
184. Król A, Pomastowski P, Rafińska K, Railean-Plugaru V, Buszewski B. Zinc oxide nanoparticles: Synthesis, antiseptic activity and toxicity mechanism. *Adv Colloid Interface Sci*. 2017;249:37–52.
[Doi: 10.1016/j.cis.2017.07.033](https://doi.org/10.1016/j.cis.2017.07.033)
185. Balavandy SK, Sameli K, Abidin ZZ. Rapid and green synthesis of silver nanoparticles via sodium alginate media. *Int J Electrochem Sci*. 2015;10(1):486–497. [https://doi.org/10.1016/S1452-3981\(23\)05007-1](https://doi.org/10.1016/S1452-3981(23)05007-1)
186. Nishimura S, Mott D, Takagaki A, Maenosono S, Ebitani K. Role of base in the formation of silver nanoparticles synthesized using sodium acrylate as dual reducing and encapsulating agents. *Phys Chem Chem Phys*. 2011;13(20):9335–9343. [Doi: 10.1039/c0cp02985](https://doi.org/10.1039/c0cp02985)
187. Gupta M, Tomar RS, Kausik S, Mishra RK, Sharma D. Effective antimicrobial activity of green ZnO nanoparticles of *Catarantus roseus*. *Front Microbiol*. 2018;9:2030. [Doi: 10.3389/fmicb.2018.02030](https://doi.org/10.3389/fmicb.2018.02030)
188. Kalaiselvi A, Roopan SM, Madhumitha G, Ramalingam C, Al-Dhabi NA, Arasu MV. *Catarantus roseus*-mediated zinc oxide nanoparticles against photocatalytic application of phenol red under UV@ 365 nm. *Current Sci*. 2016;111(11):1811–1815.
[Doi:10.18520/CS/V111/I11/1811-1815](https://doi.org/10.18520/CS/V111/I11/1811-1815)

References

189. Go EG, Xu X, McCormick PG. Effect of particle size on the UV absorbance of zinc oxide nanoparticles. *Scripta Materialia*. 2014;78-79:49-52. <https://doi.org/10.1016/j.scriptamat.2014.01.033>
190. Sing P, Kim YJ, Zhang D, Yang DC. Biological Synthesis of Nanoparticles from Plants and Microorganisms. *Trends in Biotechnology*. Elsevier Ltd. 2016;34(7):588–599. [Doi: 10.1016/j.tibtec.2016.02.006](https://doi.org/10.1016/j.tibtec.2016.02.006)
191. Wang Q, Mei S, Manivel P, Ma H, Chen X. Zinc oxide nanoparticles synthesized using coffee leaf extract assisted with ultrasound as nanocarriers for mangiferin. *Curr Res Food Sci*. 2022;5:868-877. <https://doi.org/10.1016/j.crfs.2022.05.002>
192. Huang J, Li Q, Sun D, Lu Y, Su Y, Yang X, et al. Biosynthesis of silver and gold nanoparticles by novel sundried *Cinnamomum camphora* leaf. *Nanotechnology*. 2007;18(10):105104. [Doi: 10.1088/0957-4484/18/10/105104](https://doi.org/10.1088/0957-4484/18/10/105104)
193. Khalil MMH, Ismail EH, El-Bagdady KZ, Mohamed D. Green synthesis of silver nanoparticles using olive leaf extract and its antibacterial activity. *Arabian Journal of Chemistry*. 2014;7(6):1131–1139. <https://doi.org/10.1016/j.arabjc.2013.04.007>
194. Basnet P, Chaturvedi TI, Samanta D, Chatterjee S. A review on biosynthesized zinc oxide nanoparticles using plant extracts as reductants and stabilizing agents. *J Photochem Photobiol B*. 2018;183:201–221. <https://doi.org/10.1016/j.jphotobiol.2018.04.036>
195. Gulati S, Sadeva M, Basin KK. Capping agents in nanoparticle synthesis: Surfactant and solvent system. In: *AIP Conference Proceedings*. AIP Publishing LLC. 2018;1953(1):030214. <https://doi.org/10.1063/1.5032549>
196. Moghri Moazzen MA, Borghei SM, Talebi F. Change in the morphology of ZnO nanoparticles upon changing the reactant

References

- concentration. *Appl Nanosci* [Internet]. 2013;3(4):295–302. <https://doi.org/10.1007/s13204-012-0147-z>
197. Alami ZY, Salem M, Gaidi M, Elk amk ami J. Effect of Zn concentration on structural and optical proprieties of ZnO t in films deposited by spray pyrolysis. *Adv Energy Int J*. 2015;2(4):11–24.
Doi: [10.5121/aeij.2015.2402](https://doi.org/10.5121/aeij.2015.2402)
198. Mayekar J, D ar V, Rad a S. Role of salt precursor in t e synt esis of zinc oxide nanoparticles. *Int J Res Eng Tec nol*. 2014;3(3):43–45.
Doi: [10.15623/ijret.2014.0303008](https://doi.org/10.15623/ijret.2014.0303008)
199. Gontijo LAP, Rap ael E, Ferrari DPS, Ferrari JL, Lyon JP, Sc iavon MA. pH effect on t e synt esis of different size silver nanoparticles evaluated by DLS and t eir size-dependent antimicrobial activity. *Matéria (Rio J)*. 2020;25(4):e-12845.
Doi:[10.1590/S1517-707620200004.1145](https://doi.org/10.1590/S1517-707620200004.1145).
200. Hasan M, Ulla I, Zulfiqar H, Naeem K, Iqbal A, Gul H, et al. Biological entities as c emical reactors for synt esis of nanomaterials: Progress, c allenges and future perspective. *Mater Today C em*. 2018;8:13–28. <https://doi.org/10.1016/j.mtc em.2018.02.003>
201. Tourné-Péteil C, Robin B, Lions M, Martinez J, Me di A, Subra G, et al. Combining sol–gel and microfluidics processes for t e synt esis of protein containing ybrid microgels. *C emical Communications*. 2019;55(87):13112–5. Doi: [10.1039/C9CC04963K](https://doi.org/10.1039/C9CC04963K)
202. Rafaie HA, Samat NA, Nor RM. Effect of pH on t e growt of zinc oxide nanorods using *Citrus aurantifolia* extracts. *Mater Lett*. 2014;137:297–9. <https://doi.org/10.1016/j.matlet.2014.09.033>
203. Mo ammadi FM, G asemi N. Influence of temperature and concentration on biosynt esis and c aracterization of zinc oxide nanoparticles using c erry extract. *J Nanostructure C em*. 2018;8:93–102. <https://doi.org/10.1007/s40097-018-0257-6>

References

204. Buazar F, Bavi M, Krousaoui F, Halvani M, Khaledi-Nasab A, Hossieni SA. Potato extract as reducing agent and stabiliser in a facile green one-step synthesis of ZnO nanoparticles. *J Exp Nanosci.* 2016;11(3):175–84. <https://doi.org/10.1080/17458080.2015.1039610>
205. Ali K, Dwivedi S, Azam A, Saquib Q, Al-Said MS, Alkhalairy AA, et al. Aloe vera extract functionalized zinc oxide nanoparticles as nanoantibiotics against multi-drug resistant clinical bacterial isolates. *J Colloid Interface Sci.* 2016;472:145–56. <https://doi.org/10.1016/j.jcis.2016.03.021>
206. Alartani MN, Ismail I, Bellucci S, Kardary NH, Abdel Salam M. Biosynthesis microwave-assisted of zinc oxide nanoparticles with zizipus jujuba leaves extract: Characterization and photocatalytic application. *Nanomaterials.* 2021;11(7):1682. [Doi: 10.3390/nano11071682](https://doi.org/10.3390/nano11071682)
207. Varugese G, Jitlin PW, Usa KT. Determination of optical band gap energy of wurtzite ZnO: Ce nanocrystallites. *Physical Science International Journal.* 2015;5(2):146. [Doi: 10.9734/PSIJ/2015/14151](https://doi.org/10.9734/PSIJ/2015/14151)
208. Ji X, Zhang F, Zhang R, Liu F, Peng Q, Wang M. An acidic polysaccharide from Zizipus Jujuba cv. Muzao: Purification and structural characterization. *Food Chem.* 2019;274:494–9. <https://doi.org/10.1016/j.foodchem.2018.09.037>
209. Cui T, Dong C, Huang Q. Ionothermal precipitation of highly dispersive ZnO nanoparticles with improved photocatalytic performance. *Appl Surf Sci.* 2016;384:73–82. <https://doi.org/10.1016/j.apsusc.2016.05.008>
210. Ramimogadam D, Hussein MZ bin, Taufiq-Yap YH. The effect of sodium dodecyl sulfate (SDS) and cetyltrimethylammonium bromide (CTAB) on the properties of ZnO synthesized by hydrothermal method. *Int J Mol Sci.* 2012;13(10):13275–93. [Doi: 10.3390/ijms131013275](https://doi.org/10.3390/ijms131013275)

References

211. Dobrucka R, Długaszewska J. Biosynthesis and antibacterial activity of ZnO nanoparticles using *Trifolium pratense* flower extract. *Saudi J Biol Sci.* 2016;23(4):517–23. <https://doi.org/10.1016/j.sjbs.2015.05.016>
212. Ebadi M, Zolfagari MR, Agaei SS, Zargar M, Safiei M, Zairi HS, et al. A bio-inspired strategy for the synthesis of zinc oxide nanoparticles (ZnO NPs) using the cell extract of cyanobacterium *Nostoc* sp. EA03: from biological function to toxicity evaluation. *RSC Adv.* 2019;9(41):23508–23525. [Doi:10.1039/c9ra03962g](https://doi.org/10.1039/c9ra03962g)
213. Jayachandran A, Aswathy TR, Nair AS. Green synthesis and characterization of zinc oxide nanoparticles using *Cayratia pedata* leaf extract. *Biochem Biophys Rep.* 2021;2026:100995. <https://doi.org/10.1016/j.bbrep.2021.100995>
214. Dey A, Somaia S. Green synthesis and characterization of zinc oxide nanoparticles using leaf extract of *Tryallia glauca* (Cav.) Kuntze and their role as antioxidant and antibacterial. *Microsc Res Tech.* 2022; 85(8):2835-2847. [Doi: 10.1002/jemt.24132](https://doi.org/10.1002/jemt.24132)
215. Geetha MS, Nagabhusana H, Sivananjai HN. Green mediated synthesis and characterization of ZnO nanoparticles using *Euphorbia Jatropa* latex as reducing agent. *Journal of Science: Advanced Materials and Devices.* 2016;1(3):301–310. <https://doi.org/10.1016/j.jsamd.2016.06.015>
216. Suresh J, Pradees G, Alexramani V, Sundrarajan M, Hong SI. Green synthesis and characterization of zinc oxide nanoparticle using insulin plant (*Costus pictus* D. Don) and investigation of its antimicrobial as well as anticancer activities. *Advances in Natural Sciences: Nanoscience and Nanotechnology.* 2018;9(1):015008. [Doi: 10.1088/2043-6254/aaa6f1](https://doi.org/10.1088/2043-6254/aaa6f1)
217. Pillai AM, Sivasankarapillai VS, Radar A, Josep J, Sadegfar F, Rajes K, et al. Green synthesis and characterization of zinc oxide

References

- nanoparticles with antibacterial and antifungal activity. *J Mol Struct.* 2020;1211:128107. <https://doi.org/10.1016/j.molstruc.2020.128107>
218. Kalpana VN, Devi Rajeswari V. A review on green synthesis, biomedical applications, and toxicity studies of ZnO NPs. *Bioinorg Chem Appl.* 2018;2018: 3569758. <https://doi.org/10.1155/2018/3569758>
219. Alart i MN, Ismail I, Bellucci S, Jaremko M, Abo-Aba SEM, Abdel Salam M. Biosynthesized Zinc Oxide Nanoparticles Using Zizipus Jujube Plant Extract Assisted by Ultrasonic Irradiation and Their Biological Applications. *Separations.* 2023; 10(2):78. <https://doi.org/10.3390/separations10020078>
220. Selvanathan V, Aminuzzaman M, Tan LX, Win YF, Chea ESG, Heng MH, Tey L-H, Arullappan S, Algetami N, Alart i SS, Sultana S, Sa'iduzzaman M, Abdulla H, Aktaruzzaman M. Synthesis, characterization, and preliminary in vitro antibacterial evaluation of ZnO nanoparticles derived from soursop (*Annona muricata* L.) leaf extract as a green reducing agent, *Journal of Materials Research and Technology.* 2022; 20: 2931-2941. <https://doi.org/10.1016/j.jmrt.2022.08.028>
221. Al Za'abi M, al Busaidi M, Yasin J, Scupp N, Nemmar A, Ali BH. Development of a new model for the induction of chronic kidney disease via intraperitoneal adenine administration, and the effect of treatment with gum acacia terebinth. *Am J Transl Res.* 2015;7(1):28-38. PMID: 25755826; PMCID: PMC4346521.
222. Ramadan AG, Yassein AAM, Eissa EA, Mahmoud MS, Hassan GM. Biochemical and histopathological alterations induced by subchronic exposure to zinc oxide nanoparticle in male rats and assessment of its genotoxicity. *J.Umm Al-Qura Univ. Appl. Sci.* 2022;8:41-49. <https://doi.org/10.1007/s43994-022-00008-3>

References

223. Mansouri E, K orsandi L, Orazizade M, Jozi Z. Dose-dependent epatotoxicity effects of zinc oxide nanoparticles. 2015; 2(4): 273-282. [Doi: 10.7508/nmj.2015.04.005](https://doi.org/10.7508/nmj.2015.04.005)
224. Ben SI, Mrad I, Ri ane N, Mir LEL, Sakly M, Amara S. Sub-acute oral toxicity of zinc oxide nanoparticles in male rats. 2015;6(3). [Doi: 10.4172/2157-7439.1000284](https://doi.org/10.4172/2157-7439.1000284)
225. Alebac ew M, Kinfu Y, Makonnen E, Bekuretsion Y, Urga K, Afework M. Toxicological evaluation of met anol leaves extract of Vernonia bipontini Vatke in blood, liver and kidney tissues of mice. Afr Healt Sci. 2014;14(4):1012–24. [Doi: 10.4314/a s.v14i4.33](https://doi.org/10.4314/a s.v14i4.33)
226. Me rdad M, Moz gan GP. Effect of Zingiber Extract on Histopat ologic C anges in Mice Kidneys. Res J Appl Sci. 2011;6(5):295–298. [Doi: 10.3923/rjasci.2011.295.298](https://doi.org/10.3923/rjasci.2011.295.298)
227. George SA, Al-Rus aidan S, Francis I, Soonowala D, Nampoory MRN. 2,8-Di ydroxyadenine Nep ropat y Identified as Cause of End-Stage Renal Disease After Renal Transplant. Exp Clin Transplant. 2017;15(5):574-577. [Doi:10.6002/ect.2015.0096](https://doi.org/10.6002/ect.2015.0096)
228. Cai H, Su S, Li Y, Zeng H, Z u Z, Guo J, et al. Protective effects of Salvia miltiorr iza on adenine-induced c ronic renal failure by regulating t e metabolic profiling and modulating t e NADPH oxidase/ROS/ERK and TGF- β /Smad signaling pat ways. J Et noparmacol. 2018;212:153–165. [Doi: 10.1016/j.jep.2017.09.021](https://doi.org/10.1016/j.jep.2017.09.021)
229. Törmänen S, Pörsti I, Lakkisto P, Tikkanen I, Niemelä O, Paavonen T, et al. Endot elin A receptor blocker and calcimimetic in t e adenine rat model of c ronic renal insufficiency. BMC Nep rol. 2017;18(1):1–13. [Doi: 10.1186/s12882-017-0742-z](https://doi.org/10.1186/s12882-017-0742-z)
230. Wang J, Wang F, Yun H, Z ang H, Z ang Q. Effect and mec anism of fucoidan derivatives from Laminaria japonica in experimental adenine-induced c ronic kidney disease. J Et noparmacol. 2012;139(3):807–813. [Doi: 10.1016/j.jep.2011.12.022](https://doi.org/10.1016/j.jep.2011.12.022)

References

231. Jarsia P, Nosrati A, Alizade A, Has emi-Sote SMB. Hepatotoxicity and ALT/AST enzymes activities change in therapeutic and toxic doses consumption of acetaminophen in rats. *Int Biol Biomed J.* 2017;3(3):119–124. URL: <http://ibbj.org/article-1-129-en.html>
232. Soleymaninejad M, Joursaraei S G, Feizi F, Jafari Anarkooli I. The Effects of Lycopene and Insulin on Histological Changes and the Expression Level of Bcl-2 Family Genes in the Hippocampus of Streptozotocin-Induced Diabetic Rats. *Journal of diabetes research*, 2017; 4650939. <https://doi.org/10.1155/2017/4650939>
233. Ali BH, Al-Salam S, al Suleimani Y, al Kalbani J, al Balani S, Asique M, et al. Curcumin ameliorates kidney function and oxidative stress in experimental chronic kidney disease. *Basic Clin Pharmacol Toxicol.* 2018;122(1):65–73. Doi: [10.1111/bcpt.12817](https://doi.org/10.1111/bcpt.12817)
234. Chang X ying, Cui L, Wang X z i, Z ang L, Z u D, Z ou X rong, et al. Quercetin attenuates vascular calcification through suppressed oxidative stress in adenine-induced chronic renal failure rats. *Biomed Res Int.* 2017;2017:5716204. Doi: [10.1155/2017/5716204](https://doi.org/10.1155/2017/5716204)
235. El-Maddawy ZK, Abd El Naby WSH. Protective effects of zinc oxide nanoparticles against doxorubicin induced testicular toxicity and DNA damage in male rats. *Toxicol Res (Camb).* 2019;8(5):654–662. Doi: [10.1039/c9tx00052f](https://doi.org/10.1039/c9tx00052f)
236. K aleel SMJ, Jaran AS, Haddadin MSY. Evaluation of total phenolic content and antioxidant activity of tree leaf extracts of *Ziziphus spina-christi* (Sedr) grown in Jordan. *Br J Med Med Res.* 2016;14:1–8. Doi: [10.9734/BJMMR/2016/24935](https://doi.org/10.9734/BJMMR/2016/24935)
237. K aleel SM, Almu ur RA, Al-Deeb TMF, Jaran AS. Biochemical changes in the liver, kidney and serum of rats exposed to ethanolic leaf extract of *Ziziphus spina-christi*. *Jordan Journal of Biological Sciences.* 2021;14(4): 763 – 767. <https://doi.org/10.54319/jjbs/140417>

References

238. Engle SJ, Stockelman MG, Chen JU, Boivin G, Yum MN, Davies PM, et al. Adenine phosphoribosyltransferase-deficient mice develop 2, 8-dihydroxyadenine nephrolithiasis. *Proceedings of the National Academy of Sciences*. 1996;93(11):5307–5312.
[Doi: 10.1073/pnas.93.11.5307](https://doi.org/10.1073/pnas.93.11.5307)
239. Pettitt RM, Brumbaugh AP, Gartman MF, Jackson AM. Chronic kidney disease: Detection and evaluation. *Osteopathic Family Physician*. 2020;12(1):14–19. [Doi:10.33181/12011](https://doi.org/10.33181/12011)
240. al Za'abi M, Salaby A, Manoj P, Ali BH. The in vivo effects of adenine-induced chronic kidney disease on some renal and hepatic function and CYP450 metabolizing enzymes. *Physiol Res*. 2017;66(2):263-271. [Doi: 10.33549/physiolres.933374](https://doi.org/10.33549/physiolres.933374)
241. Amin A, Mahmoud-Ghoneim D. *Zizyphus spina-christi* protects against carbon tetrachloride-induced liver fibrosis in rats. *Food and Chemical Toxicology*. 2009;47(8):2111–2119.
<https://doi.org/10.1016/j.fct.2009.05.038>
242. El Maaiden E, El Karrassi Y, Qara NAS, Essamadi AK, Moustaid K, Nasser B. Genus *Ziziphus*: A comprehensive review on ethnopharmacological, phytochemical and pharmacological properties. *Journal of Ethnopharmacology*. 2020;259:112950.
[Doi: 10.1016/j.jep.2020.112950](https://doi.org/10.1016/j.jep.2020.112950)
243. Rami G, Moammad KS, Zarei M, Sokooi M, Oskoueian E, Poorbagher MRM, et al. Zinc oxide nanoparticles synthesized using *Hyssopus Officinalis* L. Extract Induced oxidative stress and changes in the expression of key genes involved in inflammatory and antioxidant systems. *Biol Res*. 2022;55(1):24.
<https://doi.org/10.1186/s40659-022-00392-4>

الخلاصة

الجسيمات النانوية لأوكسيد الخارصين تمت دراستها على نطاق واسع في العقود الأخيرة وذلك بسبب تطبيقاتها في الطب النانوي بناءً على العوامل الفسيولوجية والكيميائية الحيوية التي تمتلكها وغالباً ما تضاف هذه الجسيمات كمكمل غذائي في اغذية الحيوانات. تهدف هذه الدراسة إلى تخليق وتوصيف جسيمات أوكسيد الخارصين النانوية بالطريقة البايولوجية باستخدام المستخلص النباتي، ثم دراسة تأثيراتها في ذكور الجرذان المعرضة للادنين. التخليق الحيوي لجسيمات أوكسيد الخارصين النانوية (ZnO-NPs) تم باستخدام المستخلص المائي الخام لأوراق السدر *Ziziphus-spina christi* ونترات الخارصين سداسي الماء $(Zn(NO_3)_2 \cdot 6H_2O)$. وسط التفاعل كان عند درجة حرارة 60 مئوية، ودالة حامضية 9. ان التغيير في لون المحلول من الأصفر إلى البني يشير الى تكوين جزيئات أوكسيد الخارصين النانوية. ان جسيمات اوكسيد الخارصين النانوية الناتجة تم تشخيصها باستخدام عدة تقنيات. حيث أظهر طيف الأشعة فوق البنفسجية-المرئية (UV-Vis) قمة عظمية عند 362 نانومتر، وهذا يعد دليلاً واضحاً على تكوين ZnO-NPs. بين طيف الأشعة تحت الحمراء (FT-IR) ظهور قمم امتصاص بين 400 و500 سم⁻¹ تعود الى اهتزاز اصرة Zn-O. اما تحليل حيود الأشعة السينية (XRD) فقد اظهر التركيب Hexagonal-Wurtzite للجسيمات النانوية الناتجة بمتوسط حجم بلوري عند 38.177 نانومتر. وبين فحص المجهر الإلكتروني (TEM) أن الجسيمات النانوية لها شكل كروي وتقع في مدى 35-45 نانومتر، كما أظهرت صور الماسح المجهر الإلكتروني (SEM) الشكل الشبه الكروي للجسيمات النانوية على شكل تجمعات بمتوسط حجم الجسيمات، D1 (39.74 نانومتر)، D2 (42.25 نانومتر)، وD3 (48.19 نانومتر). اضافة الى ذلك، اظهر مجهر القوة الذرية (AFM) عن سطحاً موحداً مع حبيبات تشبه المخروط تغطي سطح جسيمات اوكسيد الخارصين النانوية. في هذه الدراسة تم استخدام ستة وثلاثين من ذكور الجرذان وقسمت عشوائياً إلى ست مجموعات متساوية (ستة جرذان لكل مجموعة). المجموعة الأولى جرعت فقط بثنائي ميثيل سلفوكسيد عن طريق الفم (5% v/v/day) لمدة 30 يوماً واعتبرت كمجموعة سيطرة، المجموعة الثانية جرعت بمادة الأدينين عن طريق الفم (100 mg/Kg. Bw/day) لمدة 30 يوماً، المجموعة الثالثة تم اعطائها مستخلص أوراق السدر (10 mg/Kg. Bw/day) لمدة 30 يوماً، المجموعة الرابعة أعطيت ZnO-NPs (10 mg/Kg. Bw/day) لمدة 30 يوماً، المجموعة الخامسة تم إعطائها جرعة من الأدينين مع جرعة من مستخلص أوراق السدر لمدة 30 يوماً، كذلك المجموعة السادسة والأخيرة تلقت جرعة مشتركة من الأدينين و ZnO-NPs لمدة 30 يوماً. بعد نهاية 30 يوماً، تم قياس وظائف الكلية (حامض اليوريك، اليوريا والكرياتينين) ووظائف الكبد (ALT، AST، وALP). كذلك تم قياس مستويات مضادات

الأوكسدة (TAC, CAT, SOD, GSH, MDA و NO). بالإضافة الى ذلك، تم دراسة التغيرات النسيجية المرضية لكل من الكلى والكبد لدى الجرذان. أظهرت النتائج ان كل من مستخلص أوراق السدر وجسيمات اوكسيد الخارصين النانوية بجرعة (10 mg/Kg.Bw/day) لها تأثيرات فعالة ضد التعرض للأدينين، وهذا ما أكده تحسن النمو في ذكور الجرذان إضافة الى الانخفاض المعنوي في مؤشرات وظائف الكلى والكبد (حامض اليوريك، اليوريا، الكرياتينين ، ALT ، AST ALP) بعد اعطائها الجرعة اعلاه مقارنة بالجرذان المعرضة للأدينين ($P \geq 0.05$). كما تم ملاحظة ان هناك ارتفاع كبير في مستويات مضادات الأوكسدة SOD و CAT و TAC و GSH بالتوافق مع الانخفاض في مستويات كل من MDA و NO في كلا مجموعتي المعالجة (الخامسة والسادسة) عند مقارنتها بجرذان مجموعة الأدينين. إضافة الى ذلك، كان هناك تحسن ملحوظ في التغيرات النسيجية لكل من الكلى والكبد بالمقارنة مع مجموعة جرذان الأدينين. بناء على هذه النتائج يمكن الاستنتاج، أن جسيمات أوكسيد الخارصين النانوية ومستخلص اوراق السدر لها تأثيرات فعالة لدى ذكور الجرذان المعرضة للأدينين، مما يعني أنه يمكن استخدامها بشكل آمن ضد تلف الكلية والكبد الناجم من تأثير المواد السمية، حيث لم يلاحظ أي آثار ضارة في أنسجة الكلية والكبد، مما يشير إلى أنها قد تكون مضادات قوية للأوكسدة والالتهابات والتسمم وفعالة للاستخدام في التطبيقات الطبية الحيوية.



جامعة كربلاء
كلية العلوم
قسم الكيمياء

التخليق الحيوي لجسيمات أكسيد الخارصين النانوية باستخدام
مستخلص أوراق السدر: التشخيص ودراسة تأثيراته في ذكور
الجرذان المعرضة للأدنين

رسالة مقدمة الى مجلس كلية العلوم - جامعة كربلاء
كجزء من استكمال متطلبات نيل درجة الماجستير في الكيمياء

من قبل

حيدر حسين عباس

بكالوريوس علوم كيمياء/ جامعة الكوفة (2009)

بإشراف

أ.د. عايد حميد حسن

أ.د. نرجس هادي السعدي

2023 م

1445 هـ